

**Mid-Tertiary geology and geochronology of the  
Clifton-Morenci area, Greenlee and Graham  
Counties, Arizona, and adjacent New Mexico**

by  
Charles A. Ferguson<sup>1</sup>, M. Stephen Enders<sup>2</sup>,  
Lisa Peters<sup>3</sup>, and William C. McIntosh<sup>3</sup>

**Arizona Geological Survey Open-file Report 00-07**

**August, 2000**

**Arizona Geological Survey  
416 W. Congress, Suite 100, Tucson, AZ 85701**

**Also available in Adobe® PDF format with DI-18 and DGM-01**

<sup>1</sup> Arizona Geological Survey, 416 W. Congress, #100, Tucson, AZ 85701 email:wamego\_kid@hotmail.com

<sup>2</sup> Phelps Dodge Morenci, Inc., 4521 Highway 191, Morenci, AZ 85540

<sup>3</sup> New Mexico Institute of Mining and Technology, 801 Leroy Place, Socorro, NM 87801

# **Mid-Tertiary geology and geochronology of the Clifton-Morenci area, Greenlee and Graham Counties, Arizona, and adjacent New Mexico**

## **INTRODUCTION**

The geology of the Clifton-Morenci area has been investigated for nearly 100 years beginning with the pioneering work of W. Lindgren at the start of the 20<sup>th</sup> century. For most of the century, geological investigation focused on mineralization and the complex suite of Eocene porphyritic intrusive stocks and dikes in the area. Very little attention was directed at the regional structural and stratigraphic relationships in the overlying, and largely unmineralized Tertiary volcanic rocks.

From the beginning, geologists have understood that supergene enrichment played a critical role in making the Morenci district a world class porphyry copper deposit (Lindgren, 1905a). For much of the past 90 years, enrichment was thought to have occurred during two phases of exposure and erosion: pre-volcanic and post-volcanic (Lindgren, 1905a; Moolick and Durek, 1966; Langton, 1973; North and Preece, 1993). Since then, the role of pre-volcanic enrichment has been questioned (Cook, 1994; Enders, 2000). Understanding the evolution of supergene enrichment at Morenci is of critical importance, not only because of this deposit's economic significance, but also in terms of our understanding of the evolution of porphyry copper systems in general. As a result, Phelps Dodge Morenci Inc. initiated a research program in 1997 to address unanswered questions concerning the Tertiary geologic history of the Clifton-Morenci area. The principal result of this effort was a Ph.D. program undertaken by M. Stephen Enders at the University of Arizona that included a re-examination of the regional structure and Tertiary stratigraphy of the Clifton-Morenci area. The detailed geologic map, structural cross-sections, and the stratigraphic, geochronologic, and structural observations contained in this report are the principal products of this aspect of the research program.

Two basic programs of field study were enacted to clarify the regional stratigraphic framework of the Clifton-Morenci area: 1) mapping and <sup>40</sup>Ar/<sup>39</sup>Ar geochronology of the Oligocene and Miocene volcanic rocks, and 2) provenance analysis of the Miocene and Pliocene volcanoclastic sedimentary rocks in the adjacent Eagle Creek, San Francisco, and Duncan basins. A collaborative project involving geologists from the Arizona Geological Survey and Phelps Dodge Morenci Inc. funded by Phelps Dodge Morenci was initiated in 1998 with the two principal objectives: 1) compiling all new and previous mapping in the area into a single comprehensive geologic map encompassing the original Clifton 15' folio of Lindgren (1905b), and 2) constructing a detailed lithostratigraphic and chronostratigraphic framework of the Tertiary volcanic and sedimentary rocks of the area.

This report is intended to accompany the digital geologic map and cross sections of the Clifton-Morenci area published as Arizona Geological Survey Digital Geological Map 1 (DGM-01). References to details of the geologic map and cross-sections are made

frequently in this report and it is advised that, to fully appreciate the geology of the area, the map and cross sections should be available to the reader.

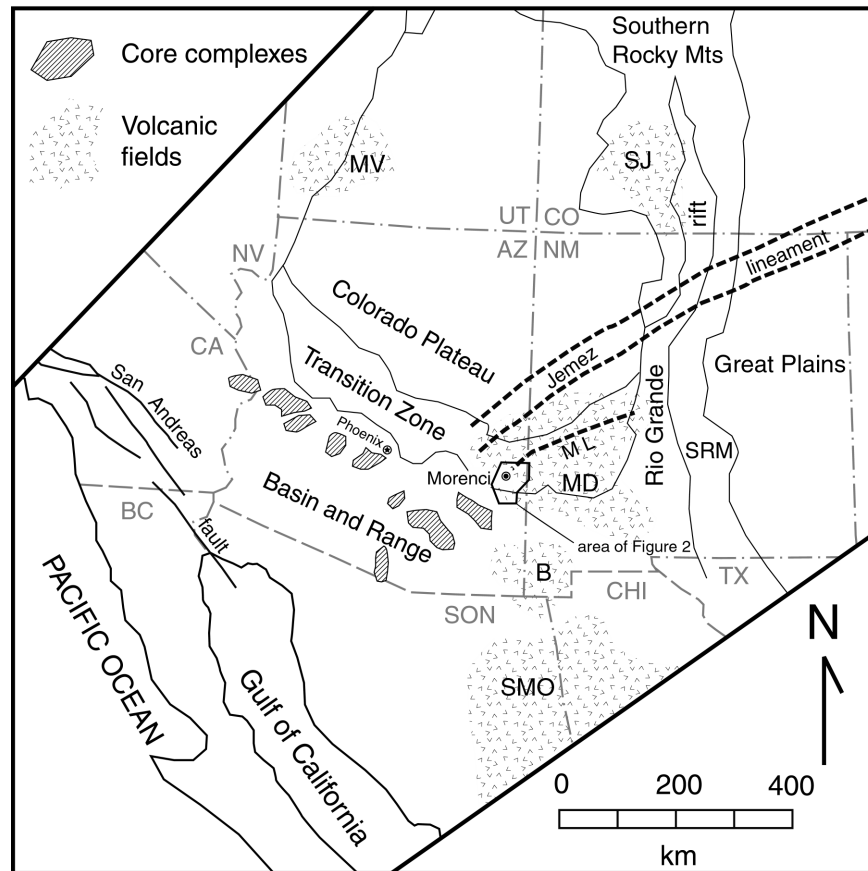


**Figure 1.** Location of the Clifton-Morenci area in relation to major tectonic provinces and Oligocene volcanic fields of the southwestern United States. ML = Morenci Lineament.

## GEOLOGIC SETTING

The Clifton-Morenci area lies at the juncture of three important geologic provinces: the Basin and Range, and Transition Zone structural provinces, and the Mogollon-Datil volcanic field (Figure 1). The Transition Zone in Arizona is a relatively narrow (40-60 km), northwest-striking belt of rugged mountains and deep canyons that intervenes between the thick (40 km) and structurally inert crust of the Colorado Plateau, and the thin (18-20 km) highly extended crust of the Basin and Range (Warren, 1969; Hauser et al., 1987; Hauser and Lundy, 1989; Hendricks and Plescia, 1991). Structurally, the Transition Zone is defined by low magnitudes of total extension at the surface ( $\ll 10\%$ ), but the dramatic decrease in crustal thickness towards the southwest implies significant structural thinning of the middle and/or lower crust (Spencer and Reynolds, 1991; Leighty, 1997). The principal evidence of this thinning is a belt of metamorphic

core-complexes strung out along the northeast margin of the Basin and Range province throughout Arizona (Spencer and Reynolds, 1989). The most southeasterly of these complexes is the Pinaleno Mountains that lie directly southwest of the Morenci area (Figure 1). The restored position of the middle crustal rocks exposed in the footwall of the Pinaleno Mountains detachment system is probably somewhere along the southwestern edge of the Transition Zone, and many of the northwest-striking, Mid-Tertiary normal faults in the Clifton-Morenci area are thought to be related to the formation of this detachment fault (Walker, 1995).

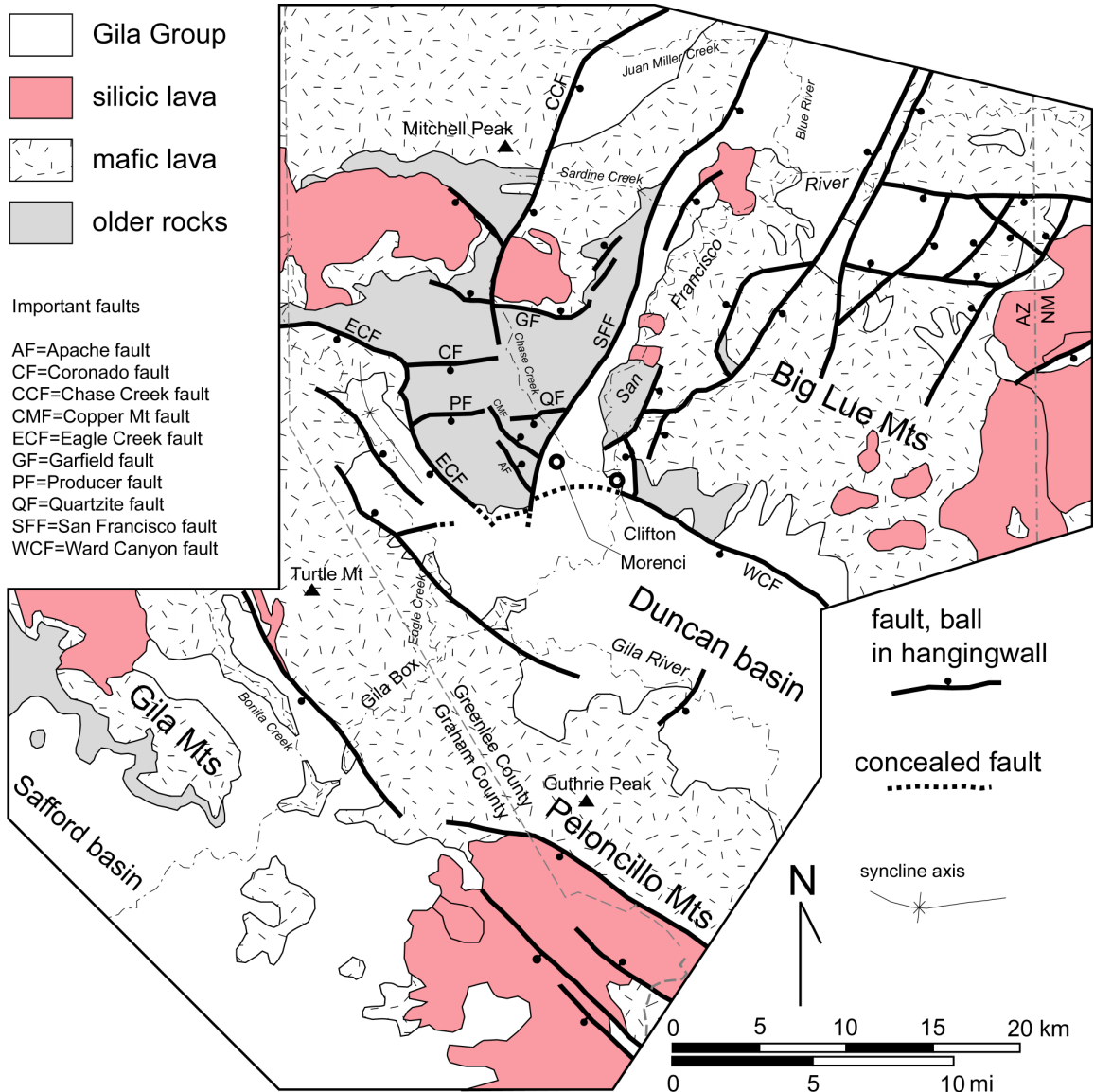


**Figure 2.** Simplified geology of the Clifton-Morenci area showing the location of important faults discussed in the text.

To the east of the Clifton-Morenci area the Transition Zone, based on the work of Aldrich and Laughlin (1984) and Schneider and Keller (1994), curves sharply to the north along trend with the Morenci lineament (Figure 1). The northeast-striking Morenci lineament extends from the Clifton-Morenci area northeast at least 300 km into central New Mexico. In New Mexico, the lineament merges into two northeast-striking structures, the Plains of San Agustin basin and the Socorro Accommodation Zone, which together act as approximate boundaries between the Colorado Plateau to the northwest and the Mogollon-Datil volcanic field to the southeast. Slightly farther to the north, the Jemez lineament or Jemez magmatic zone represents another major northeast-striking structural and magmatic zone that extends across the Rio Grande Rift and well into the Great Plains physiographic province (Aldrich and Laughlin, 1984). Together, the Morenci and Jemez lineaments have had a long history of activity inherited from the early Proterozoic northeast-striking structural grain of the basement (e.g. Karlstrom and Humphreys, 1998). The Morenci lineament has been active as an important structural element during the Laramide orogeny and during Mid-Tertiary extension (e.g. Chapin and Cather, 1981; Baldridge et al., 1982; Garmezzy, 1990).

## **GEOCHRONOLOGY**

### **Philosophy of sampling**

Prior to this study very little was known about the ages of the volcanic units in the Clifton-Morenci area. Dominating the sequence is a thick pile of basaltic andesite lava that is underlain and overlain by significantly thinner, previously dated Oligocene and Miocene felsic units (Figures 2 and 3). Just to the north of the Clifton-Morenci area the mafic lavas are overlain by the Enebro Mountain Formation, (proposed here based on Schroeder's (1996) rhyolite of Enebro Mountain) which has been dated at between 20 and 22 Ma (Marvin et al., 1987; Ratté and Brooks, 1995; Schroeder, 1996). At the base of the mafic lavas, the thin distal fringe of two regional Oligocene ignimbrites from the Mogollon-Datil volcanic field have been identified along San Francisco River (Cunningham, 1969; Ratté and Brooks, 1995).

To the south, east, and west of Clifton-Morenci, several small felsic lava fields have been described within the mafic lava sequence. Inasmuch as the mafic lavas around the Clifton-Morenci area are apparently continuous and without interruption, one of our primary goals was finding evidence for these felsic, presumably time-stratigraphic interbeds within, above, or below the monotonous pile of mafic lava around the Clifton-Morenci area.

Our dating program concentrated on three major stratigraphic problems. First, we wanted to confirm or refute a hypothesis that the Miocene Enebro Mountain Formation represents an isochronous marker unit, and if so, determine how far south and west it can be traced. Secondly, we wanted to date the upper and lower parts of the mafic lava sequence with the intent of determining if and when major hiatus occurred, and whether or not the sequence's upper and lower contacts are time-stratigraphic or time-transgressive. Finally, we wanted to trace the distal fringes of the interbedded felsic units of adjacent areas toward the Clifton-Morenci area with the hope of finding time-correlative markers in the monotonous pile of mafic lavas.

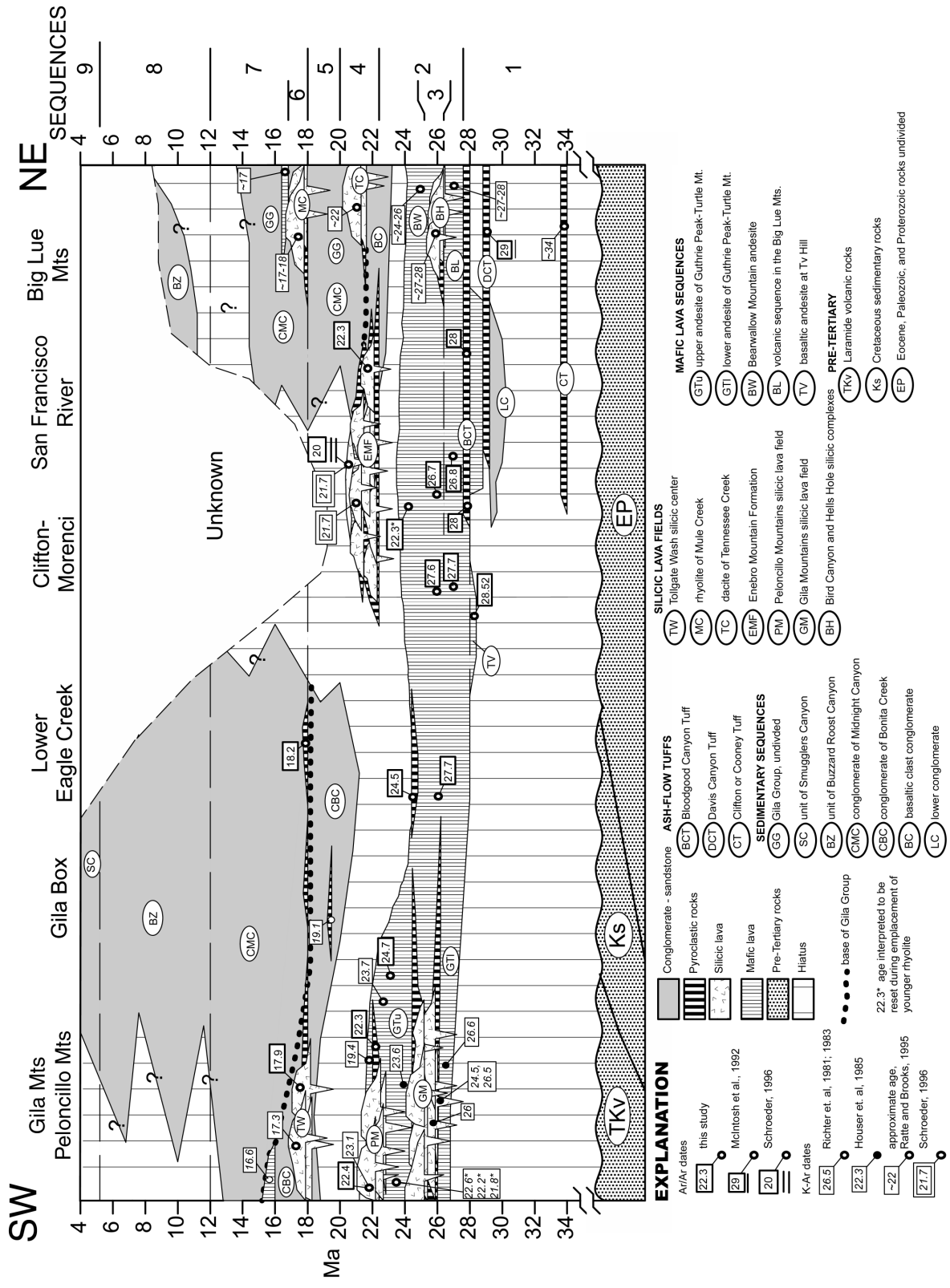


**Figure 3.** Space-time diagram for Tertiary stratigraphic units of the Clifton-Morenci area, Big Lue Mts., northern Duncan basin, eastern Gila Mts., and northern Peloncillo Mts.

A major obstacle we encountered in our sampling program was the suitability of the rock samples for dating. As reported by Schroeder (1996), the Enebro Mountain Formation proved to be exceptionally crystal-poor and practically void of sanidine phenocrysts. Samples of the mafic lava suitable for dating were also very difficult to obtain. We avoided sampling mafic lava that contained vesicles or amygdules, obvious clay alteration or extensive hematite staining, and lava with glassy matrix. Twenty samples were submitted for microprobe analysis to select the most suitable for dating. Many of the flows that we sampled were judged to be of poor or moderate quality by microprobe analysis (See Appendix C).

## Analyses

Sixteen  $^{40}\text{Ar}/^{39}\text{Ar}$  age dates were acquired from volcanic rocks in and around the Morenci- Clifton area; eight groundmass concentrate mafic lava, and eight sanidine, single-crystal, laser fusion analyses. Most of the dates are for units in the map area (Sheet 1), but a few were selected from units in adjacent areas that had been dated previously, mostly by conventional K-Ar methods (Richter et al., 1983; Houser et al., 1985; Ratté and Brooks, 1995). The analyses were done at the New Mexico Geochronological Research Laboratory (Peters and McIntosh, 1999; Peters, 1999). Results are summarized in Tables 1, 2 and 3. The details of the analytical procedures and complete data tables are presented in four Appendices; mafic lava analyses in Appendix A, felsic lavas in Appendix B, an evaluation of the quality of samples in Appendix C, and a description of laboratory procedures in Appendix D.

**Table 1.** Summary of mafic lava groundmass concentrate  $^{40}\text{Ar}/^{39}\text{Ar}$  analyses. Preferred age in **bold type**. UTM coordinates are in grid zone 12.

Sample #	Plateau	Error 2 $\sigma$	Isochron	Error 2 $\sigma$	Intercept	Error 2 $\sigma$	Integrated	Error 2 $\sigma$	UTM N	UTM E
F8-266	<b>22.33</b>	<b>0.14</b>	22.35	0.21	298.9	8.7	22.61	0.44	3671380	650935
F8-269			28.27	0.2	270.3	4.2	<b>26.68</b>	<b>0.7</b>	3674340	654240
F8-273	26.91	0.16	<b>26.81</b>	<b>0.1</b>	305.5	2.8	27.3	1.4	3673885	655885
F8-275	<b>27.62</b>	<b>0.2</b>	28.11	0.56	289	12	27.74	0.56	3663485	662610
F8-276	<b>27.73</b>	<b>0.17</b>	27.91	0.32	291	12	27.77	0.52	3663735	663610
F8-286	<b>24.74</b>	<b>0.24</b>	24.96	0.41	292.3	7.2	24.78	0.38	3641625	654650
F8-301	26.99	0.18	27.64	0.39	273	15	<b>27.2</b>	<b>1.4</b>	3650435	649085
F8-316			28.99	0.23			<b>28.52</b>	<b>0.24</b>	3663965	650145

Of the eight mafic lava groundmass samples, five yielded well-behaved plateau ages, but for one of these (F8-273) the plateau age was discarded in favor of its isochron age because of its higher than atmospheric  $^{40}\text{Ar}/^{39}\text{Ar}_{\text{in}}$  intercept value (Table 1). Three samples (F8-269, F8-301, and F8-316) yielded disturbed spectra, and for these, integrated ages are preferred. Table 1 summarizes the results for each mafic lava sample and indicates which calculated date is preferred. Figure 4 is a probability distribution diagram for all of the samples. A detailed description of the analyses, and procedures, along with plateau and isochron diagrams for each sample is provided in Appendix A.

Datable sanidine phenocrysts were recovered from seven felsic lava and tuff units in the Clifton-Morenci area and analyzed by the single crystal laser total fusion method (Table 2). Because of the paucity of sanidine phenocrysts in the Enebro Mountain Formation (Schroeder, 1996), most of our sanidine  $^{40}\text{Ar}/^{39}\text{Ar}$  dating program was focused on the numerous felsic lava flows and nonwelded tuffs to the south and west of the Morenci district. Results of the sanidine dates are summarized on a probability distribution diagram (Figure 5). Probability distribution diagrams for individual samples are in Appendix B.

**Table 2.** Summary of sanidine, single-crystal, total laser fusion  $^{40}\text{Ar}/^{39}\text{Ar}$  analyses. UTM coordinates are in grid zone 12. An asterisk (\*) indicates a pumice separate of this sample.

Sample #	Age	Error $2\sigma$	UTM N	UTM E
F8-288*	22.25	0.06	3638775	651125
F8-288	22.34	0.08	3638775	651125
F8-295	22.41	0.06	3627655	660860
F8-299	18.2	0.05	3652540	649610
F8-302	24.52	0.06	3650525	649235
F8-277	27.94	0.09	3664345	664510
F8-282	22.26	0.38	3664890	660425
F8-289	17.89	0.61	3635100	648130
F9-165	28.14	0.04	3667725	655990

**Table 3.** Radiometric ages for Laramide intrusive rocks of the Morenci district. Table also includes two previously published dates for supergene alunite from the district.

Description (sample #)	Age (Ma)	Mineral	Method	Quadrangle Name	Reference
Diorite Porphyry (L-847)	$63.0 \pm 1.9$	hornblende	K-Ar	Copperplate Gulch	McDowell (1971)
	$64.7 \pm 2.0$	hornblende	K-Ar		McDowell (1971)
Dacite Porphyry (DW-17, 268')	$58.7 \pm 1.5$	feldspar	K-Ar	Mitchell Peak	Geochron Labs (5/19/99)
Monzonite Porphyry (L-976)	$56.5 \pm 1.7$	biotite	K-Ar	Copperplate Gulch	McDowell (1971)
	$61.7 \pm 2.8$	feldspar	K-Ar	Clifton	AMAX unpubl. data (1976)
Older Granite Porphyry	$57.6 \pm 2.2$	biotite	K-Ar	Copperplate Gulch	Bennett (1975)
Molybdenite (94MOR) <sup>1</sup>	$54.9 \pm 0.91$	molybdenite	Re-Os	Clifton	McCandless et al. (1993, 1999 <sup>1</sup> )
Breccia (type unknown)	$53.9 \pm 2.0$	sericite	K-Ar	Clifton	AMAX unpubl. data (1976)
Candelaria Breccia	$52.8 \pm 2.0$	sericite	K-Ar	Copperplate Gulch	Bennett (1975)
Andesite Dike (92-23)	$30.0 \pm 0.7$	biotite	K-Ar	Clifton	Cook (1994)
Alunite (92-21)	$9.88 \pm 0.26$	alunite	K-Ar	Clifton	Cook (1994)
Alunite (92-05)	$7.19 \pm 0.27$	alunite	K-Ar	Copperplate Gulch	Cook (1994)

<sup>1</sup> The published age of  $55.8 \pm 1.0$  Ma was revised using a corrected  $\lambda = 1.666\text{E}-11$  per Tom McCandless (pers. comm.).

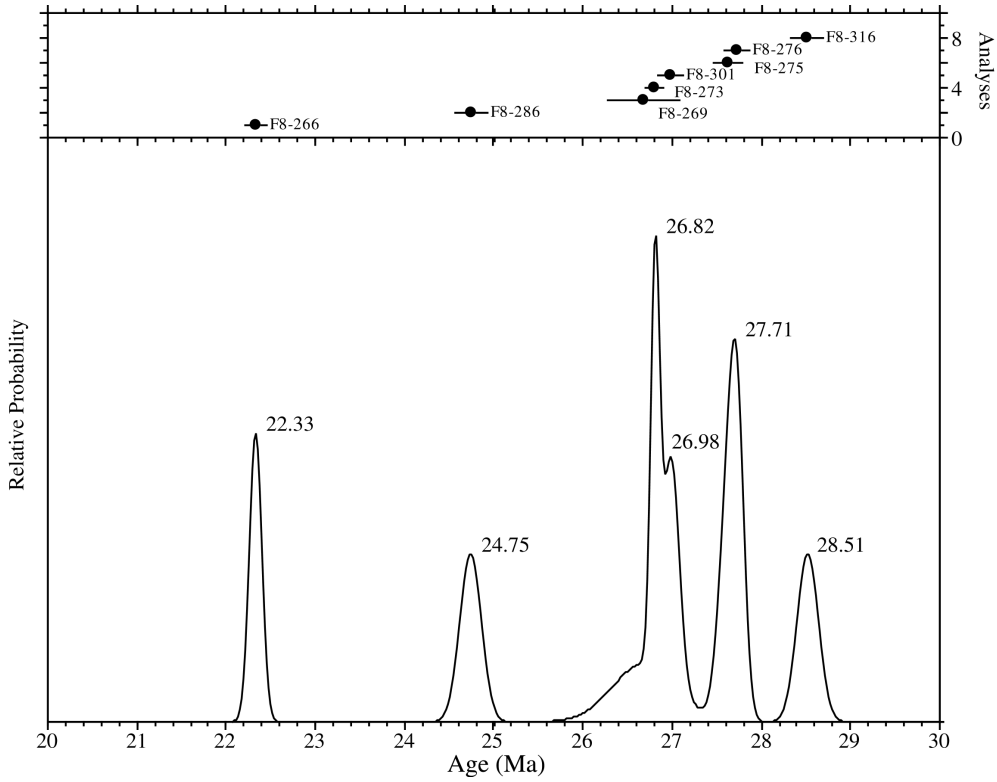


**Figure 4.** Age distribution of Morenci mafic lavas.

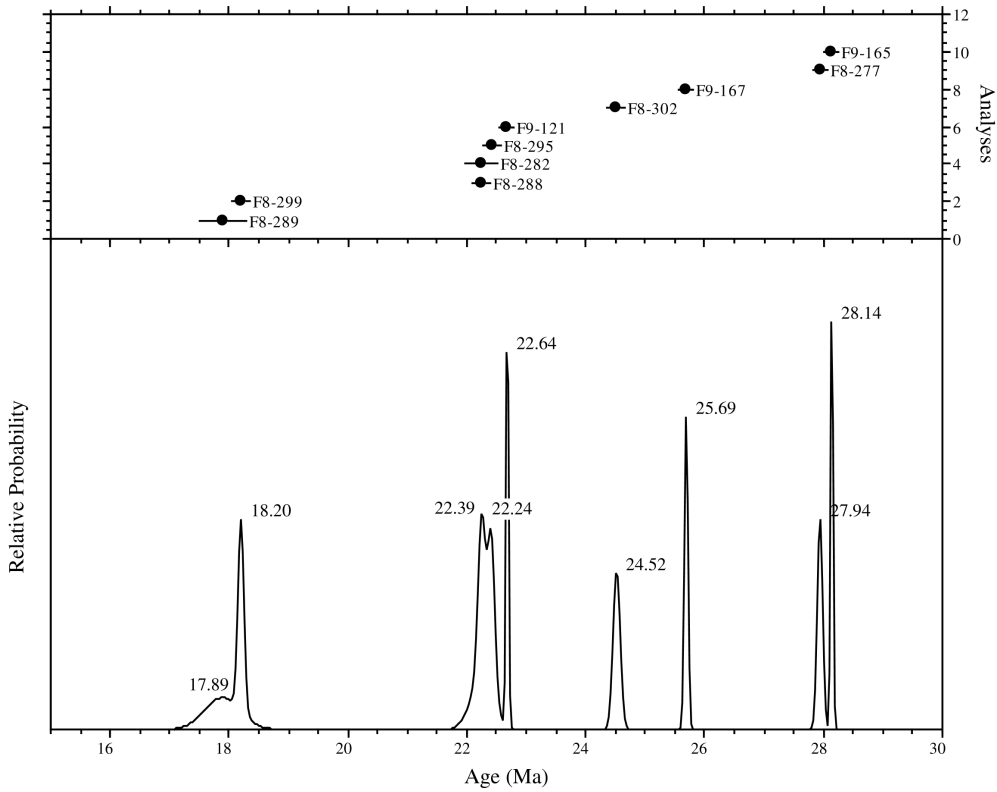


**Figure 5.** Probability distribution diagram of the weighted mean ages from the Morenci sanidine.

## Summary of results

### *Clifton-Morenci area*

The oldest mafic lava we dated in the Clifton-Morenci area is the  $28.52 \pm 0.24$  Ma basaltic andesite at Tv hill, which is a small exposure of massive lava that intrudes a cogenetic pyroclastic sequence of cinder and agglutinate. This important outcrop directly overlies lower Paleozoic rocks overlooking the western margin of the current open pit mine. A  $30.0 \pm 0.7$  Ma (K-Ar whole rock) mafic dike sampled in the Morenci pit (Cook, 1994) may be a feeder for the oldest mafic flows in the Clifton-Morenci area. Elsewhere, the oldest dates for the base of the mafic lava sequence in the Big Lue, Peloncillo, and Gila mountains consistently range between about 28-27 Ma (Richter et al., 1983; Houser et al., 1985; Ratté and Brooks, 1995).

The main thickness of basaltic andesite lava in the Clifton-Morenci area overlies the 28 Ma (McIntosh et al., 1992) Bloodgood Canyon Tuff, but a thin sequence of older basaltic andesite lava occurs between Bloodgood Canyon Tuff and the ~34 Ma Clifton Tuff along San Francisco River near Clifton. Two sanidine  $^{40}\text{Ar}/^{39}\text{Ar}$  dates from the western distal edge of the Bloodgood Canyon Tuff were acquired during this study;  $28.14 \pm 0.04$  Ma and  $27.94 \pm 0.09$  Ma. Although its possible age range is 6 million years, we place the base of this older sequence of mafic lavas at about 30 Ma. We interpret a 4 million year hiatus between the Clifton Tuff and the base of the mafic lava because sandstone and conglomerate occur between the two units in most areas, and available geochronology indicates that the oldest mafic lavas are about 30 Ma. In addition, in the northeast corner of the study area, the oldest mafic lavas overlie a crystal-poor welded ignimbrite that we correlate with the  $29.01 \pm 0.11$  Ma Davis Canyon Tuff (sanidine  $^{40}\text{Ar}/^{39}\text{Ar}$ , McIntosh et al., 1992) which in turn overlies Tertiary sandstone and conglomerate.

The age of the upper contact of the mafic sequence is poorly understood. A region-wide age of 26-25 Ma seems reasonable, based on ages published by Ratté and Brooks (1995) in the Big Lue Mountains and our  $^{40}\text{Ar}/^{39}\text{Ar}$  date of  $24.52 \pm 0.06$  Ma from sanidine in a felsic tuff at the top of the sequence in the Gila Box area. The presence of a basaltic clast conglomerate at the top of the sequence to the north, south, and southeast of Morenci, and the lack of multiple age dates younger than approximately 25 Ma suggest that the contact between the mafic lava and the overlying 23-22 Ma felsic volcanics of the Enebro Mountain Formation represents a 3-4 million year hiatus in the Clifton-Morenci area. An even longer hiatus (up to 7 million years) is possible in the lower Eagle Creek – Gila Box area where less than 100 meters of conglomerate is present between the  $24.52 \pm 0.06$  Ma tuff at the top of the mafic lavas and an  $18.20 \pm 0.05$  Ma tuff (our  $^{40}\text{Ar}/^{39}\text{Ar}$  dates) that defines the base of the Gila Group. Farther south, in the northern Peloncillo Mountains, there is good evidence that the duration of this hiatus is much shorter because a  $22.34 \pm 0.08$  Ma tuff (our sanidine  $^{40}\text{Ar}/^{39}\text{Ar}$  date) occurs within and near the top of the mafic lavas which have been dated at  $19.4 \pm 0.4$  Ma (K-Ar whole rock date of Richter et al., 1983).

### *Reset ages*

Four dates in the mafic lava sequence, all around 22 Ma, are interpreted to be reset. These come from areas invaded by abundant, approximately 22 Ma rhyolite dikes

and include our  $22.33 \pm 0.14$  Ma  $^{40}\text{Ar}/^{39}\text{Ar}$  groundmass concentrate date of basaltic andesite lava from an area named “intrusion basin” near Enebro Mountain by Schroeder (1996). The other three are K-Ar whole rock dates of approximately 22 Ma (Richter et al., 1983) from the andesite of Guthrie Peak-Turtle Mountain in the Peloncillo Mountains.

### ***Enebro Mountain Formation***

We recovered sparse, small sanidine phenocrysts from only one sample of the Enebro Mountain Formation, a dome along San Francisco River that yielded a  $^{40}\text{Ar}/^{39}\text{Ar}$  date of  $22.26 \text{ Ma} \pm 0.38 \text{ Ma}$ . At Enebro Mountain Schroeder (1996) dated a flow at 21.7 Ma ( $^{40}\text{Ar}/^{39}\text{Ar}$  biotite) and a crosscutting dike at 21.7 and 20.0 Ma (K-Ar biotite and sanidine respectively). K-Ar whole rock dates of  $20.6 \pm 0.7$  Ma and  $20.9 \pm 0.8$  Ma (Marvin et al., 1987) were also reported from these rocks. A duration of about 1 million years for the formation seems reasonable, and there is no evidence that the upper and lower contacts of the Enebro Mountain Formation are significantly time-transgressive. We interpret the formation to be an essentially isochronous unit.

### ***Gila Box area***

Numerous nonwelded tuff units occur interbedded with the mafic lava sequence in the northern Peloncillo Mountains, Gila Box area, and Gila Mountains to the south and west of the Clifton-Morenci area, but none of these correlate with the Enebro Mountain Formation. Two thin, nonwelded tuffs in the Gila Box yielded  $^{40}\text{Ar}/^{39}\text{Ar}$  sanidine single crystal dates of  $18.20 \pm 0.05$  Ma and  $24.52 \pm 0.06$  Ma. The older one is interbedded with the uppermost part of the mafic lava sequence and the younger is separated by about 100 meters of conglomerate of Bonita Creek. No intervening pyroclastic rocks are present in the section. We interpret these two tuffs as distal fringe pyroclastic deposits from the ~26-24 Ma silicic lava field in the Gila Mountains and the ~18 Ma Tollgate Wash silicic lava field in the northern Peloncillo Mountains. Farther south, a tuff we dated at  $22.34 \text{ Ma} \pm 0.08 \text{ Ma}$  (sanidine  $^{40}\text{Ar}/^{39}\text{Ar}$ ) in the northern Peloncillo Mountains might correlate with the Enebro Mountain Formation, but its proximity to nearby ~23-22 Ma lava domes in the Peloncillo Mountains, and its abundant sanidine phenocrysts, a feature atypical of nearly all the Enebro Mountain Formation rhyolites, suggest that it was locally derived.

### ***Gila and Peloncillo mountains***

The only volcanic sequence common to the Clifton-Morenci area and all adjacent areas is the mafic lavas. To the south and west of Morenci, the mafic lavas are referred to as the andesite of Guthrie Peak-Turtle Mountain (AGT) in the Peloncillo Mountains and Gila Mountains (Richter et al., 1983; Houser et al., 1985). The Gila Box area represents a region intermediate between all three areas, and the mafic lavas of the AGT are well exposed here. In the Gila Box area, Richter et al., 1983 refer to an older sequence of andesite lava as the andesite of Gila River, and based on petrographic differences, they place this unit below the AGT. Based on our study of relationships along the crest of the Peloncillo Mountains and in the Gila Box, we believe that Richter et al.'s (1983) andesite of Gila River correlates with the lower part of the AGT as it is mapped in the main part of the Gila and Peloncillo mountains. For the remainder of this discussion we refer to Richter et al.'s (1983) andesite of Gila River as part of the AGT.

In the Gila Mountains, an approximately 26-24 Ma silicic lava field occurs within the AGT, and this allows the AGT to be divided into upper and lower andesites (Tau and Tal units of Houser et al., 1985). This division is clearly defined and unequivocal based on field relationships in the Gila Mountains (Houser et al., 1985). To the east, in the Gila Box area, several thin nonwelded tuffs occur interbedded within the AGT, and the oldest one of these was used to separate the AGT from Richter et al.'s (1983) older unit, andesite of Gila River. Since our  $24.52 \pm 0.06$  Ma, single crystal sanidine  $^{40}\text{Ar}/^{39}\text{Ar}$  date is from the youngest of the tuffs interbedded with the AGT in Gila Box, we interpret it and all of the older tuffs in this area to be derived from the Gila Mountains silicic lava field. The Gila Mountains silicic volcanic field has no time-equivalent in the Clifton-Morenci area, but it does correlate roughly in time with a pair of isolated silicic lava fields in the Big Lue Mountains; the Bird Canyon and Hells Hole silicic complexes of Ratté and Brooks (1995).

The extensive silicic lava field in the northern Peloncillo Mountains has also been interpreted to occur within the AGT (Richter et al., 1983). However, geochronology (Richter et al., 1983; this study), and field relationships (this study) indicate that the Peloncillo Mountains silicic volcanics are all younger than the main thickness of the AGT (including both of Richter et al., 1983 Tal and Tau map units). The critical relationship is a steeply northeast-dipping contact near the crest of the range exposed just north of highway 191 that was mapped as a buttress unconformity by Richter et al. (1983). The unconformity places the upper part of the AGT (Tau map unit) above a thick succession of silicic lava which in turn overlies the lower part of the AGT (Tal map unit). We reinterpret this unconformity as a south-side-down normal fault based on map patterns that show the contact to dip steeply to the south instead of steeply or moderately to the north. Based on this field relationship and our geochronology, we interpret the Peloncillo Mountains silicic lava field to be younger than the main mass of the AGT and entirely younger than the Gila Mountains silicic lava field. The Peloncillo silicic lava field correlates in time with the Enebro Mountain Formation in the Clifton-Morenci area, and the dacite of Tennessee Creek farther east in the Big Lue Mountains (Ratté and Brooks, 1995). Note that on our space-time diagram (Figure 3), we show the silicic lava fields of the Peloncillo and Gila mountains hypothetically overlapping each other with an intervening thickness of AGT mafic lavas even though this relationship is not known to exist.

Two younger Miocene (17-18 Ma) rhyolite lava fields in the Big Lue Mountains (rhyolite of Mule Creek), and in the northern Peloncillo Mountains (Tollgate Wash silicic lava field) have no time-equivalent unit in the Clifton-Morenci area. The silicic lava fields in the Peloncillo Mountains are both characterized by fairly abundant sanidine phenocrysts. We interpret the  $18.20 \pm 0.05$  Ma (sanidine  $^{40}\text{Ar}/^{39}\text{Ar}$ ) nonwelded tuff in the upper Gila Box-Eagle Creek area to be derived from the Tollgate Wash silicic lava field of the northern Peloncillo Mountains. We also dated one of the isolated plugs of this small field at  $17.89 \pm 0.61$  Ma (sanidine  $^{40}\text{Ar}/^{39}\text{Ar}$ ).

### ***Discussion and recommendations***

Because of its great thickness, and lack of felsic interbeds, we consider the basaltic andesite lava sequence in the Clifton-Morenci area to be the most poorly

understood of all the volcanic sequences in the region. We recommend that this sequence receive the greatest amount of attention in terms of future geochronological studies. We find it interesting that our oldest and youngest dates in this unit come from the thinnest preserved sequence of these rocks (in the footwall of Chase Creek fault). Four samples from the thickest part of the sequence, including one pair of samples collected above and below what we believed was a major flow break all yielded similar dates of between approximately 26.5 and 27.5 Ma. A detailed petrographic, stratigraphic, and geochronologic study comparing the thickest and thinnest parts of the sequence would be very interesting. In particular, we wonder if a sequence that shows very little evidence of internal hiatus could have been deposited continually over 7 million years. We believe that the younger 2-3 million years of this interval represents a hiatus (Figure 3), but there is scant evidence to support this.

## **STRATIGRAPHY**

### **Paleozoic and Mesozoic**

The stratigraphy and sedimentology of Paleozoic and Mesozoic units was not investigated in detail for this study, and our unit descriptions for these rocks are drawn largely from Lindgren (1905b). Two features of interest however, were observed in these rocks during our mapping. The Cambrian Coronado Formation is present throughout much of the area, and it is noticeably thicker to the southwest, but along San Francisco River in the vicinity of Limestone Gulch and Ash Spring Canyon, the formation is missing or very thin. Instead, calcareous, coarse-grained, arkosic, cobble and locally boulder conglomerate is present at the base of the Ordovician Longfellow Formation in this area. Outcrop patterns indicate that a Cambrian-early Ordovician basement high was present in this area.

Lindgren (1905b) describes two upper Paleozoic units in the map area: the Mississippian Modoc Formation, and the Carboniferous Tule Canyon Formation. Modoc Formation is present throughout the southern part of the map area, and Tule Canyon Formation was mapped only to the north. The Tule Canyon Formation was recognized as a separate unit because, unlike the Modoc Formation, it contains Pennsylvanian fossils in its upper part. The lower Tule Canyon Formation probably correlates with the Modoc Formation, but it is not known exactly how. James (1999) describes a complex sequence of siliciclastic and carbonate strata at this interval coinciding with the large area of Tule Canyon Formation mapped by Lindgren (1905b) in the northwest part of the study area. We believe that this sequence probably deserves the most attention in terms of refining the Paleozoic stratigraphy in the area.

### **Early Tertiary**

Paleogene rocks in the map area are all hypabyssal intermediate to mafic porphyritic stocks, dikes and sills that range in age from 65-53 Ma. These rocks are closely associated with the porphyry copper mineralization (Figure 6). The rocks are divided into four main suites, from oldest to youngest: diorite porphyry, monzonite porphyry, and older and younger granite porphyries. In addition, some of the diabase dikes in the area may be Paleogene in age, and the Candalaria breccia probably represents

the deep-seated remains of a volcanic vent. See the unit descriptions for detailed descriptions of the various Paleogene hypabyssal rocks in the Clifton-Morenci area. Available geochronology results for the porphyries are listed in Table 3. No volcanic rocks of Late Cretaceous, Paleocene, or Eocene age are preserved in the Clifton-Morenci area, nor are they well represented in the oldest Mid-Tertiary conglomeratic units. The closest preserved volcanic rocks of this age are exposed in the southeastern Gila Mountains, and a subsurface continuation of this volcanic belt is shown hypothetically on cross-section D-D' (Sheet 2).

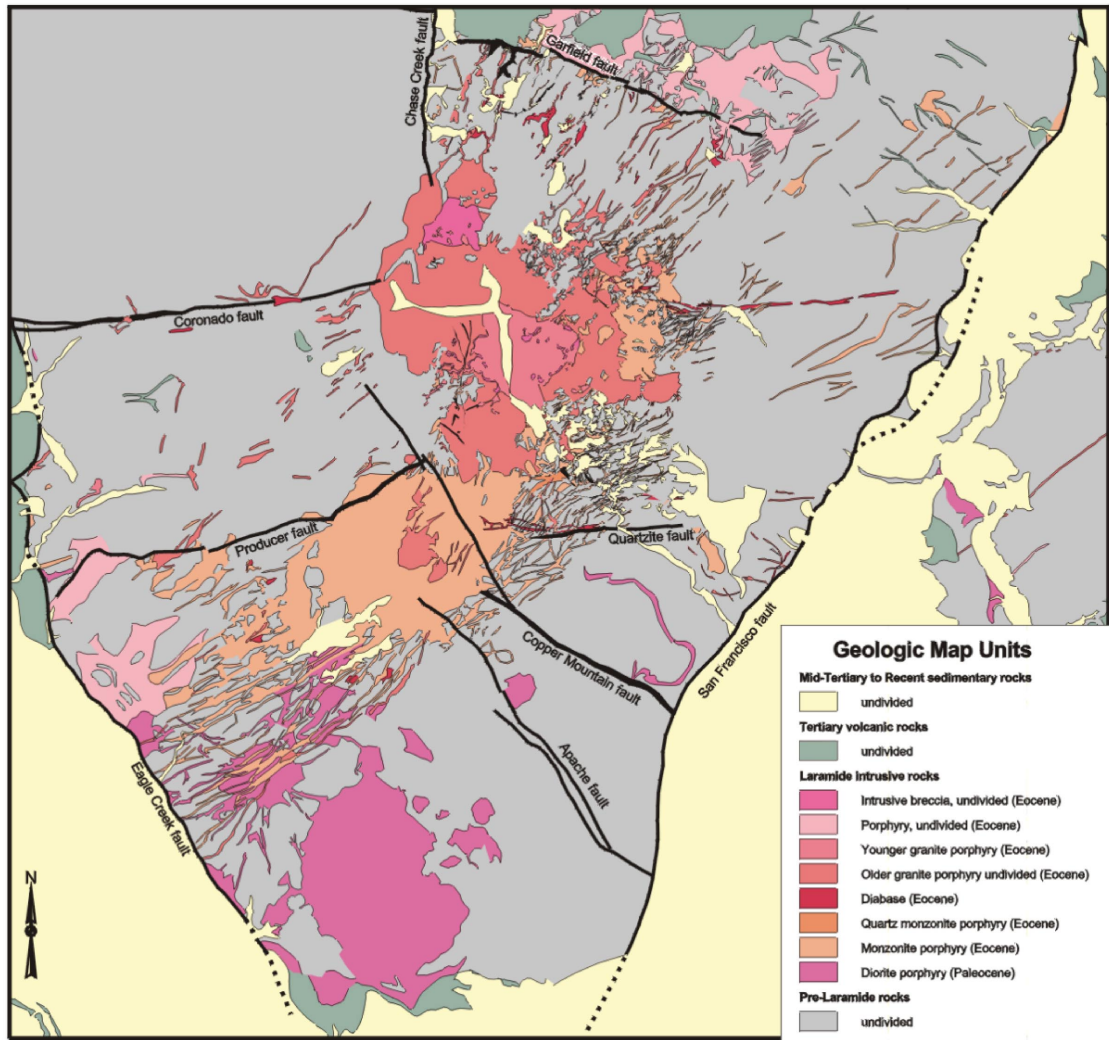


**Figure 6.** Eocene intrusive rocks in the Morenci area.

## Mid- to Late-Tertiary volcanic and sedimentary sequence

### *Volcanic rocks*

The Mid-Tertiary volcanics of the Clifton-Morenci area are easily divisible into three general sequences; an Oligocene sequence of three separate approximately 34, 29, and 28 Ma regional ash-flow tuffs, a thick succession of basaltic andesite lava, and a

capping sequence of rhyolite lava and tuff called the Enebro Mountain Formation. Because of their regional importance, formal names have long been in use for the Oligocene tuffs (Cunningham, 1969; McIntosh et al., 1992; Ratté and Brooks, 1995). Field relationships and geochronology show that the thick mafic volcanic rocks of the Clifton-Morenci area correlate in time and space with previously, and differently named sequences to the east and southwest. The mafic lavas in the Clifton-Morenci area represent an important link between the volcanic stratigraphy of the Mogollon-Datil volcanic field, the Peloncillo volcanic field, and other volcanic fields farther west. We do not believe the mafic lavas in the Clifton-Morenci area have been studied in enough detail to be given a name. The nearest named sequences are the Bearwallow Mountain andesite and volcanic sequence Big Lue Mountains to the east (Ratté and Brooks, 1995), but without more detailed chronology, it would be very difficult to make this division in the Clifton-Morenci area. Extending the nomenclature of the Peloncillo and Gila mountains to the northeast is more appealing, because only one name, the andesite of Guthrie Peak-Turtle Mountain, would be needed to describe the whole sequence.

### ***Enebro Mountain Formation designation***

The youngest volcanic sequence in the Clifton-Morenci area, the Enebro Mountain Formation, has been studied in enough detail, and its chronostratigraphic relationships well enough established to merit elevation to formal status. We believe that the unit's areal extent (100 km<sup>2</sup>), relatively high volume (60 km<sup>3</sup>), and importance as a stratigraphic marker unit are ample reasons to merit this designation. The Enebro Mountain Formation is herein proposed as a formal name for the unit mapped by Schroeder (1996) as rhyolite of Enebro Mountain. In addition to the outcrops mapped by Schroeder (1996) we include all of the area mapped as rhyolite by Lindgren (1905a) to the west of Enebro Mountain, the extensive field of rhyolite lava and tuff in the Chesser Gulch area to the east, and a series of domes, lava flows and nonwelded tuff along San Francisco River. Schroeder (1996) recognized four variations of rhyolite lava and two variations of tuff on his map; devitrified and vitric coherent facies lava, altered and unaltered autobreccia, fused tuff and nonwelded tuff. Our map lumps together these variations so that the Enebro Mountain Formation is divided into lava (Ter), tuff (Tet), intrusive (Tei), or undifferentiated (Te) units. The thickest preserved section of the Enebro Mountain Formation is about 335 meters on the south face of Enebro Mountain, but the best exposures here are cut by two faults (Schroeder, 1996). We designate a type section on the east slope of a 7160' peak just to the southwest of Enebro Mountain. The section starts in the upper part of Wood Canyon (approximate UTM coordinates: 3670450N, 648585E) and goes to the top of the peak (approximate UTM coordinates: 3670630N, 647840E). The type section consists of from bottom to top; 18 meters of tuff that directly overlies mafic lava, 85 meters of lava, 12 meters of tuff, 85 meters of lava, 9 meters of tuff, and 122 meters of lava. The top of the formation is not exposed in this area, but elsewhere it is typically overlain by basal conglomeratic rocks of the Gila Group, principally conglomerate of Midnight Canyon.

Although the Enebro Mountain Formation has approximate time equivalents in the Big Lue Mountains to the east (the dacite of Tennessee Creek of Ratté and Brooks, 1995) and the Peloncillo Mountains to the south (Richter et al., 1983), these other units

are distinct and non-contiguous. The Enebro Mountain Formation is characterized by very crystal-poor, nearly aphyric rhyolite lava and nonwelded tuffs, and to the west, it may include thin basaltic lava flows (based on the mapping of Lindgren, 1905a). The unit is restricted to an east-west striking belt just to the north of the north-side-down Garfield fault. Motion on this fault may be related to emplacement of the rhyolite.

### ***Gila Group***

The mid-Tertiary volcanic rocks of the Clifton-Morenci are overlain by a thick succession of conglomeratic sedimentary rocks and partially indurated sand and gravel. The deposits are well-exposed along the canyons of the Gila, and San Francisco rivers, and Eagle Creek, and these sections represent most of the type areas for Gilbert's (1875) Gila Conglomerate, the other two being in New Mexico. The Gila conglomerate has since been elevated to group level (Heindl, 1963) and is currently referred to either as Gila Group (e.g. Cather et al., 1994), as Gila Conglomerate (e.g. Knechtel, 1938; Ratté et al., 1969; Richter et al., 1983; Houser et al., 1985), or as Gila Formation (Ratté and Brooks, 1995). Because the unit includes lithologies other than conglomerate, we prefer the term Gila Group. In the Clifton-Morenci area Richter et al. (1983) and Houser et al. (1985) defined the Gila Conglomerate as "unlithified to lithified, dominantly clastic sediments deposited in closed basins," and they divide it into several informal units. Based on the descriptions of Gilbert (1875) and Knechtel (1936; 1938) the upper contact is defined as the onset of incision related to the integration of a through-going drainage system. Defining the base of the Gila Group is more equivocal, and has been a subject of debate for many years (e.g. Heindl, 1962). Heindl (1962; 1963) discussed this problem and stated that of the three classes of alluvial units that might be confused with actual Gila Group deposits, the class that is most difficult to distinguish is "certain alluvial deposits older than the basin fill that have been separated because they are clearly related to volcanic rocks older than the basin fill or are in marked angular unconformity with the basin fill." Whereas this may be a problem farther to the west towards the interior of the Basin and Range province (Heindl, 1963), it is not a significant problem in the Clifton-Morenci area. Richter et al. (1983) and Houser et al. (1985) defined the base of the Gila Conglomerate as the top of a distinctive basalt-clast conglomerate called the conglomerate of Bonita Creek. This contact is also marked by a thin sequence of nonwelded tuff that we have dated at  $18.20 \pm 0.05$  Ma.

### ***Time-stratigraphic sequences***

We use our  $^{40}\text{Ar}/^{39}\text{Ar}$  dating results in combination with the 25 previously published K-Ar and  $^{40}\text{Ar}/^{39}\text{Ar}$  dates (Table 4) from other volcanic rocks in and adjacent to the Clifton-Morenci region to construct a detailed chronostratigraphic framework. We define nine time-stratigraphic sequences of Oligocene through Miocene volcanic and sedimentary rock. The framework embraces a 3200 km<sup>2</sup> area which includes the Big Lue Mountains (Ratté and Brooks, 1995), Clifton-Morenci area (Schroeder, 1996; this report), Gila Box (Richter and Lawrence, 1981; this report), northern Peloncillo Mountains (Richter et al., 1983; this report), and eastern Gila Mountains (Houser et al., 1985). Since the sequences are defined by age instead of lithostratigraphic criteria they show dramatic changes in thickness and composition across the region. These changes can be used to

interpret the migration of volcanic, sedimentary, and tectonic environments across the study area. The age range, composition, variations, and volume of volcanic materials for each sequence are summarized in Table 5. Details of each sequence's components and a list of all correlative map units in this and adjacent areas are described in the following sections.

**Table 4.** Ages of mid-Tertiary volcanic rocks in the Clifton-Morenci region, including the Big Lue Mountains, Gila Box, eastern Gila Mountains, and northern Peloncillo Mountains. Entries are listed by increasing age. Map unit symbols are from the associated reference. Marvin et al.'s (1987) sample numbers are sequence numbers.

Sample #	Age (Ma)	Error (±)	Method	Mineral	Unit	Reference
R81:A	16.2	?	K-Ar	groundmass	Tb	Richter et al. (1981)
R81:A	16.6	?	K-Ar	plagioclase	Tb	Richter et al. (1981)
F8-289	17.89	0.61	$^{40}\text{Ar}/^{39}\text{Ar}$	sanidine	Trp	this study, Richter et al.'s (1983) map unit
1 (198)	17.7	0.6	K-Ar	whole rock	Tb	Ratte and Brooks (1995)
4 (36)	17.7	0.6	K-Ar	glass	Tr	Ratte and Brooks (1995)
F8-299	18.2	0.05	$^{40}\text{Ar}/^{39}\text{Ar}$	sanidine	Ttt	this study, Copperplate Gulch quadrangle
5 (35)	18.3	0.7	K-Ar	glass	Tr	Ratte and Brooks (1995)
2 (38)	19.0	1.2	K-Ar	whole rock	Tb	Ratte and Brooks (1995)
6 (37)	19.0	0.7	K-Ar	whole rock	Tr	Ratte and Brooks (1995)
A	19.1	0.4	K-Ar	sanidine	Ttt	Richter et al. (1983)
3 (39)	19.1	1.1	K-Ar	whole rock	Tb	Ratte and Brooks (1995)
C	19.4	0.4	K-Ar	whole rock	Tau	Richter et al. (1983)
dike	20	?	$^{40}\text{Ar}/^{39}\text{Ar}$	sanidine	Tei	Schroeder (1996)
203b	20.6	0.7	K-Ar	whole rock	Tei	Marvin et al. (1987)
203a	20.9	0.8	K-Ar	whole rock	Tei	Marvin et al. (1987)
7 (195)	21.3	1.8	K-Ar	plagioclase	Tr	Ratte and Brooks (1995)
dike	21.7	?	K-Ar	biotite	Tei	Schroeder (1996)
dome	21.7	?	K-Ar	biotite	Ter	Schroeder (1996)
8 (33)	21.8	1.4	K-Ar	hornblende	Tr	Ratte and Brooks (1995)
R83:G	21.8	0.5	K-Ar	whole rock	Tal	Richter et al. (1983)
R83:F	22.2	0.5	-Ar	whole rock	Tal	Richter et al. (1983)
F8-288	22.25	0.06	$^{40}\text{Ar}/^{39}\text{Ar}$	pumice sanidine	Ttt	this study, Richter et al.'s (1983) map unit
F8-282	22.26	0.38	$^{40}\text{Ar}/^{39}\text{Ar}$	sanidine	Tei	this study, Clifton quadrangle
F8-266	22.33	0.14	$^{40}\text{Ar}/^{39}\text{Ar}$	groundmass	Tb	this study, Coronado quadrangle
F8-288	22.34	0.08	$^{40}\text{Ar}/^{39}\text{Ar}$	matrix sanidine	Ttt	this study, Richter et al.'s (1983) map unit
F8-295	22.41	0.06	$^{40}\text{Ar}/^{39}\text{Ar}$	sanidine	Tabr	this study, Richter et al.'s (1983) map unit
R83:E	22.6	0.5	K-Ar	whole rock	Tal	Richter et al. (1983)
I	23.1	0.5	K-Ar	biotite, sanidine	Tabr	Richter et al. (1983)
H85:A	23.6	0.5	K-Ar	whole rock	Tau	Houser et al. (1985)
D	23.7	0.5	K-Ar	whole rock	Tau	Richter et al. (1983)
13 (196)	24.2	0.9	K-Ar	whole rock	Tba	Ratte and Brooks (1995)
9 (43)	24.5	0.8	K-Ar	plagioclase	Tba	Ratte and Brooks (1995)

H85:D	24.5	0.6	K-Ar	biotite	Tbbc	Houser et. al. (1985)
F8-302	24.52	0.06	<sup>40</sup> Ar/ <sup>39</sup> Ar	sanidine	?	this study, unit not shown on Richter et al. (1983)
F8-286	24.74	0.24	<sup>40</sup> Ar/ <sup>39</sup> Ar	groundmass	Tb	this study, Richter et al.'s (1983) map unit
10 (31)	25.0	0.9	K-Ar	plagioclase	Tba	Ratte and Brooks (1995)
H85:C	25.9	0.6	K-Ar	oxyhornblende	Tbld	Houser et. al. (1985)
11 (32)	26.2	1.0	K-Ar	plagioclase	Tba	Ratte and Brooks (1995)
H85:D	26.5	0.6	K-Ar	plagioclase	Tbbc	Houser et. al. (1985)
H85:B	26.6	0.6	K-Ar	whole rock	Tal	Houser et. al. (1985)
F8-269	26.68	0.7	<sup>40</sup> Ar/ <sup>39</sup> Ar	groundmass	Tb	this study, Mitchell Peak quadrangle
F8-273	26.81	0.1	<sup>40</sup> Ar/ <sup>39</sup> Ar	groundmass	Tb	this study, Mitchell Peak quadrangle
F8-301	27.2	1.4	<sup>40</sup> Ar/ <sup>39</sup> Ar	groundmass	Tau	this study, Richter et al.'s (1983) map unit
22 (199)	27.5	1.0	K-Ar	whole rock	Tau	Ratte and Brooks (1995)
F8-275	27.62	0.2	<sup>40</sup> Ar/ <sup>39</sup> Ar	groundmass	Tb	this study, Clifton quadrangle
F8-276	27.73	0.17	<sup>40</sup> Ar/ <sup>39</sup> Ar	groundmass	Ta	this study, Ratte and Brooks (1995) map unit
23 (17)	27.9	1.0	K-Ar	whole rock	Tau	Ratte and Brooks (1995)
F8-277	27.94	0.09	<sup>40</sup> Ar/ <sup>39</sup> Ar	sanidine	Tbc	this study, Ratte and Brooks (1995) map unit
F9-165	28.14	0.04	<sup>40</sup> Ar/ <sup>39</sup> Ar	sanidine	Tbc	this study, Mitchell Peak quadrangle
F8-316	28.52	0.24	<sup>40</sup> Ar/ <sup>39</sup> Ar	whole rock	Tbl	this study, Copperplate Gulch quadrangle
unknown	29.01	0.11	<sup>40</sup> Ar/ <sup>39</sup> Ar	sanidine	Tdc	McIntosh et al. (1992)
92-23	30.0	0.7	K-Ar	whole rock	Ta	Cook (1994)
67	33.1	2.8	fission-track	zircon	Tc	Wahl (1980)
66	33.7	1	K-Ar	biotite	Tc	Marvin et al. (1987)

### Sequence 1 (34 to 28 Ma): Older andesitic lavas

The 34 Ma Clifton Tuff and the 28 Ma Bloodgood Canyon Tuff define the lower and upper boundaries of this sequence. Both of these regional ash-flow tuff sheets were derived from silicic cauldron complexes in the Mogollon-Datil volcanic field of southwestern New Mexico (McIntosh et al., 1992), and they pinch-out just to the west of the San Francisco River. In between these tuffs, up to 200 meters of basaltic andesite is present. Because the Bloodgood Canyon Tuff has a limited aerial extent, there are many areas where lava older than the Bloodgood Canyon Tuff may be lumped with the younger andesitic lavas of sequence 2. Other units that can be assigned to this sequence include a thin conglomerate unit and a crystal-poor, welded ash-flow tuff that is present only in the extreme northeastern part of the map area in the footwall of San Francisco fault north of Sardine Creek. This crystal-poor tuff is tentatively correlated with the 29 Ma Davis Canyon Tuff (Ratté and Brooks, 1995) despite that fact that we were unable to extract datable sanidine phenocrysts from two fairly fresh samples. The onset of andesitic lava volcanism of sequence 1 probably did not commence until after about 30 Ma. This is based on the oldest dates for basaltic lava in the Morenci area of  $30.0 \pm 0.7$  Ma for a dike at Metcalf (K-Ar whole rock, Cook, 1994) and our groundmass concentrate <sup>40</sup>Ar/<sup>39</sup>Ar date of  $28.52 \pm 0.24$  Ma for the basaltic andesite lava at Tv Hill, part of an isolated cinder

cone that overlies Paleozoic rocks just to the west of the Morenci Pit. Map units from Sheet 1 that are assigned to sequence 1 are: Tc, Tcl, Tdc, Tbl, and Tbc. In some areas near Clifton, map unit Tb may also be correlative to this sequence.

**Table 5.** Age, composition, and volume of volcanic rocks in the time-stratigraphic Tertiary sequences of the Clifton-Morenci area. The volume of volcanic rocks is shown only for our study area which includes the 15' Clifton Quadrangle.

#	Sequence name	Age (Ma)	Composition
9	Unit of Smugglers Canyon	5?-2	Heterolithic conglomerate containing clasts of locally derived rocks, including copper-bearing and polished hematite clasts
8	Unit of Buzzard Roost Canyon	12?-5?	Heterolithic conglomerate containing basalt, rhyolite, porphyry, Paleozoic, and Proterozoic clasts
7	Conglomerate of Midnight Canyon	18-12?	Heterolithic conglomerate containing subequal amounts of basalt and rhyolite clasts. Sequence named for the dominant unit, conglomerate of Midnight Canyon, but the base of this lithostratigraphic unit is time-transgressive, becoming older to the north where it crosses into our sequence #5.
6	Younger silicic lavas	18-17	Two isolated rhyolite lava fields in the Peloncillo and Big Lue mountains produced thin pyroclastic deposits that define a sporadic time-line. One of these tuffs dated at 18.2 Ma in Gila Box marks the base of the Gila Group in this area. Silicic lavas of this age are not present in the Clifton-Morenci area.
5	Conglomerate of Bonita Creek	20-18	Represents the prelude to Gila Group sedimentation in the south and the onset of Gila Group sedimentation in the north. Named for its dominant lithofacies, which consists of Basaltic-clast rich conglomerate. In the north, this sequence includes the basal unit of the Gila Group, conglomerate of Midnight Canyon.
4	Middle silicic lavas	22.5-20	Three isolated early Miocene silicic lava fields overlie the younger andesitic lavas. In the Clifton-Morenci area, this sequence is represented by the 60 km <sup>3</sup> Enebro Mountain Formation. Correlative silicic lava fields also occur in the Peloncillo Mountains, and the Big Lue Mountains. The sequence also includes a basaltic-clast conglomerate in the northern part of our map area, along San Francisco River.
3	Older silicic lavas	26.5-24.5	Two separate late Oligocene silicic lava fields occur within the younger andesitic lava sequence of the Gila Mountains to the southwest and Big Lue Mountains to the east. No silicic lavas of this age are present in the Clifton-Morenci area.
2	Younger andesitic lavas	28-22.5	A very thick sequence of amalgamated basaltic andesite lava flows. The sequence is uninterrupted in the Clifton-Morenci area, but to the northeast and southwest, silicic lavas of sequence #3 are interleaved within this sequence. The younger 2 million years of this interval is probably represented by a hiatus throughout most of the region. Volume of lava in study area is ~ 360 km <sup>3</sup> .
1	Older andesitic lavas	34-28	All units older than and including the 28 Ma Bloodgood Canyon Tuff. Includes the 29 Ma Davis Canyon Tuff, the 34 Ma Clifton Tuff, a series of andesitic lavas, and minor sedimentary rocks. Volume of volcanic rocks in study area is 5-10 km <sup>3</sup> .

Sequence 2 (28 to 22.5 Ma): Younger andesitic lavas

This sequence represents the main pulse of basaltic volcanism in the Clifton-Morenci area. It produced a pile of mafic lava (map units Tb, Tbb, and Tbs of Sheet 1) up to 1 km thick that blanketed the entire area and accounted for at least 360 km<sup>3</sup> of erupted material in the study area. Regionally, the volume of the mafic flows erupted in this sequence is probably well over 1,000 km<sup>3</sup>. The thickest accumulation of lava was directly north of the Clifton-Morenci area, and the thinnest was probably directly above the mineralized zone of the Morenci district. Our groundmass concentrate <sup>40</sup>Ar/<sup>39</sup>Ar dates from the sequence range between 27.73 ± 0.17 Ma, and 22.33 ± 0.14 Ma, but we believe the true range of ages for this sequence is between ~28 and 24 Ma. In the Clifton-Morenci area, sequence 2 consists of monotonous, amalgamated lava flows of basaltic andesite to andesite composition (all mapped as Tb, Sheet 1) but to the east, west and south felsic lavas and tuffs intertongue and partition the mafic lavas into different map units. To the east, Ratté and Brooks (1995) divided lavas correlative to our sequence 2 into two units; the 27-28 Ma volcanic sequence in the Big Lue Mountains (including map units Ta, Tacc, Tac, and Tbl), and the 24-26 Ma Bearwallow Mountain andesite Brooks (1995) recognized a younger Miocene (17-20 Ma) basalt lava unit (including map units Tb, Tbs, and Tbcc) based on one K-Ar whole rock date of 17.7 ± 0.6 Ma about 7 Along the eastern edge of the study area, sequence 2 includes at least one prominent flow break defined by interbedded volcanoclastic rocks (unit Tbs of our map), but it is not certain how this break correlates with the division(s) mapped by Ratté and Brooks (1995) to the east. It is also not clear how well the age assignment of Ratté and Brooks' (1995) younger basalt unit can be applied to the sequence we mapped just to the east of San Francisco River. For example, Ratté and Brooks' (1995) 17-20 Ma Miocene basalt unit can be traced into this study area without obvious disruption by faults or changes in stratigraphy down to the upper San Francisco River where it is intruded by a 22.26 ± 0.38 Ma (sanidine <sup>40</sup>Ar/<sup>39</sup>Ar) rhyolite lava dome. A younger unit is clearly present upstream, based on Ratté and Brooks' (1995) geochronology and the fact that in this area basalt is interbedded with Gila Group conglomerates along the Dix Creek fault. However, based on discussions with Jim Ratté (personal communication, 2000) we believe that much of the younger basalt mapped by Ratté and Brooks (1995) in the northwest corner of their map area is actually late Oligocene to earliest Miocene in age.

Farther south, in the Big Lue Mountains, we traced the contact between Ratté and Brooks' (1995) two older mafic units into the eastern part of our map area just north of Limestone Gulch. We interpret this contact to correlate with a prominent flow break (mapped as an intraformational contact on Sheet 1) in Ash Spring Canyon that overlaps a major east-side-down fault. Lavas from above and below this contact were dated (groundmass concentrate <sup>40</sup>Ar/<sup>39</sup>Ar) for this study and gave essentially the same age; 27.62 ± 0.20 Ma and 27.73 ± 0.17 Ma respectively.

To the south of the map area in the northern Peloncillo Mountains, Richter et al. (1983) subdivide mafic lavas correlative to sequence 2 into two main sequences of younger and older andesite flows, assigned to the andesite of Guthrie Peak-Turtle Mountain and andesite of Gila River (AGT). The younger sequence is referred to as upper andesite flows (including map units Tau, Tad, Tac, and Tpf of Richter et al., 1983) throughout their map area, but the younger sequence overlies two different mafic lava

units in different areas. In the northwest it overlies the andesite of Gila River (Ta), and to the south it overlies lower andesite flows of the AGT (map unit Tal). In both areas, thin pyroclastic flows (Richter et al., 1983 map units Ttg and Tab) mark the contact between the older and upper andesites.

Richter et al. (1983) published two K-Ar whole rock dates from their upper andesite unit;  $23.7 \pm 0.5$  Ma from a flow at the top of the sequence along lower Gila River, and  $19.4 \pm 0.4$  Ma for a lava near the top of the sequence along the southern margin of the outcrop area. Richter et al. (1983) also published three K-Ar whole rock dates from their lower andesite sequence;  $22.6 \pm 0.5$ ,  $22.2 \pm 0.5$ , and  $21.8 \pm 0.5$  Ma. These younger dates are puzzling, because these lavas clearly underlie andesitic lava that we dated at  $24.74 \pm 0.24$  Ma (groundmass concentrate  $^{40}\text{Ar}/^{39}\text{Ar}$ ), and Richter et al. (1983) dated at  $23.7 \pm 0.5$  Ma (K-Ar whole rock). The andesites which yielded the young dates clearly underlie sanidine-bearing rhyolitic lavas that have been dated at  $23.1 \pm 0.5$  Ma (Richter et al., 1983 K-Ar biotite and sanidine) and at  $22.41 \pm 0.06$  Ma (sanidine  $^{40}\text{Ar}/^{39}\text{Ar}$ , this study). We interpret Richter et al.'s (1983) ages of the lower andesite to have been reset during emplacement of the  $\sim 22$  Ma rhyolite lavas in the area.

In the Gila Mountains directly northeast of Safford our sequence 2 is correlated with the AGT of Houser et al., (1985). This succession includes upper and lower andesite lava units (Tau, Taut, Taup, Tad, and Tal map units) which occur above and below a felsic lava (Houser et al., 1985). The interbedded felsic volcanic rocks of the Gila Mountains range in age from 26.5 to 24.5 Ma (Houser et al., 1985) and can be traced eastward onto the western slopes of Turtle Mountain, just to the northwest of Gila Box. Nonwelded tuff, dated at  $24.52 \pm 0.06$  Ma (sanidine  $^{40}\text{Ar}/^{39}\text{Ar}$ , this study) from the top of sequence 2 in lower Eagle Creek near the Gila Box, and an older layer of undated nonwelded tuff mapped as Ttg by Richter et al. (1983) in Gila Box, are interpreted as pyroclastic units derived from the Gila Mountains silicic lava field.

### Sequence 3 (26.5 to 24.5 Ma): Older silicic lavas

Sequence 3 is enclosed within sequence 2. Its eruptive products are recognized in the extreme western part of the Clifton-Morenci area, the Gila Mountains, and the Big Lue Mountains. If present in the Peloncillo Mountains, rocks of this age are buried by older flows of the AGT. In the Gila Mountains, sequence 3 consists of a suite of felsic lavas and associated nonwelded tuff that has yielded three K-Ar dates of  $26.5 \pm 0.6$  Ma (plagioclase),  $25.9 \pm 0.6$  Ma (oxyhornblende), and  $24.5 \pm 0.6$  Ma (biotite, Houser et al., 1985). The felsic volcanic rocks occur between the upper and lower divisions of the AGT (Houser et al., 1985) and are subdivided into a number of map units: Trp, Tr, Tbdp, Tbhd, Tbdb, Tbud, Tbuf, Tblf, Tbp, Tbl, Tba, Tbrd, Tbbc, Tbcd, and Tbc. Richter et al. (1983) mapped one flow of this lava field northwest of the Gila Box as Tdf. In the Gila Box area, a thin nonwelded tuff (Ttg) is present in between the upper andesite flows (Tau) and andesite of Gila River (Ta) of Richter et al. (1983). This Ttg unit and another unmapped nonwelded tuff higher in the section near the mouth of Eagle Creek, are interpreted to be derived from the silicic lava field in the Gila Mountains. The upper, unmapped nonwelded tuff was dated at  $24.52 \pm 0.06$  Ma (sanidine  $^{40}\text{Ar}/^{39}\text{Ar}$ , this study), but the lower one (the Ttg unit of Richter et al., 1983) has not been dated.

In the Big Lue Mountains, sequence 3 consists of two separate silicic lava fields mapped by Ratté and Brooks (1995); the complex of Bird Canyon (map unit Tbd), and the rhyolite of Hells Hole (map units Thr, and Thp).

Sequence 4 (22.5 to 20 Ma): Middle silicic lavas

In the Clifton-Morenci area, sequence 4 is represented by the Enebro Mountain Formation, an east-southeast-striking swarm of rhyolite lava domes that extends eastward from upper Eagle Creek through Enebro Mountain across the Chesser Gulch area to San Francisco River. Schroeder (1996) dated a lava dome at 21.7 Ma (biotite  $^{40}\text{Ar}/^{39}\text{Ar}$ ) and a crosscutting dike at 21.7 Ma (biotite K-Ar) and 20 Ma (sanidine K-Ar). One of the lava domes along San Francisco River was dated at  $22.25 \pm 0.38$  Ma (sanidine  $^{40}\text{Ar}/^{39}\text{Ar}$ ) as part of this study. In addition, Marvin et al. (1987) reported K-Ar whole rock dates of  $20.6 \pm 0.7$  Ma and  $20.9 \pm 0.8$  Ma from these rocks. The Enebro Mountain Formation lava field produced voluminous nonwelded tuffs that blanketed much of the area just north of the Morenci–Clifton area. The Enebro Mountain Formation is divided into four map units on Sheet 1: Te, Ter, Tet, and Ter.

The Enebro Mountain Formation of the Clifton-Morenci area is correlated with an extensive field of felsic lavas in the northern Peloncillo Mountains including map units Tabr, Tab, Tar, Tapd, Tapi, Tap, Tard, Tda, Ttrb, and Ttrd of Richter et al. (1983). Richter et al. (1983) reported dates for two lavas from this succession in the northern Peloncillo Mountains at  $23.1 \pm 0.5$  (K-Ar biotite and sanidine) and  $21.2 \pm 0.4$  Ma (K-Ar whole rock). The oldest of these lavas (Richter et al.'s (1983) unit Tabr) was re-sampled in this study and gave a sanidine  $^{40}\text{Ar}/^{39}\text{Ar}$  age of  $22.41 \pm 0.06$  Ma. The felsic lava sequence in the Peloncillo Mountains also includes a thin sequence of basaltic andesite lava flows that overlie the  $22.34 \pm 0.08$  Ma nonwelded tuff (our sanidine  $^{40}\text{Ar}/^{39}\text{Ar}$  date of Richter et al.'s (1983) Ttt map unit) in the Guthrie Peak area.

In the eastern Big Lue Mountains, Ratté and Brooks (1995) reported K-Ar plagioclase and K-Ar hornblende ages of  $21.3 \pm 1.8$  Ma and  $21.8 \pm 1.4$  Ma, respectively from the dacite of Tennessee Creek. This small silicic lava field is correlative to the Enebro Mountain Formation and is considered part of sequence 4.

Also included in our sequence 4 is a basaltic clast conglomerate (our map unit Tcb, Sheet 1) which underlies nonwelded tuff of the Enebro Mountain Formation in the northeast corner of the study area. The basalt clast conglomerate (Tcb) represents a similar lithofacies to the conglomerate of Bonita Creek (Tbck), which is a considerably younger unit found to the southwest. The appearance of this lithofacies first in this area, compared to the rest of the region, indicates that the prelude to basin-fill style sedimentation of the Gila Group was earliest in this area, and supports structural data which indicate that the San Francisco half-graben basin is relatively old.

Sequence 5 (20 to 18 Ma): “Conglomerate of Bonita Creek”

Sequence 5 represents an interval of waning volcanism, the prelude to Gila Group basin-fill sedimentation in the south and the onset of Gila Group style basin-fill sedimentation in the north. Since the sequence consists of lithostratigraphic units with time-transgressive contacts, it includes many different lithologic units, in order of abundance; conglomerate, rhyolite lava, nonwelded rhyolite tuff, and basalt lava. The

sequence is named for its most abundant lithofacies, represented by the basaltic-clast rich conglomerate of Bonita Creek (map unit Tbck of Sheet 1). The top of sequence 5 is a hypothetical time-line connecting the base of two small, 17-18 Ma silicic lava fields; the rhyolite of Mule Creek in the Big Lue Mountains, and the Tollgate Wash silicic lava field in the northern Peloncillo Mountains. In the Gila Box area, the time-line is a real feature, marked by an  $18.20 \pm 0.05$  Ma (sanidine  $^{40}\text{Ar}/^{39}\text{Ar}$ ) nonwelded tuff (map unit Ttt of Sheet 1), but elsewhere it is imaginary.

The lithostratigraphic unit, conglomerate of Bonita Creek's upper and lower contacts are time-transgressive, being younger to the south and older to the north. For example, at the southern edge of the Guthrie quadrangle in the northern Peloncillo Mountains, the top of the conglomerate of Bonita Creek is marked by a thin basalt flow that correlates with a thick sequence of 16.6 and 16.2 Ma basalt lava flows farther south (K-Ar plagioclase and groundmass concentrate dates of Richter et al., 1981). This part of the conglomerate of Bonita Creek is assigned to our sequence 7. In the northeast part of the study area, the conglomerate of Bonita Creek lithofacies is represented by an older unit; a basalt-clast conglomerate (our map unit Tbc) which underlies the 22.5-21.0 Ma Enebro Mountain Formation. In the northeast, sequence 5 is represented by the basal unit of the Gila Group, the conglomerate of Midnight Canyon (Tgmc of Sheet 1).

#### Sequence 6 (18 to 17 Ma): Younger silicic lavas

The sequence consists of two widely separated silicic lava fields; the rhyolite of Mule Creek in the Big Lue Mountains, and the Tollgate Wash silicic lava field in the northern Peloncillo Mountains. We connect these two lava fields with a hypothetical time-line which coincides with a thin layer of nonwelded tuff (map unit Ttt of Sheet 1) in the Gila Box area dated at  $18.20 \pm 0.05$  Ma (sanidine  $^{40}\text{Ar}/^{39}\text{Ar}$ ). This tuff marks the division between the conglomerates of Bonita Creek and Midnight Canyon and the base of the Gila Group in the Gila Box area.

The Tollgate Wash silicic lavas of the northern Peloncillo Mountains, mapped as Ttd, Ttv, Ttb, Trp, Trb, and Trd by Richter et al. (1983) are part of this sequence. There are no volcanic rocks of this age in the Clifton-Morenci area, but in the Big Lue Mountains, sequence 6 is represented by the ~17-18 Ma rhyolite of Mule Creek (map units Tmf, Tmp, Tmo, and Tmb of Ratté and Brooks, 1995).

#### Sequence 7 (18 to ~12 Ma): "Conglomerate of Midnight Canyon"

This time interval represents the cessation of volcanism throughout the region and the onset of Gila Group sedimentation in the south. This sequence is named for its dominant lithofacies, the conglomerate of Midnight Canyon (map unit Tgmc of Sheet 1), a succession of heterolithic conglomerate that contains sub-equal amounts of basalt and rhyolite clasts. This unit (map symbol Tgmc of Richter et al., 1983, Houser et al, 1985, and this report), which is considered to be the base of the Gila Group in this area, is present in the San Francisco, Eagle Creek, and Duncan basins around the Clifton-Morenci area, and in Pigeon Creek to the north of the map area. The unit was mapped as rhyolite by Lindgren (1905a,b), as rhyolite conglomerate by Heindl (1960), and as QTg by Richter and Lawrence (1981).

At the southern edge of the region sequence 7 includes the upper part of Richter et al.'s (1983) conglomerate of Bonita Creek, and to the north, its base is well up within the conglomerate of Midnight Canyon. The basal contact is marked by thin tuff lenses (Ttt of this study) dated at  $18.20 \pm 0.05$  Ma (sanidine  $^{40}\text{Ar}/^{39}\text{Ar}$ ) in the Gila Box, or by indistinct downward gradation into the basaltic conglomerate of the conglomerate of Bonita Creek (Tbck). The upper contact is conformable with the overlying unit of Buzzard Roost Canyon (Tgbr), but it is not known how close this contact represents a time-line. Richter et al. (1983) assign a Miocene age for the conglomerate of Bonita Creek, and indicate that the conglomerate of Midnight Canyon is late Miocene to Pliocene in age. However, using the  $18.20 \pm 0.05$  Ma (sanidine  $^{40}\text{Ar}/^{39}\text{Ar}$ ) rhyolite tuff (Ttt of our study) of sequence 6 as a marker, deposition of sequence 7 rocks began in the early Miocene (around 18 Ma) and extended to an unknown time in the mid-Miocene (~12 Ma), rather than Pliocene. Our reassignment of the age range of these rocks is based on 13.4 and 11.0 Ma  $^{40}\text{Ar}/^{39}\text{Ar}$  age dates (Enders, 2000) from alunite in the Morenci deposit which suggest that the volcanic rocks and some of the underlying Cretaceous, Paleozoic, and Proterozoic rocks had been stripped from the top of portions of the Morenci block by the end of the mid-Miocene. This detritus was deposited in the unit of Buzzard Roost Canyon of sequence 8, described below.

Sequence 8 (~12 to ~5 Ma): “Unit of Buzzard Roost Canyon”

The unit of Buzzard Roost Canyon (map units QTgg and QTgd of Sheet 1) is a succession of heterolithic conglomerate that contains clasts of basalt, rhyolite, Laramide-age porphyry, Paleozoic sedimentary rocks, and Proterozoic granite. These rocks correlate with the Tgre and Tgor units of Richter et al. (1983) and Houser et al. (1985) in the Guthrie and Safford quadrangles to the south and southwest of the study area, the Quaternary gravels of Lindgren (1905a,b), map units Qgcc and Qgsf of Pawlowski (1980), and map unit QTg of Richter and Lawrence (1981). The unit of Buzzard Roost Canyon has a gradational lower contact that is marked by the first appearance of Paleozoic limestone or quartzite and typically contains 1-5% red granitic clasts. The abundance of non-volcanic clasts increases upwards to 15-30% at the top of the unit. In places the unit contains rare clasts of skarn and oxidized copper-sulfides in veined and altered porphyry and Proterozoic host clasts. Richter et al. (1983) and Houser et al. (1985) assign a Pliocene age to this sequence. However, the 13.4 and 11.0 Ma alunite  $^{40}\text{Ar}/^{39}\text{Ar}$  age dates of Enders (2000) suggest that rocks of sequence 8 were probably deposited beginning at the end of the mid-Miocene (~12 Ma) and continued into the early Pliocene.

Sequence 9 (~5 to ~2 Ma) “Unit of Smugglers Canyon”

Conglomerates of the unit of Smugglers Canyon (map unit QTgs of Sheet 1) contain clasts of local provenance. This unit was included with the Quaternary gravels of Lindgren (1905a,b), as Qgsb by Pawlowski (1980), and with unit QTg of Richter and Lawrence (1981). The conglomerates of sequence 9 contain highly variable amounts of locally derived red Proterozoic granite, Paleozoic sedimentary rocks, Laramide porphyritic plutonic rocks, and Tertiary volcanic rocks. Clasts are weakly to strongly imbricated in places and may be rounded to sub-angular in shape, depending on proximity to source area. The unit contains <1 to 15% black polished hematite and magnetite clasts,

and copper-oxide mineralized, veined, altered and leached clasts of skarn, porphyry, quartzite, and granite. The formation of significant copper enrichment was completed by about 7 Ma and thick leached capping was exposed around 5 Ma, based on  $^{40}\text{Ar}/^{39}\text{Ar}$  age dates from alunite and jarosite in the Morenci (Enders, 2000). Base level drop and incision of the Gila River and its tributaries began in the early Pleistocene.

## STRUCTURAL GEOLOGY

The structural patterns in the Clifton-Morenci area are complex, but can be summarized as being the interaction of an older northeast-striking and a younger northwest-striking structural grain. The northeast-striking structures are expressed as a tectonic-metamorphic fabric in Early Proterozoic rocks, a preferred orientation of the Eocene igneous dikes and elongate stocks related to the porphyry copper mineralization, and a set of high-angle Paleogene faults. The northwest-striking structures are dominated by Neogene normal faults related to the formation of the nearby Pinaleño Mountains detachment fault system and opening of the Safford basin.

### Early Proterozoic

Proterozoic rocks exposed in the Clifton-Morenci area are dominated by Middle or Early Proterozoic granitoids. The granitic rocks show little or no evidence of ductile deformation, but they intrude a close to tightly folded sequence of quartzite and metapelitic rocks of probably Early Proterozoic age. The metamorphic rocks are found only in the footwall of Chase Creek fault in the northern part of the map area. Warren (1999) and Chillingworth (1999) defined an east- to northeast-striking, southeast vergent fold-belt with an associated steeply northwest-dipping axial planar schistosity by mapping out resistant beds of quartzite in these rocks. There is no evidence that this folding affected the younger Middle or Early Proterozoic granitic rocks in this area.

### Laramide

Very little evidence of Paleozoic or Mesozoic deformation is present in the map area. Throughout most of the map area, the Paleozoic sequence is not duplicated or folded in any way that might indicate compressional deformation, and there are no major angular unconformities between units to suggest tectonic disturbances during the Paleozoic. Along the extreme southwest edge of the Morenci block in upper Horseshoe Gulch near the west end of Coronado fault, there is evidence of northeast-directed compression in the form of a minor set of low-angle east-directed thrust faults duplicating section in the upper Coronado quartzite. In addition, nearby patterns of apparent duplication of the Devonian Morenci and Modoc formations in the immediate footwall of Eagle Creek fault are tentatively interpreted as evidence for northeast-directed thrusting (Sheet 1). The orientation of compressional structures in this area suggests a Laramide ancestry.

Between 100 and 150 meters of Cretaceous sedimentary rocks of the Pinkard Formation are preserved only in the extreme southwestern part of the Morenci block. The presence of these rocks only in the southwest suggests that a phase of Paleogene southwesterly tilting affected this part of the map area. The Cretaceous rocks in this area are also broadly folded about upright, northeast-striking open folds (section D-D', Sheet

2). Just to the southwest, thickness calculations from drill holes in the hanging wall of Eagle Creek fault, indicate over 300 meters of Upper Cretaceous rocks in the Eagle Creek graben.

In the main part of the Morenci block, evidence of Laramide faulting is limited to a few of the high-angle normal, oblique slip faults that show evidence of intrusion by some of the Eocene porphyritic rocks (Walker, 1995).

## **Mid-Tertiary**

### ***The Morenci lineament, and the Transition Zone in the Clifton-Morenci area***

The principal expression of the Morenci lineament in the Clifton-Morenci area is the southeast-side-down San Francisco and Chase Creek faults, two of the most recently active and most dramatic faults in the area (Figure 2). The San Francisco fault, and all apparent expression of the Morenci lineament ends abruptly at the south end of the Morenci block, a structurally high-standing massif in the footwall of the San Francisco and Eagle Creek faults which includes all of the exposed mineralized rocks of the copper porphyry system. About 5 km to the east, the Chase Creek fault mimics the orientation of San Francisco fault, but near its south end it curves to the south and loses displacement in the swarm of Eocene intrusive bodies in the middle of the Morenci district.

The northwest-striking, southwest-side-down Eagle Creek fault bounds the southwest side of the Morenci block and represents the northeast side of a narrow half-graben that broadens to the southeast into the much larger and wider Duncan basin (Figures 2, 7). At the southern tip of the Morenci block, younger conglomeratic deposits of the Gila Group conceal the intersection of Eagle Creek and San Francisco faults. Drill hole data just to the south (Dames and More, 1997) indicate that San Francisco fault is either abruptly truncated or that it turns sharply to the west and merges with Eagle Creek fault. There is no evidence along the southern boundary of the Eagle Creek half graben or Duncan basin for a continuation of San Francisco fault. There is however, a good candidate for the southeasterly continuation of Eagle Creek fault along the northeast flank of the Duncan basin southeast of Clifton in the form of the Ward Canyon fault. Younger deposits of the Gila Group also bury the intersection of the Ward Canyon and San Francisco faults. Based on drill hole data (Dames and More, 1997), we show the buried connection between the Eagle Creek and Ward Canyon faults offset slightly in a sinistral sense across the southern tip of San Francisco fault (Sheet 1), and suggest that the major south-side-down fault that bounds the southern tip of the Morenci block is an Eagle Creek – Ward Canyon connection (Sheet 3, section F-F'). The surface trace of the Ward Canyon fault does not emerge until it crosses San Francisco River at the Clifton town site. Just to the southeast of the map area, some strands of the Ward Canyon fault are the only structures in the area with documented Holocene offset (Pearthree, 1998).

The orthogonal interaction of northeast- and northwest-striking normal faults in the Clifton-Morenci area probably reflects the abrupt, dramatic change in orientation of the Colorado Plateau – Transition Zone boundary to the north (Figure 1).

### ***Duncan basin***

The Duncan basin borders the Morenci block to the southwest, south, and southeast. The basin strikes north-northwest, is about 60 km long, and the valley ranges

from 8 km to over 14-km wide covering a 700-km<sup>2</sup> area (Figures 2, 7). It is bordered on the northeast by the Big Lue Mountains, on the east by the Summit (Steeple Rock) Mountains, on the south by Lordsburg Mesa, and on the west and northwest by the Peloncillo Mountains and Black Hills. The Gila River enters the basin from the southeast and drains the valley to the northwest. The Duncan basin terminates to the northwest about one mile upstream from the confluence of the Gila and San Francisco Rivers where the volcanic rocks of the Peloncillo Mountains are continuously exposed across the valley. The Eagle Creek basin is a half-graben that extends for over 16 km to the northwest of the confluence and separates the Morenci block from the Turtle Mountains of the northern Peloncillo range on the west. The San Francisco basin is a half-graben that extends for over 20-km northeast of Clifton and separates the Morenci block from the Big Lue range on the east. The Duncan basin north of York, Arizona, the Eagle Creek and San Francisco basins, and Bonita Creek and the Gila Box have been deeply incised by their current drainages. They contain inner gorges that range from 200 m in depth in the upper reaches of the canyons to over 315 meters in the lower stretches (Sheet 1).

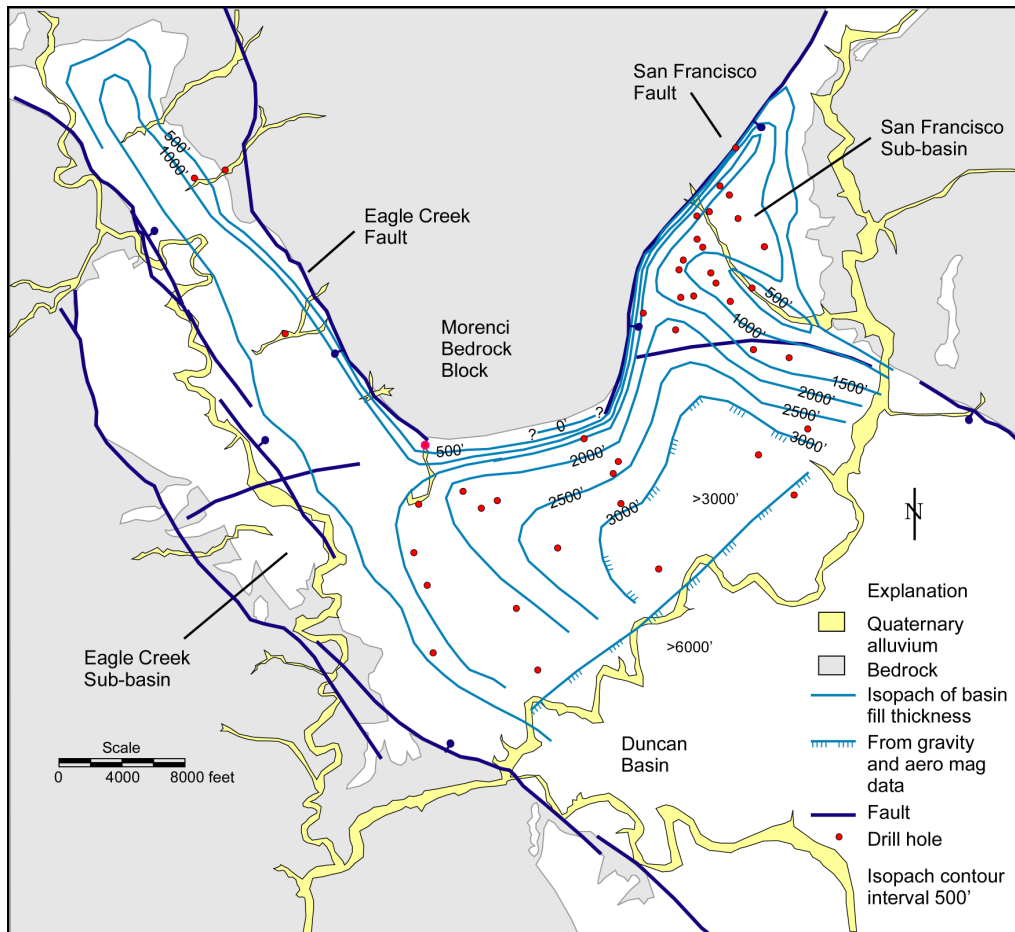


**Figure 7.** Thickness of basin-fill in the Duncan basin and the San Francisco and Eagle Creek sub-basins.

The Duncan basin is filled with volcanoclastic and sedimentary rocks derived from bedrock of the surrounding mountains since the early Miocene. The Peloncillo, Big Lue, Summit, and Steeple Rock Mountains that surround the basin are composed chiefly of mid-Tertiary volcanic rocks and include units of Sequences 1, 2, 3, 4, and 6. Pre-Basin and Range sediments of probable lower Miocene age (Drewes et al., 1985) are poorly exposed along the margins of the basin. These rocks include the volcanic conglomerate and “tilted tuffaceous beds” of Heindl (1962) and the pre-Gila Group Miocene conglomerate of Bonita Creek of Richter et al. (1983) of Sequence 5. The sedimentary rocks of the lower basin fill are predominantly conglomerates with lesser amounts of sandstone and mudstone near the range-fronts. The conglomerate facies occur dominantly in the Eagle Creek and San Francisco sub-basins and in a one to three km wide zone along the northeast margin of the basin (Halpenney, et al, 1946; Morrison, 1965). Towards the center of the basin the lower basin fill grades into finer grained beds that further grade into lacustrine and playa deposits in the vicinity of Duncan. The thickness of the lower basin fill ranges up to 625 m thick in the Clifton-Morenci area to almost 2 km thick in the center of the basin (Enders, 2000). Lower basin fill includes the conglomerate of Midnight Canyon (Tgmc) of Sequence 7, the unit of Buzzard Roost Canyon (Tgbr) of sequence 8, and the unit of Smuggler Canyon (QTgs) of Sequence 9. The upper basin fill consists of tuffaceous sediments probably deposited in a lacustrine environment and rest disconformably upon coarse-grained red beds near the center of the basin, in the vicinity of Duncan (Harbour, 1966). The Older Alluvial Deposits (QTao) in the surrounding Eagle Creek and San Francisco sub-basins may represent the remnants of upper basin fill the Clifton-Morenci area. A series of seven graded Pleistocene and younger surfaces that slope toward the interior of the valley have cut into the upper and lower basin fill (Morrison, 1965). Stream alluvium (Qa, Qao) consisting of unconsolidated gravel, sand, and silt of channel, point bar and floodplain deposits fills the inner valleys to depths ranging from 1 to 50 m.

Although the structure of the Duncan basin is complex, it is distinctly bounded on the west by a set of 040° striking, step-like normal faults. These basin-bounding structures dip steeply towards the basin at 75° to 85° and are exposed continuously for about 24 km along the northeastern margin of the basin. The Ward Canyon fault southeast of Clifton bounds the northeastern margin of the basin for about 8 km. These structures link up with the Eagle Creek fault system to the northwest and are cut by the northeast-striking faults of the San Francisco system to the northeast. From Guthrie to Duncan the Gila River hugs the western margin of the basin along the Peloncillo range-front. South of Apache Creek, the basin-forming structures are either poorly exposed or buried by basin fill and their presence have been inferred from geophysical data.

Aeromagnetic, gravity, and drill hole data show the basin to be separated into segments with very different depths (Enders, 2000). Gravity data indicates that basin depth decreases from >1,800 m at its northwest end near Clifton to 760 m near Duncan. In the vicinity of Franklin, Arizona, an inferred, north-south-striking, normal fault coupled with northeast and northwest-striking segments are coincident with a change in the alignment of the Gila River and increase the basin depth to 1,800 m. Further to the south, another normal fault, striking east-northeast is coincident with a decrease in basin

depth to about 600 m. Magnetic lineaments suggest that several step faults and cross faults also occur in addition to the major normal faults (Enders, 2000).

### ***Eagle Creek fault and half-graben basin***

The Eagle Creek half-graben is a narrow (1-4 km wide) basin bounded to the northeast by the southwest-side-down Eagle Creek fault and to the southwest by a gently northeast dipping depositional contact between Miocene basaltic andesite lava and volcanoclastic sedimentary rocks of the unit of Bonita Creek (>18 Ma) and the Gila Group (<18 Ma). The southwestern boundary is also defined locally by minor, high-angle, northeast-side-down faults, but the main fault offset is clearly along the northeast side of the basin.

Drill hole thickness data (Dames and More, 1997) indicate that 800-1,100 meters of Tertiary sedimentary rocks are preserved in the center of the Eagle Creek basin near its convergence with the Duncan basin. The greatest thickness of basin-fill is not found along the northeastern margin of the northeast-tilted half-graben because an older phase of southerly to southwesterly tilting influenced the pre-northeasterly tilting geometry of the basin floor. Evidence of this older tilting is preserved in an embayment near the north end of the basin formed by a sharp westerly turn of Eagle Creek fault. The oldest rocks in the hanging wall of Eagle Creek fault in this embayment are basaltic andesite lava overlain by moderately to steeply south-dipping volcanoclastic sedimentary rocks. This southerly tilting is interpreted to have resulted from an older phase of north- or northeast-side-down normal faulting and at least one fault of this orientation is preserved within the basaltic andesite lava in the hanging wall of Eagle Creek fault (Sheet 1). This older phase of southerly tilting may also have affected the pre-Tertiary rocks in the footwall of Eagle Creek fault and explain why the Cretaceous strata, preserved only at the southern tip of the Morenci block, are gently tilted to the south.

### ***San Francisco fault and half graben***

Even though San Francisco fault is one of the youngest structures in the Clifton-Morenci area, a prolonged history of Paleogene through Neogene northeast-striking normal faulting is evident in its west-tilted hanging wall and half-graben basin north and east of Clifton. Directly east of Clifton, Cunningham (1981) shows numerous east-side-down normal faults cutting Paleozoic units that apparently do not cut the overlying basal Tertiary sequence of Clifton Tuff and basaltic andesite lava. To the north of Clifton, there is evidence of faulting during the Oligocene in at least two areas. Near its southern termination, a splay of the major northeast-striking fault that extends from lower Limestone Gulch to Ash Spring Canyon offsets 34 Ma Clifton Tuff, but the same fault is apparently overlapped by the 29 Ma Bloodgood Canyon Tuff. Farther northeast, the main strand of this fault zone cuts the lower part of the basaltic andesite map unit (Tb), but it is clearly buried by the upper part of the same sequence. Both parts of the basaltic andesite sequence have been dated at approximately 27 Ma. Fault intersections are complex in the area near the mouth of Limestone Gulch, but it appears that the main, southeast-side-down strand of the fault system discussed previously is overlapped by the basal sedimentary rocks of the Gila Group just to the west of San Francisco River.

Just northwest of Clifton, drill hole data (Dames and More, 1997) shows that the San Francisco fault must have a steep (greater than 75°) easterly dip (Preece and Menzer, 1982; Walker, 1995). However, at several localities farther north, major strands of the fault are exposed that have moderate (less than 60°) easterly dips. In particular, relationships preserved where the San Francisco fault crosses Sardine Creek in the northeast part of the map area suggest that a younger, steeply dipping strand truncates an older, moderately east-dipping strand of the San Francisco fault. This relationship is depicted somewhat hypothetically on all of the east-west structural cross-sections (Sheet 2). We speculate that the older, moderately dipping strands are evidence of Oligocene and possibly older offset along the San Francisco fault, and that the younger steeply-dipping strand propagated as a Neogene structure.

Evidence of a prolonged history of motion along the San Francisco fault is also preserved in the sedimentary record. The base of the Gila Group is significantly older (by at least 2 million years) along the upper part of San Francisco River than in areas to the south.

### ***Faults in the Morenci block***

The Morenci block includes a number of east-side-down and south-side-down normal faults that mimic the orientations and kinematics of the major faults that bound the block to the southwest and southeast; the Eagle Creek and San Francisco faults respectively. Detailed studies of some of the fault zones indicate a prolonged Early through Mid- and Late Tertiary history of motion (Walker, 1995). Using cross-cutting relationships of Eocene intrusive rocks and evidence of mineralization of the fault gouge Walker (1995) recognized phases of Paleogene and Neogene motion along the Coronado, Producer, Kingbolt, and Quartzite faults. Walker (1995) also noted that a significant amount of the Paleogene motion along Coronado fault was sinistral oblique. Motion along the other main faults; Eagle Creek, Apache, Copper Mountain, Garfield, Chase Creek, and Las Terrazas were judged (Walker, 1995) to be mostly post-Laramide in age. The Copper Mountain fault is judged to be fairly young (10-7 Ma) based on the presence of a well-developed supergene blanket prior to movement. Final movement along the Garfield, Chase Creek, and Las Terrazas faults may be of similar age based on offsets of supergene mineral zones (Enders, 2000) and the presence of delicate oxide minerals in the gouge (Walker, 1995). Motion along the Garfield and Chase Creek faults is primarily Neogene since stratigraphic offset of Paleozoic and early Miocene supracrustal units across both faults are similar. Although strike-slip indicators have been documented along some of the faults in the Morenci block (e.g. Walker, 1995), there is little evidence of major strike-slip motions. Nearly all of the apparent dextral or sinistral map-view offsets of fault traces truncated by younger faults in the Morenci block can be accounted for by normal dip-slip motion.

Faults of the Morenci block are well exposed around the periphery of the main mineralized district, and stratigraphic offsets are well documented in the Phanerozoic supracrustal sequence that occurs in the area. However, most faults either lose displacement or are lost in the complex maze of intrusive rocks in the center of the district. The Quartzite, Coronado, and Producer faults are major south- or southeast-side-down structures that die out or transfer displacement towards the center of the district.

Emanating from the north-central part of the district, the east-side-down Chase Creek fault mimics the San Francisco fault in orientation and displacement. Maximum stratigraphic offset across Chase Creek fault is between 600 and 900 meters. The Chase Creek fault strikes due north directly north of the district and makes a dogleg jog to the NNE where it leaves Chase Creek and splays into a southwest-side-down fault that dies out to the northwest near the head of Chase Creek. The main strand continues NNE to another northeasterly dogleg turn at Pigeon Creek just to the north of the study area, at about the same latitude as a similar NE-turn in the San Francisco fault. The Chase Creek fault cuts units as young as the Gila Group where it leaves the study area to the north. At its southern end, it appears to have acted as a transfer zone for displacement along the south-side-down, Coronado, Producer, and Quartzite faults.

The southern termination of the Chase Creek fault is poorly understood, but most of its east-side-down displacement appears to be balanced by south-side-down motion along Coronado fault. If so, this would require that much of the displacement along Coronado fault postdates emplacement of the Miocene volcanic flows of the Enebro Mountain Formation. Even though Walker (1995) documents that a main strand of the Coronado fault is intruded by an Eocene diabase dike (Sheet 1), we conclude that another important strand must carry the approximately 600 meters of south-side-down stratigraphic displacement of the Cambrian Coronado Quartzite and the Oligocene basaltic andesite lavas of sequence 2 that are present on either side of the fault. Much of the Paleogene motion along Coronado fault was probably sinistral oblique based on the low ( $12^{\circ}$ - $28^{\circ}$ ) plunges of slickenlines (Walker, 1995). South of the Coronado fault, the definition of Chase Creek fault fades into the mineralized Proterozoic and Eocene plutonic rocks in the central part of the district, but it may emerge farther south in the form of two modest (total offset of about 220 meters) east-side-down normal faults, the Apache and Copper Mountain faults.

The Garfield fault is the northernmost east-west striking fault in the Morenci block, and the only major north-side-down fault in the district. Its greatest displacement (500 m) is in the immediate hanging wall of the Chase Creek fault. The Garfield fault dies out to the east near Copper King Mountain, but continues west of the Chase Creek fault into a poorly understood termination in the upper Eagle Creek drainage basin. The Garfield fault marks the southern boundary of a swarm of early Miocene rhyolite lava domes and west-northwest-striking dikes (Enebro Mountain Formation) that extend along strike, well beyond the eastern and western ends of the fault. North-side-down motion along Garfield fault may have been in response to evacuation of the approximately  $60 \text{ km}^3$  of magma that was erupted as the rhyolite lava and tuff of the Enebro Mountain Formation. In general, the thickest accumulation of lava coincides with zones of maximum fault displacement. Although it is clear that Chase Creek fault is not offset by Garfield fault, the exact location of the truncated ends of Garfield fault along Chase Creek fault is poorly defined, since the footwall is composed of homogeneous Proterozoic granite, and the immediate hanging wall is buried by alluvium. The Garfield fault is shown offset slightly in an apparent dextral sense on Sheet 1, a pattern that is consistent with approximately 600 meters of purely dip-slip, east-side-down offset across Chase Creek fault.

## CONCLUSIONS

### Stratigraphy and geochronology

The oldest Mid-Tertiary volcanic rocks in the Clifton-Morenci area are the thin, western distal edges of three regional ash-flow tuffs from the Mogollon-Datil volcanic field; the ~34 Ma Clifton Tuff, the 29 Ma Davis Canyon Tuff, and the 28 Ma Bloodgood Canyon Tuff. All three tuffs pinch out just west of San Francisco River. The Clifton and Bloodgood Canyon tuffs are present only around Clifton, and the Davis Canyon Tuff is found only to the north of Sardine Creek. Pre 28 Ma basaltic andesite lavas are documented only along San Francisco River, but thin equivalents of this older interval may be present farther west, and might be represented by the small remnant vent complex at Tv hill. Elsewhere in the region, the base of the mafic lava sequence is consistently ~27-28 Ma.

A small exposure of intrusive basaltic andesite dated at 28.5 Ma is preserved along the west margin of the Morenci pit at Tv hill. This intrusive basaltic andesite is associated with a cinder – agglutinate deposit indicating that this locality preserves the sub-volcanic unconformity and provides important constraints on the depth of erosion of the Morenci deposit in this area at this time. Reliable groundmass concentrate  $^{40}\text{Ar}/^{39}\text{Ar}$  dates of the basaltic andesite in the Clifton-Morenci area range between 24.7 and 28.5 Ma. A 22.3 Ma date from basaltic andesite lava in intrusion basin near Enebro Mountain is interpreted to be reset during emplacement of the ~ 22 Ma rhyolite lavas in the area. Likewise, a set of three K-Ar whole rock ages of about 22 Ma (Richter et al., 1983) from basaltic andesite lava in a similar setting in the northern Peloncillo Mountains are also interpreted to be reset during emplacement of a voluminous overlapping series of ~ 22 Ma felsic lavas.

The basaltic andesite lava sequence is uninterrupted and monotonous in the Clifton-Morenci area, but in adjacent areas to the east and southwest it is interbedded with ~24.5-26 Ma silicic lava fields in the Gila Mountains (Houser et al., 1985) and in the Big Lue Mountains (Ratté and Brooks, 1995). Cryptic breaks in the basaltic andesite lava sequence related to these felsic intervals can be traced into the edges of the Clifton-Morenci area. To the east of San Francisco River a thin interval of volcanoclastic sandstone can be traced into an important unconformity that overlaps a major east-side-down normal fault, but our attempt to define the duration of this hiatus by dating lava above and below the contact was unsuccessful (both samples gave the same ~ 27 Ma age). Pyroclastic deposits derived from the Gila Mountains silicic lava field can be traced into the Gila Box area and lower Eagle Creek basin where they occur interbedded with the basaltic andesite lavas. The youngest tuff occurs at the top of the basaltic andesite lava sequence and was dated at ~ 24.5 Ma consistent with its derivation from the Gila Mountains silicic lava field.

An extensive field of approximately 22.5 - 20 Ma rhyolite lava and nonwelded tuff that overlies the basaltic andesite lava sequence directly north of the Morenci district is formally designated as the Enebro Mountain Formation (based on Schroeder's (1996) rhyolite of Enebro Mountain). This new unit includes an approximately 60 km<sup>3</sup> suite of rhyolite lava domes, flows, nonwelded tuff, and sparse basaltic lava that covers a 100 km<sup>2</sup> area in an east-west striking belt north of Garfield fault. Deposits of this formation do not

extend to the south of the Morenci district, but they are roughly equivalent in time to an extensive field of silicic lava in the northern Peloncillo Mountains, and an isolated field of dacitic lava in the Big Lue Mountains.

The silicic lava field in the northern Peloncillo Mountains was originally interpreted (Richter et al., 1983) to intertongue with the basaltic andesite lava sequence. Based on our reinterpretation of a north-facing buttress unconformity (mapped by Richter et al., 1983) as a south-side-down fault near the crest of the Peloncillo Mountains, we interpret all of the exposed silicic lavas of the northern Peloncillo Mountains as younger than the main mass of mafic flows. This reinterpretation is supported by Richter et al.'s (1983), and our geochronology which shows that the oldest silicic lavas are younger than the main mass of mafic flows.

The youngest phase of silicic volcanism in the region is represented by two isolated lava fields; the 17-18 Ma Tollgate Wash silicic center in the northern Peloncillo Mountains, and the 17-18 Ma rhyolite of Mule Creek in the Big Lue Mountains. The Tollgate Wash silicic center is the probable origin for an  $18.20 \pm 0.05$  Ma (sanidine  $^{40}\text{Ar}/^{39}\text{Ar}$ ) nonwelded tuff that defines the base of the Gila Group in the Gila Box area.

New  $^{40}\text{Ar}/^{39}\text{Ar}$  geochronology combined with many previously published K-Ar and  $^{40}\text{Ar}/^{39}\text{Ar}$  dates are used to construct a time-stratigraphic framework of a 3200 km<sup>2</sup> area including Clifton-Morenci area, Big Lue Mountains, Gila Mountains, and the northern Peloncillo Mountains. The framework reveals changes in volcanic and depositional settings across the boundary of the Transition Zone – Basin and Range tectonic provinces. The principal observation is that the base of the Gila Group is time-transgressive, and older to the north by at least 4 million years.

The onset of Gila Group style, basin-filling sedimentation is defined by the first appearance of the conglomerate of Midnight Canyon, a mixed clast, volcanoclastic conglomerate that is present throughout the region (Richter et al., 1983; Houser et al., 1985; this study). Based on new and previously published age dates, the lithostratigraphic boundaries of the sedimentary units at the base of the Gila Group are time-transgressive, and consistently older to the north. The base of the Bonita Creek lithofacies, which represents the prelude to Gila Group sedimentation, changes from ~ 18 Ma in the south to ~ 23 Ma to the north. Likewise, the base of the conglomerate of Midnight Canyon changes in age from <16 Ma in the south to ~ 20 Ma in the north. Where the sedimentary sequence is thickest and well-exposed in the Gila Box area, a nonwelded tuff dated at  $18.20 \pm 0.05$  Ma (sanidine  $^{40}\text{Ar}/^{39}\text{Ar}$ ) marks the base of the Gila Group.

The first appearance of non-volcanic clasts, including copper-bearing clasts, in the Gila Group is used to define the contact between the conglomerate of Midnight Canyon and unit of Buzzard Roost Canyon. Based on Enders' (2000) alunite  $^{40}\text{Ar}/^{39}\text{Ar}$  age dates for the supergene blanket at Morenci, we shift the age of this contact from the Pliocene (5-7 Ma) to the Miocene (~10-12 Ma).

### **Implications for supergene enrichment at Clifton-Morenci**

Mid- to late-Tertiary erosion, tectonism, and associated volcanism and sedimentation played a profound role in the formation and preservation of supergene enrichment in the Morenci porphyry copper deposit. Eocene to early Oligocene erosion had removed approximately 1.8 km of rocks above the pre-mining land surface as

indicated by the 28.5 Ma sub-volcanic unconformity at Tv Hill. Although it was permissible for enrichment to have occurred prior to Oligocene volcanic activity, there is no evidence preserved in the rocks to substantiate this interpretation (Enders, 2000), and no early-Oligocene or Eocene sedimentary rocks were identified in the study area from this erosional period. The Clifton-Morenci area was covered by a thick succession of volcanic rocks beginning with the Clifton Tuff (34 Ma) and Bloodgood Canyon Tuff (28 Ma), and continuing with the basaltic-andesite (28.5 to 24.7 Ma), and finally the Enebro Mountain Formation (22.5 to 20 Ma). This mid-Tertiary volcanic cover effectively preserved the Morenci porphyry copper deposit from further erosion until the mid-Miocene. Much of the volcanic cover over the deposit was removed and deposited in the adjacent basins as the conglomerate of Midnight Canyon beginning around 18 Ma. The Morenci porphyry copper deposit was re-exposed and initial supergene enrichment had been formed by at least 13.4 Ma (Enders, 2000). Further erosion of the deposit and surrounding rocks contributed detritus to the overlying unit of Buzzard Roost Canyon beginning at the end of the mid-Miocene (~12 Ma) and continuing into the early Pliocene. Most of the supergene enrichment at Morenci appears to have been formed during episodic uplift and basin subsidence as a result of Basin and Range deformation between ~13 and ~4 Ma (Enders, 2000).

### **Structural geology**

Minor, east-directed thrust faults occur within Paleozoic strata along the south side of the Morenci block. The faults are interpreted as Laramide, but no other evidence of Phanerozoic compressional deformation was observed in the region.

We interpret a prolonged history of motion along the San Francisco fault based on the burial by Oligocene (~27 Ma) mafic lava flows of related faults in its hanging wall, and the presence of an older, moderately dipping strand of the main fault in many localities along upper San Francisco River. The ancestry of this fault system is supported by evidence that the onset of Gila Group style sedimentation began in the San Francisco half-graben at least 4 million years prior to its onset in the Gila Box and areas farther south.

An older phase of southerly tilting of the floor of the Eagle Creek half-graben is interpreted as a late Oligocene phase of northeast-side-down normal faulting, and is possibly related to initial motion along the Pinaleno detachment system.

The north-side-down Garfield fault defines the southern limit of Enebro Mountain Formation volcanic rocks and its hypabyssal feeder dikes. The fault's greatest offset coincides with the thickest accumulation of volcanic rocks of the formation. It is possible that magma draw-down concomitant with eruption of the Enebro Mountain Formation was the principal reason for motion along the Garfield fault.

## **REFERENCES**

- Aldrich, M. J. Jr., and Laughlin, A. W., 1984, A model for the tectonic development of the southeastern Colorado Plateau boundary: *Journal of Geophysical Research*, v. 89, p. 10207-10218.
- Baldridge, W. S., Barlov, Y., and Kron, A., 1982, Structural setting of the central Rio Grande Rift; relationship to basement grain in New Mexico and Arizona, *in* Gabrielsen, R. H., Ramberg, I. V.,

- Roberts, D., and Steinlein, O. A., eds., Proceedings of the Fourth international conference on basement tectonics: Basement Tectonics Committee, p. 370.
- Bennett, K.C., 1974 (?), Miscellaneous handwritten notes and sketches on the genesis and skarn alteration of the Morenci porphyry copper deposit: from the Phelps Dodge Morenci, Inc. Geology Department files, 12p.
- Bennett, K.C., 1975, Geology and origin of the breccias in the Morenci-Metcalf district, Greenlee Co., Arizona, unpublished M.S. thesis, The University of Arizona, 153 p.
- Cather, S.M., Chamberlin, R.M., and Ratté, J.C., 1994, Tertiary stratigraphy and nomenclature for western New Mexico and eastern Arizona: New Mexico Geological Society Guidebook, 45<sup>th</sup> annual field conference, Mogollon Slope, west-central New Mexico and east-central Arizona, p. 259-268.
- Chapin, C. E., and Cather, S. M., 1981, Eocene tectonics and sedimentation in the Colorado Plateau-Rocky Mountains area: Arizona Geological Society Digest, v. 14, p. 173-198.
- Chillingworth, G., 1999, Geology of an area north of Morenci, Arizona (Coronado Spring): unpublished. Part II Field Project map, Department of Earth Sciences, University of Cambridge, Cambridge, UK, 47 p. report with map, scale 1:10,000.
- Cook, S.S., 1994, The geologic history of supergene enrichment in the porphyry copper deposits of southwestern North America: unpublished Ph.D. dissertation, University of Arizona, 163 p.
- Cunningham, J.E., 1981, Preliminary untitled geologic map of the San Francisco River area north of Clifton, Arizona: Arizona Bureau of Geology and Mineral Technology, Open-file Report: OFR 81-22, scale 1:24,000.
- Dalrymple, G.B., Alexander, E.C., Jr., Lanphere, M.A., and Kraker, G.P., 1981. Irradiation of samples for <sup>40</sup>Ar/<sup>39</sup>Ar dating using the Geological Survey TRIGA reactor. USGS, Prof. Paper, 1176.
- Dames and Moore, 1997, Basin-fill stratigraphic study - draft summary report, Phelps Dodge Morenci District: unpublished consultants report for Phelps Dodge Morenci Inc., 16p with maps, scale 1:18,000.
- Deino, A., and Potts, R., 1990. Single-Crystal <sup>40</sup>Ar/<sup>39</sup>Ar dating of the Olorgesailie Formation, Southern Kenya Rift, J. Geophys. Res., 95, 8453-8470.
- Deino, A., and Potts, R., 1992. Age-probability spectra from examination of single-crystal <sup>40</sup>Ar/<sup>39</sup>Ar dating results: Examples from Olorgesailie, Southern Kenya Rift, Quat. International, 13/14, 47-53.
- Enders, M. S., 2000, The evolution of Supergene Enrichment in the Morenci Porphyry Copper deposit, Greenlee County, Arizona: unpublished Ph.D. dissertation, University of Arizona, Tucson, 3 plates, 1:24,000 scale, 517 pp.
- Fleck, R.J., Sutter, J.F., and Elliot, D.H., 1977. Interpretation of discordant <sup>40</sup>Ar/<sup>39</sup>Ar age-spectra of Mesozoic tholeiites from Antarctica, Geochim. Cosmochim. Acta, 41, 15-32.
- Force, E., 1998, personal communication, U.S. Geological Survey, Southwest Field Office, Tucson, Arizona.
- Garnezy, L., 1990, Strike-slip deformation along the southeastern margin of the Colorado Plateau: Geological Society of America Abstracts with Programs, v. 22, p. A-276.
- Gilbert, G.K., 1875, Geology of portions of New Mexico and Arizona, explored and surveyed in 1873, in Wheeler, G.M., Report on geographical and geological exploration and surveys west of the 100th meridian, v. 3, part 5, Washington, Government Printing office.
- Griffin, J.B., Ring, J.A., and Lowery, R.E., 1993, Laramide intrusive complex of the Morenci district, Greenlee County, Arizona: Arizona Conference A.I.M.E., Geology Division Spring Field Trip, Morenci, Arizona, unpublished Phelps Dodge Morenci, Inc. extended abstract, 3 p.
- Halpenny, L.C., Babcock, H.M., Morrison, R.B. and Hem, J.D., 1946, Groundwater resources of the Duncan basin, Arizona: U.S. Geological Survey, Open-file Report No. (04B H163), 21 p.
- Harrison, T. M. and McDougall, I. 1981. Excess <sup>40</sup>Ar in metamorphic rocks from Broken Hill, New South Wales: implications for <sup>40</sup>Ar/<sup>39</sup>Ar age spectra and the thermal history of the region, Earth and Planetary Science Letters, 55, 123-149.
- Hauser, E. C., and Lundy, J., 1989, COCORP deep reflections: Moho at 50 km (16 s) beneath the Colorado Plateau: Journal of Geophysical Research, v. 94, p. 7071-7082.
- Hauser, E. C., Gephart, J., Latham, T., Oliver, J., Kaufman, S., Brown, L., and Lucchitta, I., 1987, COCORP Arizona transect: Strong crustal reflections and offset Moho beneath the transition zone: Geology, v. 15, p. 1103-1106.

- Heindl, L.A., 1960, Geology of the lower Bonita Creek area: Arizona Geological Society Digest, v. 3, p. 35-40.
- Heindl, L.A., 1962, Should the term "Gila Conglomerate" be abandoned?: Arizona Geological Society Digest, v. V, p. 73-88.
- Heindl, L.A., 1963, Cenozoic geology in the Mammoth area, Pinal County, Arizona: United States Geological Survey Bulletin 1141-E, 2 sheets, scale 1:63,360, 41 pp.
- Heizler, M. T., and Harrison, T. M., 1988. Multiple trapped argon components revealed by  $^{40}\text{Ar}/^{39}\text{Ar}$  analysis, *Geochim. Cosmochim. Acta*, 52, 295-1303.
- Hendricks, J. D., and Plescia, J. B., 1991, A review of the regional geophysics of the Arizona transition zone: *Journal of Geophysical Research*, v. 96, p. 12351-12373.
- Houser, B.B., Richter, D.H., and Shafiqullah, M., 1985, Geologic map of the Safford Quadrangle, Graham County, Arizona: U.S. Geological Survey, Miscellaneous Investigations Series, Map I-1617, scale 1:48,000.
- IUGS subcommission on the systematics of igneous rocks, 1973, Classification and nomenclature of plutonic rocks: *Geotimes*, v. 18, p. 26-30.
- James, R., 1999, The geology of part of the northern Clifton Quadrangle, Arizona (Granville Recreation Area): unpublished Part II Field Project map, Department of Earth Sciences, University of Cambridge, Cambridge, UK, scale 1:10,000.
- Karlstrom, K. E., and Humphreys, E. D., 1998, Persistent influence of Proterozoic accretionary boundaries in the tectonic evolution of southwestern North America; interaction of cratonic grain and mantle modification events, *in* Karlstrom, K. E., ed., *Lithospheric structure and evolution of the Rocky Mountains; Part I*, University of Wyoming, Laramie, p. 161-179.
- Knechtel, M. M., 1936, Geologic relations of the Gila conglomerate in south-eastern Arizona: *American Journal of Science*, 5<sup>th</sup> series, v. 31, p. 81-92.
- Knechtel, M. M., 1938, Geology and ground-water resources of the valley of Gila River and San Simon Creek, Graham County, Arizona, with a section on the chemical character of the ground water by E. W. Lohr: United States Geological Survey Water-Supply Paper 796-F, p. 181-222.
- Kruger, J.M., Johnson, R.A., and Houser, B.B, 1995, Miocene-Pliocene half-graben evolution, detachment faulting and late-stage core complex uplift from reflection seismic data in south-east Arizona: *Basin Research*, v. 7, p. 129-149.
- Langton, J.M, 1973, Ore genesis in the Morenci-Metcalf district: *American Institute of Mining Engineers Transactions*, v. 254, p. 247-257.
- Lee, J.S., 1994, Petrographic and geochemical study of mafic intrusives encountered in DDH 1731 and DDH 1755, deep hypogene program, Morenci, Arizona: unpublished Phelps Dodge Morenci, Inc. memorandum to R.K. Preece, July 27, 1994, 6 p., plus appendices.
- Leighty, R.S., 1997, Evolution of tectonism and magmatism across the Basin and Range-Colorado Plateau boundary, central Arizona: Tempe, Arizona State University, unpublished Ph.D. dissertation, 1019 p.
- Lindgren, W., 1905a, The copper deposits of the Clifton-Morenci district, Arizona: U.S. Geological Survey, Professional Paper No. 43, Pl. 1, scale 1:62,500.
- Lindgren, W., 1905b, Description of the Clifton Quadrangle: U.S. Geological Survey, Clifton Folio, scale 1:62,500.
- Lo, Ching-Hua, and Onstott, T.C., 1989,  $^{39}\text{Ar}$  recoil artifacts in chloritized biotite, *Geoch. Cosmoch. Acta*, 53, 2967-2711.
- Lock, T., 1999, Geologic map of the Chesser Gulch area north of Morenci, Greenlee County, Arizona: unpublished Part II Field Project map, Dept. of Earth Sciences, University of Cambridge, Cambridge, UK, scale 1:10,000.
- Mahon, K.I., 1996. The New "York" regression: Application of an improved statistical method to geochemistry, *International Geology Review*, 38, 293-303.
- Marvin, R.F., Naeser, C.W., Bikerman, M. Mehnert, H.H., and Ratté, J.C., 1987, Isotopic ages of post-Paleocene igneous rocks within and bordering the Clifton 1 X 2 quadrangle, Arizona-New Mexico: New Mexico Bureau of Mines and Mineral Resources, Bulletin 118, p. 5-63.
- McCandless, T. E., and Ruiz, J., 1993, Rhenium-osmium evidence for regional mineralization in southwestern North America, *Science*, v, 261, p. 1282-1286.
- McDougall, I and Harrison, T.M., 1988. Geochronology and thermochronology by the  $^{40}\text{Ar}/^{39}\text{Ar}$  Method, *Oxford Monographs of Geology and Geophysics* No. 9, 212 p.

- McDowell, F.W., 1971, K-Ar ages of igneous rocks from the Western United States, *Isocron/West*, no. 2, p. 1-17.
- McIntosh, William C., Chapin, Charles E., Ratté, James C., and Sutter, John F., 1992, Time-stratigraphic framework for the Eocene-Oligocene Mogollon-Datil volcanic field, southwest New Mexico: *Geological Society of America Bulletin*, v. 104, p. 851-871.
- Menzer, F.J., 1980, The Laramide intrusive complex at Morenci-Metcalf, Arizona: Arizona Conference A.I.M.E., Mining Geology Division, unpublished report on file in Phelps Dodge Morenci, Inc. Geology Department.
- Moolick, R.T. and Durek, J.J., 1966, The Morenci District: in *Geology of the Porphyry Copper Deposits, Southwestern North America*, Titley, S.R. and Hicks, C.L., editors, University of Arizona Press, Tucson, p. 221-231.
- More, S.W., 1995, Project Report: Walker Butte Evaluation, unpubl. Phelps Dodge Exploration Corp. internal report, 10 p. with Figure 2, scale 1:6,000.
- North, R.M. and Preece, R.K., 1993, Supergene ore-forming processes in the Morenci district: Arizona Conference A.I.M.E., Geology Division Spring Field Trip, Morenci, Arizona, unpublished Phelps Dodge Morenci, Inc. extended abstract, 2 p.
- Pawlowski, M.R., 1980, Facies map of the Gila Conglomerate: unpublished Phelps Dodge Corporation report on Aggregate Resources, compiled from mapping by Richardson, W.F. (1971, 1976), scale 1:9,600.
- Pearthree, P. A. (Compiler), 1998, Quaternary fault data and map for Arizona: Arizona Geological Survey Open-File Report 98-24, 122 pp, scale 1:750,000, 1 HD DOS disk.
- Peters, L., 1999,  $^{40}\text{Ar}/^{39}\text{Ar}$  geochronology results from the Morenci Project Sanidine: unpublished New Mexico Geochronological Research Laboratory, internal report # NMGR-L-IR-28, 3 p., 6 figures, 3 tables.
- Peters, L., and McIntosh, W.C., 1999,  $^{40}\text{Ar}/^{39}\text{Ar}$  geochronology results from the Morenci Project Basalts: unpublished New Mexico Geochronological Research Laboratory, internal report # NMGR-L-IR-36, 3 p., 9 figures, 2 tables, with appendices.
- Phelps Dodge Corporation, 1969, A summary of the western exploration program (Gold Belt claims and leases – Southwest claims and leases): unpublished company report by the Geology Staff to G.B. Monroe, October 24, 1969.
- Phelps Dodge Morenci, Inc., 1996, Geology Department – Employee education and training manual: unpublished notebook compiled by the staff.
- Preece, R.K., 1984, Geology of the Morenci district as of 4/84: unpublished Phelps Dodge Morenci, Inc. geologic map, scale 1:9,600; updated 9/95, scale 1:24,000.
- Preece, R.K. and Menzer, F.J., 1982, Geology and economic potential of the Western Copper Exchange (W.C.E.) property: internal Phelps Dodge company report.
- Preece, R.K. and Menzer, F.J., 1992, Geology of the Morenci copper deposit, Greenlee County, Arizona: unpublished extended abstract for the Northwest Mining Association Short Course, Porphyry Copper Model – Regional Talks and Settings, Tucson, Arizona and Spokane, Washington, 4 p.
- Preece, R.K., Stegen, R.J., and Weiskopf, T.A., 1993, Hydrothermal alteration and mineralization of the Morenci porphyry copper deposit, Greenlee County, Arizona: Arizona Conference A.I.M.E., Geology Division Spring Field Trip, Morenci, Arizona, unpublished Phelps Dodge Morenci, Inc. extended abstract, 4 p.
- Ratté, J.C., Landis, E. R., Gaskill, D. L., and Raabe, R. G., 1969, Mineral Resources of the Blue Range Primitive area, Greenlee County, Arizona, and Catron County, New Mexico: United States Geological Survey Bulletin 1261-E, 2 maps, 1:62,500 scale, 91 pp.
- Ratté, J.C. and Brooks, W.E., 1995, Preliminary geologic map of the Big Lue Mountains 15-minute Quadrangle, Greenlee County, Arizona, and Catron and Grant Counties, New Mexico: Arizona Geological Survey, Open-file Report: OFR 95-263, sheet 1 of 1, scale 1:48,000.
- Ratté, J.C. and Hedlund, D.C., 1981, Geologic map of the Hells Hole further planning area (RARE II) Greenlee County, Arizona, and Grant County, New Mexico: U.S. Geological Survey, Miscellaneous Field Studies Map, MF-1344-A, scale 1:62,500.
- Reber, L.E., 1916, The mineralization at Clifton-Morenci: *Economic Geology*, v. 11, p. 528-573.

- Richter, D.H. and Lawrence, V.A., 1981, Geologic map of the Gila-San Francisco Wilderness Study Area, Graham and Greenlee Counties, Arizona: U.S. Geological Survey, Miscellaneous Field Studies, Map MF-1315A, scale 1:62,500.
- Richter, D.H., Shafiqullah, M., and Lawrence, V.A., 1981, Geologic map of Whitlock Mountains, Graham County, Arizona: U.S. Geological Survey, Miscellaneous Investigations Series, Map I-1302, scale 1:48,000.
- Richter, D.H., Houser, B.B., and Damon, P.E., 1983, Geologic map of the Guthrie Quadrangle, Graham and Greenlee Counties, Arizona: U.S. Geological Survey, Miscellaneous Investigations Series, Map I-1455, scale 1:48,000.
- Samson, S.D., and Alexander, E.C., Jr., 1987. Calibration of the interlaboratory  $^{40}\text{Ar}/^{39}\text{Ar}$  dating standard, Mmhb-1, Chem. Geol., 66, 27-34.
- Schneider, R. V., and Keller, G. R., 1994, Crustal structure of the western margin of the Rio Grande rift and Mogollon-Datil volcanic field, southwestern New Mexico and southeastern Arizona, in Keller, G. R., and Cather, S. M., eds., Basins of the Rio Grande Rift: Structure, Stratigraphy, and Tectonic Setting: Geological Society of America Special Paper 291, p. 207-226.
- Schroeder, T.J., 1996, Geologic map of the Enebro Mountain Rhyolite: Arizona Geological Survey, Contributed Map: CM-96-A, sheet 1 of 2, scale 1:12,000.
- Spencer, J.E. and Reynolds, S.J., 1989, Late Cenozoic tectonism in Arizona and its impact on regional landscape evolution: Arizona Geological Society Digest 17, Jenney, J.P., and Reynolds, S.J., editors, p. 539-574.
- Spencer, J. E., and Reynolds, S. J., 1991, Tectonics of mid Tertiary extension along a transect through west central Arizona: Tectonics, v. 10, p. 1204-1221.
- Steiger, R.H., and Jäger, E., 1977. Subcommittee on geochronology: Convention on the use of decay constants in geo- and cosmochronology. Earth and Planet. Sci. Lett., 36, 359-362.
- Taylor, J.R., 1982. An Introduction to Error Analysis: The Study of Uncertainties in Physical Measurements, Univ. Sci. Books, Mill Valley, Calif., 270 p.
- Wahl, D.E., 1980, Mid-Tertiary volcanic geology in parts of Greenlee County, Arizona, Grant and Hidalgo Counties, New Mexico: unpublished Ph.D. dissertation, Arizona State University, 144 p.
- Walker, M.A., 1995, Structural interpretation of the Morenci Mining district, Greenlee, County: unpublished M.S. thesis, New Mexico Institute of Mining and Technology, 130 p.
- Warren, D. H., A seismic refraction survey of crustal structure in central Arizona: Geological Society of America Bulletin, v. 80, p. 257-282.
- Warren, J.M., 1999, The geology of a region north of Morenci, Arizona (Pinal Point): Part II Field Project map, Department of Earth Sciences, University of Cambridge, Cambridge, UK, 31 p. report with map, scale 1:10,000.
- Wright, E.G., 1997, Dispatch Hill geological report: unpublished Phelps Dodge Morenci, Inc. report, 10 p., 1 plate, scale 1:4,800.
- York, D., 1969. Least squares fitting of a straight line with correlated errors, Earth and Planet. Sci. Lett., 5, 320-324.

## APPENDIX A: MAFIC LAVA GROUNDMASS CONCENTRATE ANALYSES

### <sup>40</sup>Ar/<sup>39</sup>Ar analytical methods and results

The groundmass concentrates were analyzed by the furnace incremental heating age spectrum method. Abbreviated analytical methods for the samples are given in Table A1, and details of the overall operation of the New Mexico Geochronology Research Laboratory are provided in Appendix D. The argon isotopic results are listed in Table A2.

**Table A1.** Sample preparation, analytical methods and age calculation methods.

<b>Sample preparation and irradiation:</b>
<ul style="list-style-type: none"> <li>Groundmass concentrates were treated with dilute HCl, washed and hand-picked.</li> <li>Groundmass concentrates were loaded into a machined Al disc and irradiated for 7 or 3 hours in D-3 position, Nuclear Science Center, College Station, TX.</li> <li>Neutron flux monitor Fish Canyon Tuff sanidine (FC-1). Assigned age = 27.84 Ma (Deino and Potts, 1990) relative to Mmhb-1 at 520.4 Ma (Samson and Alexander, 1987).</li> </ul>
<b>Instrumentation:</b>
<ul style="list-style-type: none"> <li>Mass Analyzer Products 215-50 mass spectrometer on line with automated all-metal extraction system.</li> <li>Samples step-heated in Mo double-vacuum resistance furnace. Heating duration 7 minutes.</li> <li>Reactive gases removed by reaction with 3 SAES GP-50 getters, 2 operated at ~450°C and 1 at 20°C. Gas also exposed to a W filament operated at ~2000°C.</li> </ul>
<b>Analytical parameters:</b>
<ul style="list-style-type: none"> <li>Electron multiplier sensitivity averaged <math>1 \times 10^{-16}</math> moles/pA.</li> <li>Total system blank and background for the furnace averaged 902, 4.3, 0.6, 2.0, <math>3.2 \times 10^{-18}</math> moles at masses 40, 39, 38, 37, and 36, respectively for temperatures &lt;1300°C.</li> <li>J-factors determined to a precision of <math>\pm 0.1\%</math> by CO<sub>2</sub> laser-fusion of 4 single crystals from each of 6 radial positions around the irradiation tray.</li> <li>Correction factors for interfering nuclear reactions were determined using K-glass and CaF<sub>2</sub> and are as follows: <math>(^{40}\text{Ar}/^{39}\text{Ar})_{\text{K}} = 0.00020 \pm 0.0003</math>; <math>(^{36}\text{Ar}/^{37}\text{Ar})_{\text{Ca}} = 0.00026 \pm 0.00002</math>; and <math>(^{39}\text{Ar}/^{37}\text{Ar})_{\text{Ca}} = 0.00070 \pm 0.00005</math>.</li> </ul>
<b>Age calculations:</b>
<ul style="list-style-type: none"> <li>Total gas ages and errors calculated by weighting individual steps by the fraction of <sup>39</sup>Ar released.</li> <li>Plateau definition: 3 or more analytically indistinguishable contiguous steps comprising at least 50% of the total <sup>39</sup>Ar (Fleck et al., 1977).</li> <li>Preferred age calculated for indicated steps when the sample does not meet plateau criteria.</li> <li>Plateau or preferred ages calculated by weighting each step by the inverse of the variance.</li> <li>Plateau and preferred age errors calculated using the method of (Taylor, 1982).</li> <li>MSWD values are calculated for n-1 degrees of freedom for plateau and preferred ages.</li> <li>Isochron ages, <sup>40</sup>Ar/<sup>36</sup>Ar<sub>i</sub> and MSWD values calculated from regression results obtained by the methods of York (1969).</li> <li>Decay constants and isotopic abundances after Steiger and Jäger (1977).</li> <li>All final errors reported at <math>\pm 2\sigma</math>, unless otherwise noted.</li> </ul>

**Table A2.** Analytical results of resistance-furnace step-heating analyses. Isotopic ratios corrected for blank, radioactive decay, and mass discrimination, not corrected for interfering reactions. Analyses in *italics* are excluded from final age calculations.

<b>F8-266, H1:98, 27.92mg wr, J=0.000769481, D=1.00361, NM-98, Lab#=9769-01</b>											
ID	Temp (°C)	<sup>40</sup> Ar/ <sup>39</sup> Ar	<sup>37</sup> Ar/ <sup>39</sup> Ar	<sup>36</sup> Ar/ <sup>39</sup> Ar (x 10 <sup>-3</sup> )	<sup>39</sup> Ar <sub>K</sub> (x 10 <sup>-15</sup> mol)	K/Ca	Cl/K (x 10 <sup>-3</sup> )	<sup>40</sup> Ar* (%)	<sup>39</sup> Ar (%)	Age (Ma)	±1σ (Ma)
A	625	1335.5	1.157	4453.2	0.939	0.44	3.4	1.5	1.0	27.1	14.7
B	700	51.74	1.071	119.0	2.36	0.48	0.68	32.2	3.4	22.99	0.39
D	800	24.95	0.8784	26.64	4.57	0.58	0.30	68.7	8.1	23.66	0.15
E	875	20.76	0.7780	14.87	11.2	0.66	0.21	79.1	19.5	22.68	0.09
F	975	18.28	0.6896	7.161	21.7	0.74	0.18	88.7	41.6	22.39	0.06
G	1075	17.30	0.4370	3.691	15.9	1.2	0.22	93.9	57.8	22.41	0.06
H	1250	18.31	0.5650	7.693	21.5	0.90	0.21	87.8	79.7	22.20	0.06
I	1650	22.89	3.915	22.49	20.0	0.13	0.36	72.3	100.0	22.89	0.09
<b>total gas age</b>			n=9		98.1	0.69				22.61	0.44*
<b>plateau</b>											
MSWD = 4.46**			n=3	steps F-H	59.0	0.91			60.2	22.33	0.14*
<b>F8-269, H2:98, 17.58 mg wr, J=0.000771407, D=1.00361, NM-98, Lab#=9770-01</b>											
ID	Temp (°C)	<sup>40</sup> Ar/ <sup>39</sup> Ar	<sup>37</sup> Ar/ <sup>39</sup> Ar	<sup>36</sup> Ar/ <sup>39</sup> Ar (x 10 <sup>-3</sup> )	<sup>39</sup> Ar <sub>K</sub> (x 10 <sup>-15</sup> mol)	K/Ca	Cl/K (x 10 <sup>-3</sup> )	<sup>40</sup> Ar* (%)	<sup>39</sup> Ar (%)	Age (Ma)	±1σ (Ma)
A	625	963.2	0.7873	3205.5	0.586	0.65	5.1	1.7	1.0	22.2	14.6
B	700	146.2	0.6544	438.4	0.150	0.78	0.29	11.4	1.3	23.2	3.7
C	750	75.35	0.6266	191.2	0.147	0.81	-0.192	25.1	1.5	26.1	2.2
D	800	49.69	0.7159	108.0	2.26	0.71	-0.607	35.9	5.4	24.67	0.40
E	875	30.84	0.7795	38.52	5.70	0.65	0.15	63.3	15.1	26.98	0.15
F	975	26.86	0.6685	23.57	10.7	0.76	0.17	74.3	33.4	27.56	0.11
G	1075	25.17	0.5076	17.74	11.1	1.0	0.18	79.3	52.4	27.59	0.10
H	1250	35.94	0.8568	57.78	18.8	0.60	0.32	52.7	84.5	26.17	0.16
I	1650	67.78	4.341	166.4	9.06	0.12	0.20	27.9	100.0	26.24	0.41
<b>total gas age</b>			n=9		58.6	0.64				26.68	0.70*
<b>F8-273, H6:98, 25.93 mg wr, J=0.000769924, D=1.00361, NM-98, Lab#=9774-01</b>											
ID	Temp (°C)	<sup>40</sup> Ar/ <sup>39</sup> Ar	<sup>37</sup> Ar/ <sup>39</sup> Ar	<sup>36</sup> Ar/ <sup>39</sup> Ar (x 10 <sup>-3</sup> )	<sup>39</sup> Ar <sub>K</sub> (x 10 <sup>-15</sup> mol)	K/Ca	Cl/K (x 10 <sup>-3</sup> )	<sup>40</sup> Ar* (%)	<sup>39</sup> Ar (%)	Age (Ma)	±1σ (Ma)
A	625	6572.7	0.9185	22070.3	0.228	0.56	33.6	0.8	0.3	70	199
B	700	620.3	1.066	2044.7	0.377	0.48	1.8	2.6	0.7	22.3	10.1
C	750	226.9	1.184	691.3	0.393	0.43	2.2	10.0	1.2	31.3	3.5
D	800	74.87	1.415	179.8	4.40	0.36	0.82	29.2	6.4	30.11	0.57
E	875	40.44	1.167	69.10	7.03	0.44	0.10	49.7	14.7	27.74	0.23
F	975	28.02	0.9716	28.45	13.0	0.53	0.29	70.3	30.1	27.16	0.12
G	1075	21.25	0.6351	5.832	16.1	0.80	0.26	92.1	49.2	27.00	0.07
H	1250	20.42	0.4323	3.432	23.5	1.2	0.26	95.2	77.1	26.81	0.06
I	1650	21.54	2.767	7.816	19.3	0.18	0.34	90.3	100.0	26.85	0.07
<b>total gas age</b>			n=9		84.3	0.67				27.3	1.4*
<b>plateau</b>											
MSWD = 3.03			n=4	steps F-I	71.9	0.71			85.3	26.91	0.16*

**Table A2 (cont.).** Results of argon isotopic analysis.

<b>F8-275, K5:98, 27.39 mg wr, J=0.000764924, D=1.00361, NM-98, Lab#=9795-01</b>											
ID	Temp (°C)	<sup>40</sup> Ar/ <sup>39</sup> Ar	<sup>37</sup> Ar/ <sup>39</sup> Ar	<sup>36</sup> Ar/ <sup>39</sup> Ar (x 10 <sup>-3</sup> )	<sup>39</sup> Ar <sub>K</sub> (x 10 <sup>-15</sup> mol)	K/Ca	Cl/K (x 10 <sup>-3</sup> )	<sup>40</sup> Ar* (%)	<sup>39</sup> Ar (%)	Age (Ma)	±1σ (Ma)
A	625	2850.6	0.3525	9509.1	0.307	1.4	21.7	1.4	0.2	55	63
B	700	165.7	0.3371	519.8	0.501	1.5	2.1	7.3	0.6	16.7	2.6
C	750	59.79	0.2682	142.0	0.273	1.9	-1.077	29.9	0.8	24.5	1.5
D	800	42.07	0.2507	74.47	8.29	2.0	0.39	47.7	6.7	27.51	0.23
E	875	27.18	0.2342	21.43	19.1	2.2	0.17	76.8	20.4	28.57	0.09
F	975	24.93	0.2156	15.80	36.9	2.4	0.067	81.3	46.8	27.77	0.09
G	1075	26.89	0.2191	23.21	33.4	2.3	0.19	74.6	70.7	27.46	0.10
H	1250	32.56	0.3548	42.22	24.1	1.4	0.24	61.8	87.9	27.55	0.15
I	1650	52.41	1.208	109.6	16.9	0.42	0.44	38.4	100.0	27.56	0.29
<b>total gas age</b>			n=9		139.7	1.9				27.74	0.56*
<b>plateau</b>											
MSWD = 2.03			n=4	steps F-I	111.2	1.9			79.6	27.62	0.20*

<b>F8-276, C5:98, 25.86mg wr, J=0.00078785, D=1.00361, NM-98, Lab#=9734-01</b>											
ID	Temp (°C)	<sup>40</sup> Ar/ <sup>39</sup> Ar	<sup>37</sup> Ar/ <sup>39</sup> Ar	<sup>36</sup> Ar/ <sup>39</sup> Ar (x 10 <sup>-3</sup> )	<sup>39</sup> Ar <sub>K</sub> (x 10 <sup>-15</sup> mol)	K/Ca	Cl/K (x 10 <sup>-3</sup> )	<sup>40</sup> Ar* (%)	<sup>39</sup> Ar (%)	Age (Ma)	±1σ (Ma)
A	625	3292.5	0.8970	11057.9	0.196	0.57	-4.392	0.8	0.2	35	96
B	700	139.3	1.004	421.4	0.447	0.51	-2.618	10.7	0.6	21.0	2.1
C	750	48.38	0.9612	91.98	0.220	0.53	-1.007	44.0	0.7	30.0	1.5
D	800	38.67	0.8817	64.80	4.27	0.58	0.73	50.7	4.4	27.65	0.25
E	875	23.65	0.7379	12.28	11.5	0.69	0.30	84.9	14.3	28.34	0.09
F	975	20.94	0.5516	4.158	23.8	0.92	0.16	94.3	34.7	27.87	0.08
G	1075	21.10	0.3807	4.783	31.7	1.3	0.096	93.4	61.9	27.82	0.07
H	1250	22.57	0.3980	10.47	22.3	1.3	0.13	86.4	81.1	27.52	0.08
I	1650	27.03	1.374	25.64	22.1	0.37	0.46	72.4	100.0	27.62	0.11
<b>total gas age</b>			n=9		116.6	0.96				27.77	0.52*
<b>plateau</b>											
MSWD = 4.19**			n=4	steps F-I	100.0	1.01			85.7	27.73	0.17*

<b>F8-286, C6:98, 32.32 mg wr, J=0.000787513, D=1.00361, NM-98, Lab#=9735-01</b>											
ID	Temp (°C)	<sup>40</sup> Ar/ <sup>39</sup> Ar	<sup>37</sup> Ar/ <sup>39</sup> Ar	<sup>36</sup> Ar/ <sup>39</sup> Ar (x 10 <sup>-3</sup> )	<sup>39</sup> Ar <sub>K</sub> (x 10 <sup>-15</sup> mol)	K/Ca	Cl/K (x 10 <sup>-3</sup> )	<sup>40</sup> Ar* (%)	<sup>39</sup> Ar (%)	Age (Ma)	±1σ (Ma)
A	625	777.4	0.9613	2532.8	0.237	0.53	7.0	3.7	0.2	41	16
B	700	142.9	0.9300	445.2	0.500	0.55	-1.095	7.9	0.5	16.1	2.1
C	750	93.67	0.8686	263.7	0.730	0.59	0.16	16.9	1.0	22.4	1.2
D	800	56.32	0.7944	131.3	7.07	0.64	0.35	31.2	5.7	24.80	0.38
E	875	25.54	0.8571	26.20	13.3	0.60	0.35	69.9	14.6	25.21	0.12
F	975	24.23	0.6733	22.38	30.1	0.76	0.19	72.9	34.8	24.94	0.10
G	1075	24.74	0.3500	24.77	32.9	1.5	0.13	70.5	56.9	24.63	0.09
H	1250	31.38	0.3537	47.61	41.1	1.4	0.15	55.2	84.5	24.47	0.14
I	1650	45.06	1.799	92.67	23.1	0.28	0.29	39.5	100.0	25.16	0.27
<b>total gas age</b>			n=9		149.0	1.0				24.78	0.38*
<b>plateau</b>											
MSWD = 3.84**			n=4	steps F-I	127.2	1.1			85.4	24.74	0.24*

**Table A2 (cont.).** Results of argon isotopic analysis.

<b>F8-301, C2:98, 36.86mg wr, J=0.00078769, D=1.00361, NM-98, Lab#=9731-01</b>											
ID	Temp (°C)	<sup>40</sup> Ar/ <sup>39</sup> Ar	<sup>37</sup> Ar/ <sup>39</sup> Ar	<sup>36</sup> Ar/ <sup>39</sup> Ar (x 10 <sup>-3</sup> )	<sup>39</sup> Ar <sub>K</sub> (x 10 <sup>-15</sup> mol)	K/Ca	Cl/K (x 10 <sup>-3</sup> )	<sup>40</sup> Ar* (%)	<sup>39</sup> Ar (%)	Age (Ma)	±1σ (Ma)
A	625	20175	0.3414	67036	0.042	1.5	-12.181	1.8	0.0	457	2171
B	700	107.6	0.9467	325.3	0.707	0.54	1.2	10.7	0.5	16.3	1.5
C	750	36.35	0.8359	70.92	0.915	0.61	0.42	42.5	1.1	21.84	0.47
D	800	26.50	0.6975	25.21	8.40	0.73	0.19	72.1	6.9	26.96	0.12
E	875	22.67	0.8422	10.31	18.7	0.61	0.27	86.9	19.6	27.79	0.08
F	975	21.08	0.8232	5.849	31.9	0.62	0.13	92.1	41.3	27.40	0.07
G	1075	21.81	0.4159	8.894	34.0	1.2	0.22	88.1	64.5	27.10	0.09
H	1250	23.15	0.4195	13.81	35.2	1.2	0.26	82.5	88.5	26.95	0.08
I	1650	26.93	3.023	27.65	16.9	0.17	0.46	70.5	100.0	26.84	0.12
<b>total gas age</b>			n=9		146.8	0.86				27.22	1.4*
<b>plateau</b>											
MSWD = 1.74			n=3	steps G-I	86.2	1.01			58.7	26.99	0.18*

<b>F8-316, F3:103, 14.93 mg wr, J=0.000740741, D=1.00361, NM-103, Lab#=50141-01</b>											
ID	Temp (°C)	<sup>40</sup> Ar/ <sup>39</sup> Ar	<sup>37</sup> Ar/ <sup>39</sup> Ar	<sup>36</sup> Ar/ <sup>39</sup> Ar (x 10 <sup>-3</sup> )	<sup>39</sup> Ar <sub>K</sub> (x 10 <sup>-15</sup> mol)	K/Ca	Cl/K (x 10 <sup>-3</sup> )	<sup>40</sup> Ar* (%)	<sup>39</sup> Ar (%)	Age (Ma)	±1σ (Ma)
A	625	205.2	1.151	621.1	0.640	0.44	1.7	10.6	1.5	28.95	1.96
B	700	33.78	1.067	40.33	1.12	0.48	0.092	65.0	4.0	29.13	0.30
C	750	26.65	0.9723	15.47	1.49	0.52	0.024	83.1	7.4	29.39	0.18
D	800	24.17	1.065	7.721	3.49	0.48	0.026	90.9	15.3	29.16	0.10
E	875	22.70	1.134	2.970	6.45	0.45	0.30	96.5	29.9	29.08	0.07
F	975	21.99	0.8121	1.284	9.30	0.63	0.26	98.6	51.0	28.76	0.07
G	1075	21.85	0.5937	1.908	8.06	0.86	0.40	97.6	69.3	28.30	0.07
H	1250	22.46	0.9071	4.941	12.4	0.56	0.24	93.8	97.3	27.97	0.07
I	1650	26.97	10.62	26.24	1.18	0.048	0.82	74.5	100.0	26.91	0.25
<b>total gas age</b>			n=9		44.1	0.59				28.52	0.12
<b>plateau</b>											
MSWD = 3.78**			n=6	steps A-F	22.5	0.53			51.0	29.00	0.17*

K/Ca = molar ratio calculated from reactor produced <sup>39</sup>Ar<sub>K</sub> and <sup>37</sup>ArCa. n= number of heating steps.  
 \* 2s error      \*\* MSWD outside of 95% confidence interval

**Table A3.** Summary of plateau and isochron ages and errors. Preferred ages are in bold text. \*MSWD's outside of 95% confidence level.

Sample name	Plateau Age (Ma)	MSWD	Isochron Age (Ma)	MSWD	<sup>40</sup> Ar/ <sup>36</sup> Ar <sub>I</sub> Intercept	Integrated Ages
F8-266	<b>22.33±0.14</b>	4.46*	22.35±0.21	6.6*	298.9±8.7	22.61±0.44
F8-269	-	-	28.27±0.20	0.86	270.3±4.2	<b>26.68±0.70</b>
F8-273	26.91±0.16	3.03	<b>26.81±0.10</b>	1.73	305.5±2.8	27.3±1.4
F8-275	<b>27.62±0.20</b>	2.03	28.11±0.56	16.3*	289±12	27.74±0.56
F8-276	<b>27.73±0.17</b>	4.19*	27.91±0.32	10.0*	291±12	27.77±0.52
F8-286	<b>24.74±0.24</b>	3.84*	24.96±0.41	6.53*	292.3±7.2	24.78±0.38
F8-301	26.99±0.18	1.74	27.64±0.39	11.83*	273±15	<b>27.2±1.4</b>
F8-316	29.00±0.17	3.78*	28.99±0.23	5.41*	298.0±4.2	<b>28.52±0.24</b>

\*MSWD's outside of 95% confidence level.

Five of the analyzed Morenci basalt samples yielded relatively flat, well-bd age spectra (Figures A1a-A7a). The calculated plateau ages are listed in Table A3. Two plateau ages (F8-273 and F8-275) have MSWD values within the 95% confidence level. The MSWD values for the plateau ages of samples F8-266, F8-276 and F8-286, are slightly outside the 95% confidence level, so the uncertainties on these ages have been adjusted accordingly. All of these samples were also evaluated with inverse isochron analysis (Figures A1b-A7b) and a summary of this data is given in Table A3. Four have  $^{40}\text{Ar}/^{36}\text{Ar}_i$  intercept values that are within error of the atmospheric value of 295.5. F8-273, has an  $^{40}\text{Ar}/^{36}\text{Ar}_i$  intercept value that is significantly greater the atmospheric value.

The groundmass concentrate from F8-269 (Figure A2a) yielded a disturbed age spectrum. A plateau age was not calculated for this sample. The early low-temperature heating-steps rise to older apparent ages, and in general higher K/Ca and radiogenic yields than the high-temperature heating-steps. Isochron analysis (Figure A2b) reveals an unrealistic  $^{40}\text{Ar}/^{36}\text{Ar}_i$  intercept of  $270.3 \pm 4.2$ , although the MSWD value is very low (0.86).

Although not as dramatic, groundmass concentrate from F8-301 (Figure A7a) yielded an age spectrum similar to the age spectrum from F8-269. After an early low-temperature increase in apparent ages there is a steady decline in the apparent ages. The decline is so gradual that a plateau age ( $26.99 \pm 0.18$  Ma) calculated across steps G-I has an acceptable MSWD value (Mahon, 1996). The results are also similar for the isochron analysis, with an  $^{40}\text{Ar}/^{36}\text{Ar}_i$  intercept for F8-301 of  $273 \pm 15$ .

The groundmass concentrate from sample F8-316 yields a disturbed age spectrum (Figure A8a). There is a consistent drop in apparent age from the low temperature to the high temperature heating steps. The K/Ca ratios are variable but do not correspond to the drop in apparent age. The integrated age of this sample is  $28.52 \pm 0.24$  Ma. A weighted mean of steps A-F yields an apparent age of  $29.00 \pm 0.17$  Ma. Isochron analysis of this sample for heating steps A-F yields an isochron age of  $28.99 \pm 0.23$  Ma (Figure A8b). The  $^{40}\text{Ar}/^{36}\text{Ar}_i$  value of  $298.0 \pm 4.2$  is within error of the atmospheric intercept of 295.5. The MSWD values for both of these ages is twice the acceptable value and to account for this, the errors have been increased.

The preferred age of all samples are displayed on a probability distribution diagram in Figure 4 (main text).

## Discussion

Four of the analyzed basalts (F8-266, F8-275, F8-276, F8-286), yielded fairly well-behaved age spectra. For these samples the plateau ages listed in Tables A2 and Table 2 (main text) are the preferred eruption ages. The isochron analysis of these samples indicated an atmospheric trapped component and the plateau ages have acceptable MSWD values or at least lower MSWD values than those of the isochron ages.

Although the groundmass concentrate from F8-273 also yields a well-behaved age spectrum, the preferred age for the eruption of F8-273 is the isochron age of  $26.81 \pm 0.10$  Ma. Isochron analysis reveals a  $^{40}\text{Ar}/^{36}\text{Ar}_i$  of 305.5 (above the atmospheric ratio of 295.5) and an acceptable MSWD value (Mahon, 1996). This age was, therefore, chosen as being more accurate than the plateau age.

### F8-266 Groundmass Concentrate

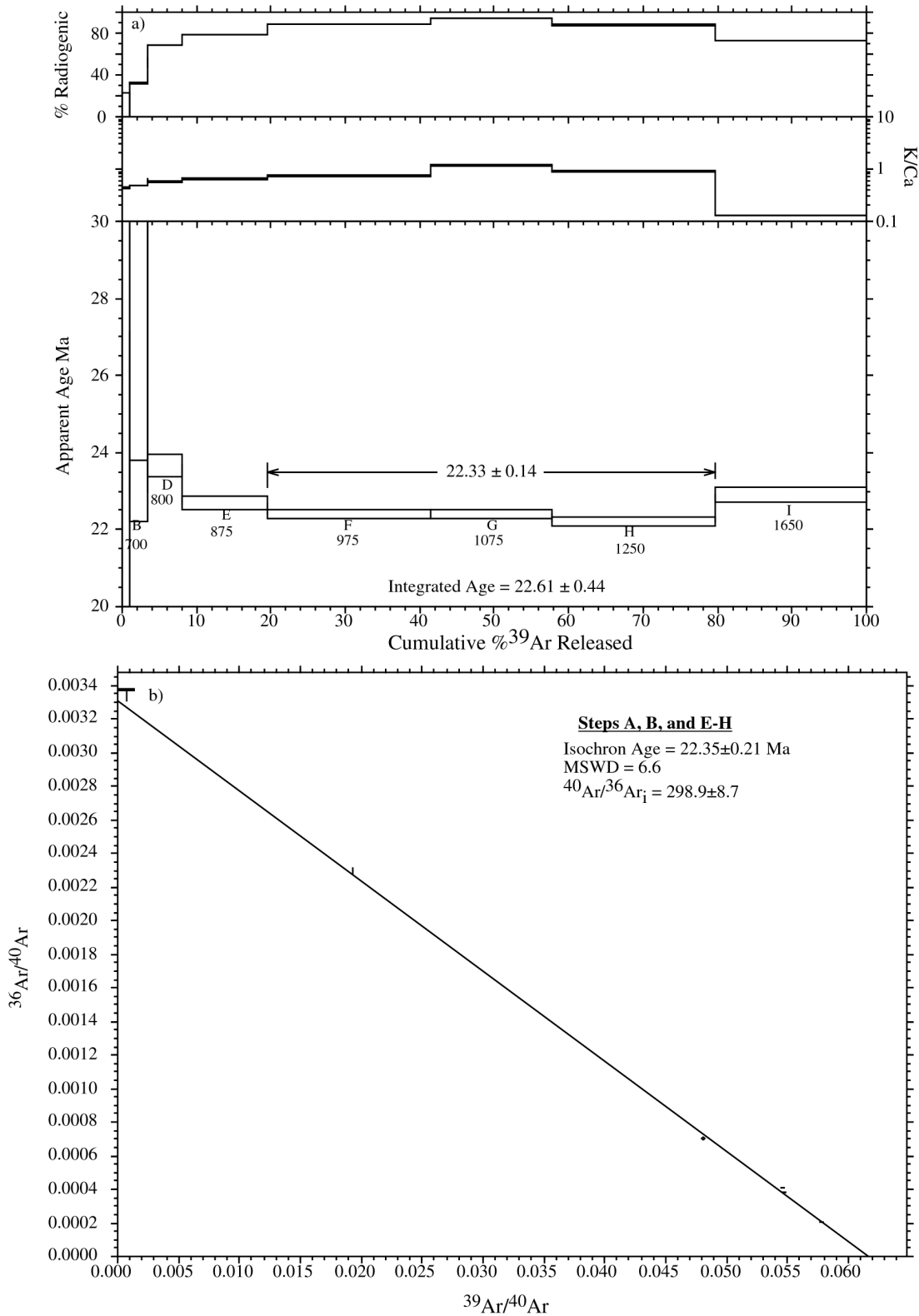


**Figure A1.** Age spectrum (a) and isochron (b) for resistance-furnace  $^{40}\text{Ar}/^{39}\text{Ar}$  of F8-266.

### F8-269 Groundmass Concentrate

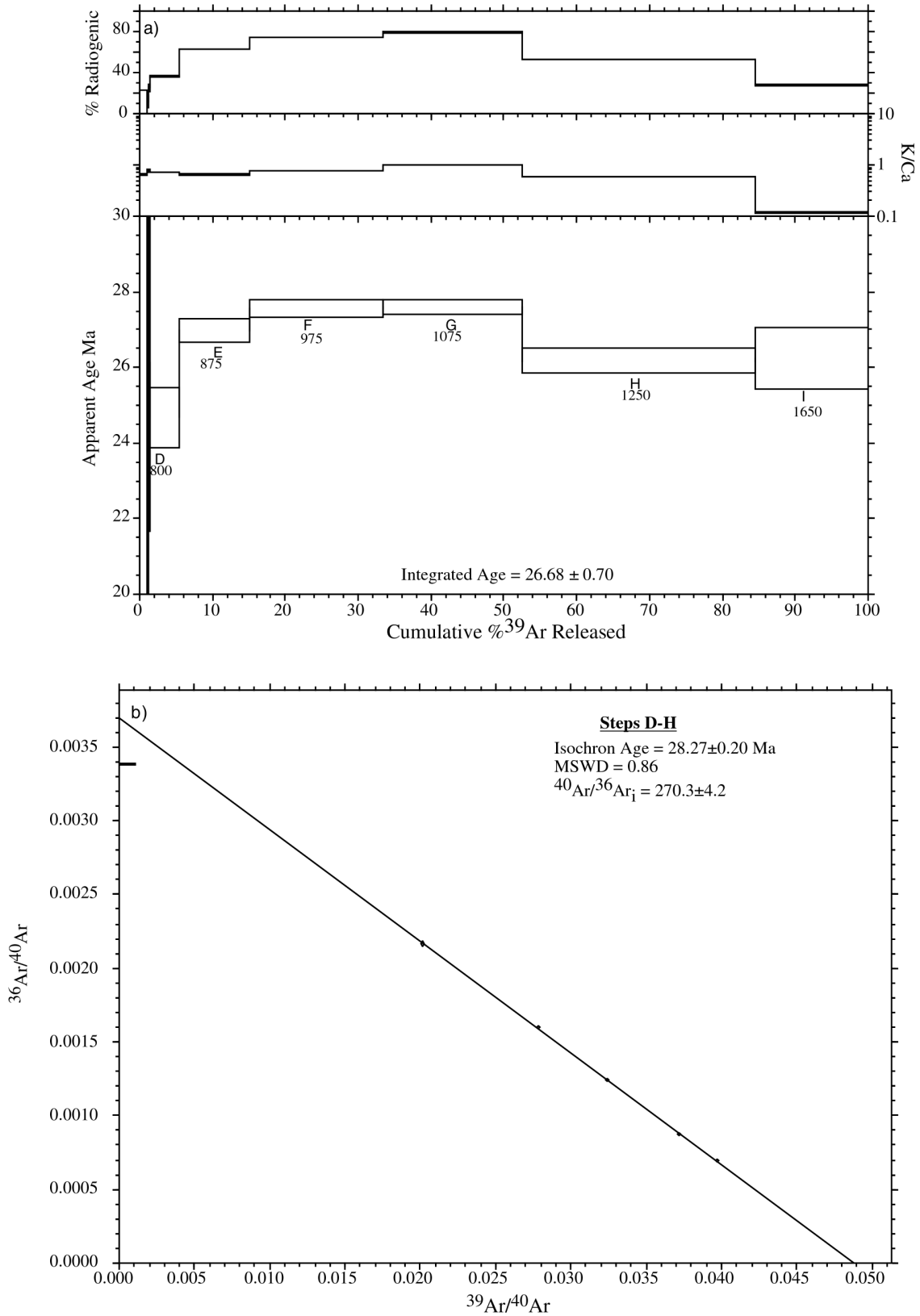


**Figure A2.** Age spectrum (a) and isochron (b) for resistance-furnace  $^{40}\text{Ar}/^{39}\text{Ar}$  of F8-269.

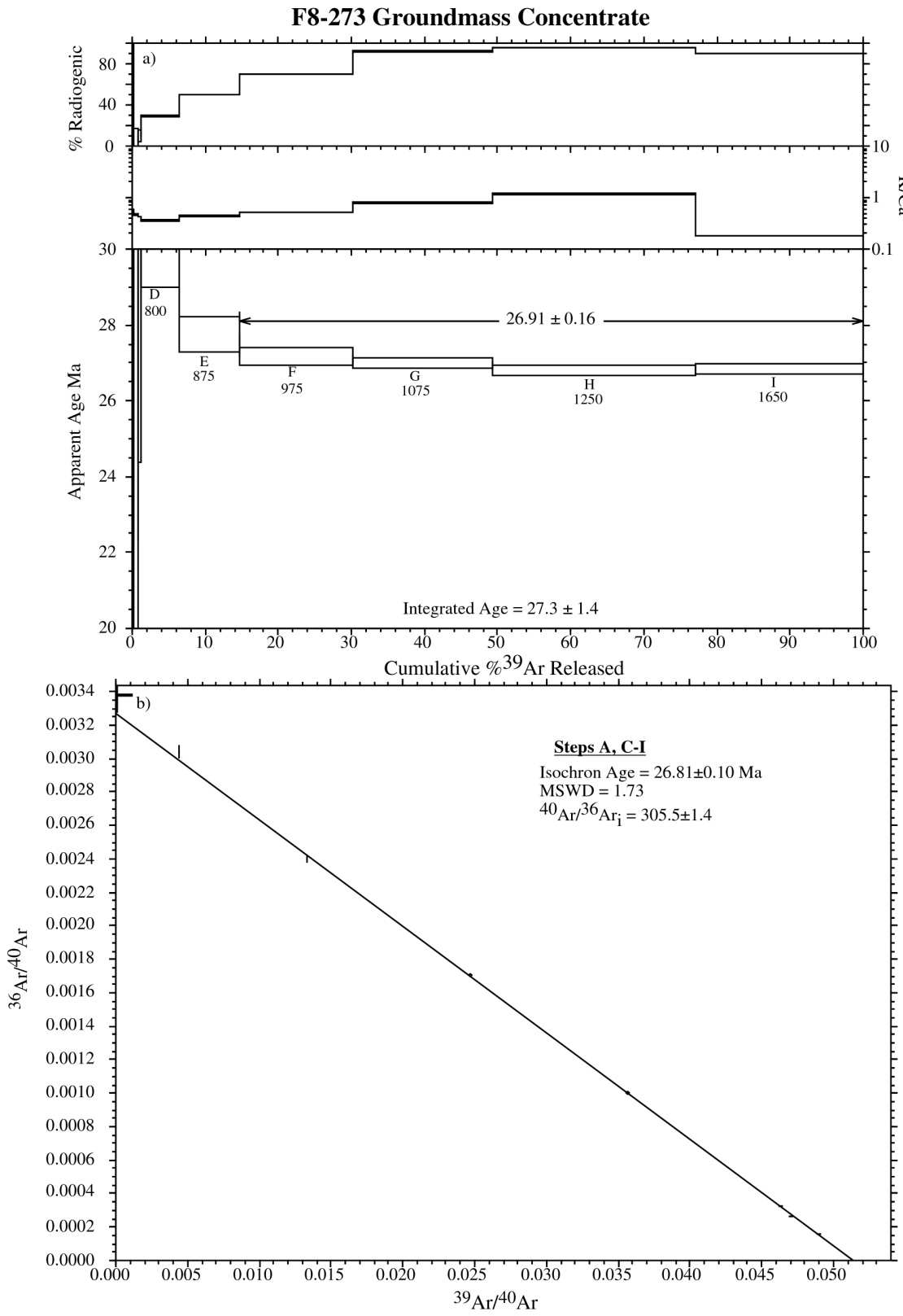


**Figure A3.** Age spectrum (a) and isochron (b) for resistance-furnace  $^{40}\text{Ar}/^{39}\text{Ar}$  of F8-273.

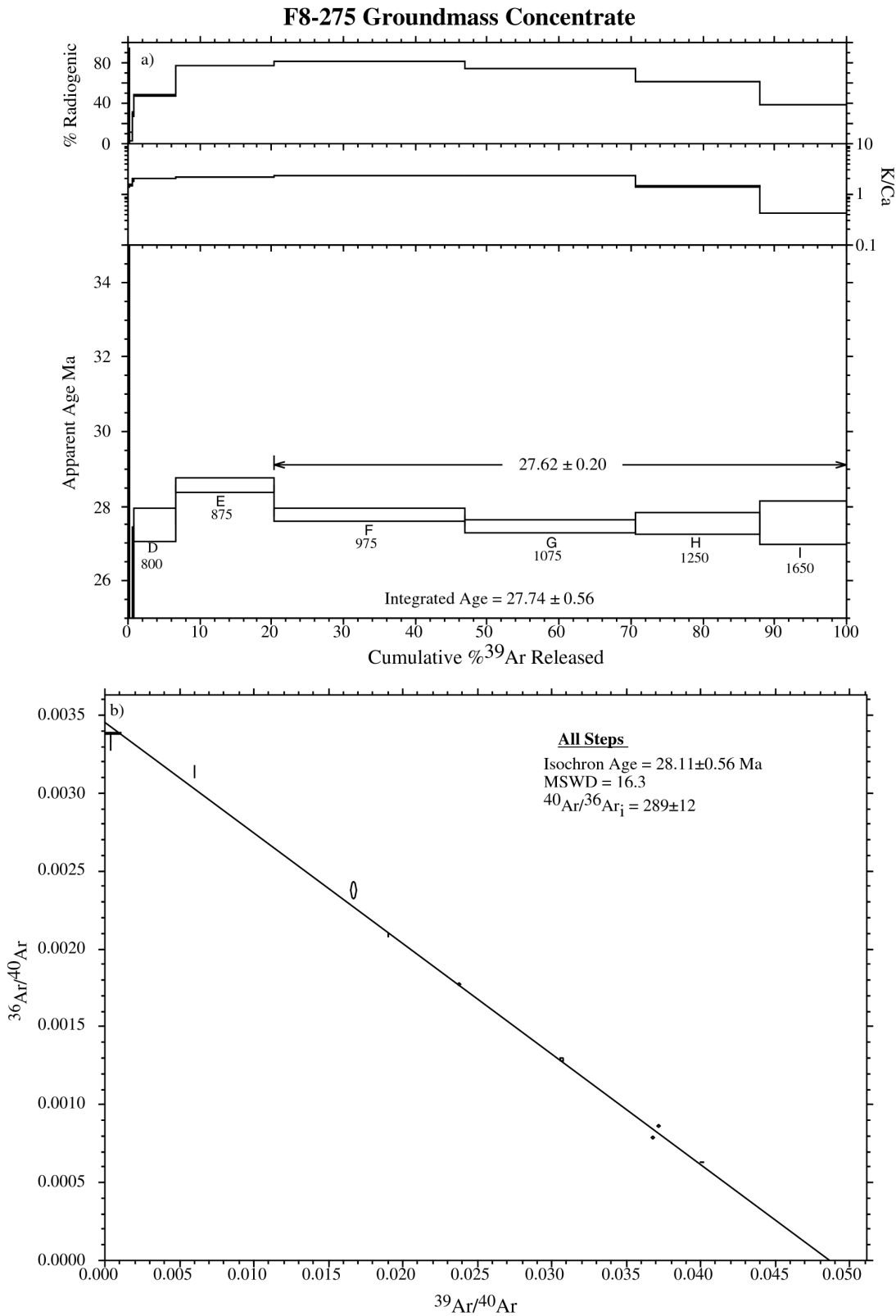


**Figure A4.** Age spectrum (a) and isochron (b) for resistance-furnace  $^{40}\text{Ar}/^{39}\text{Ar}$  of F8-275.

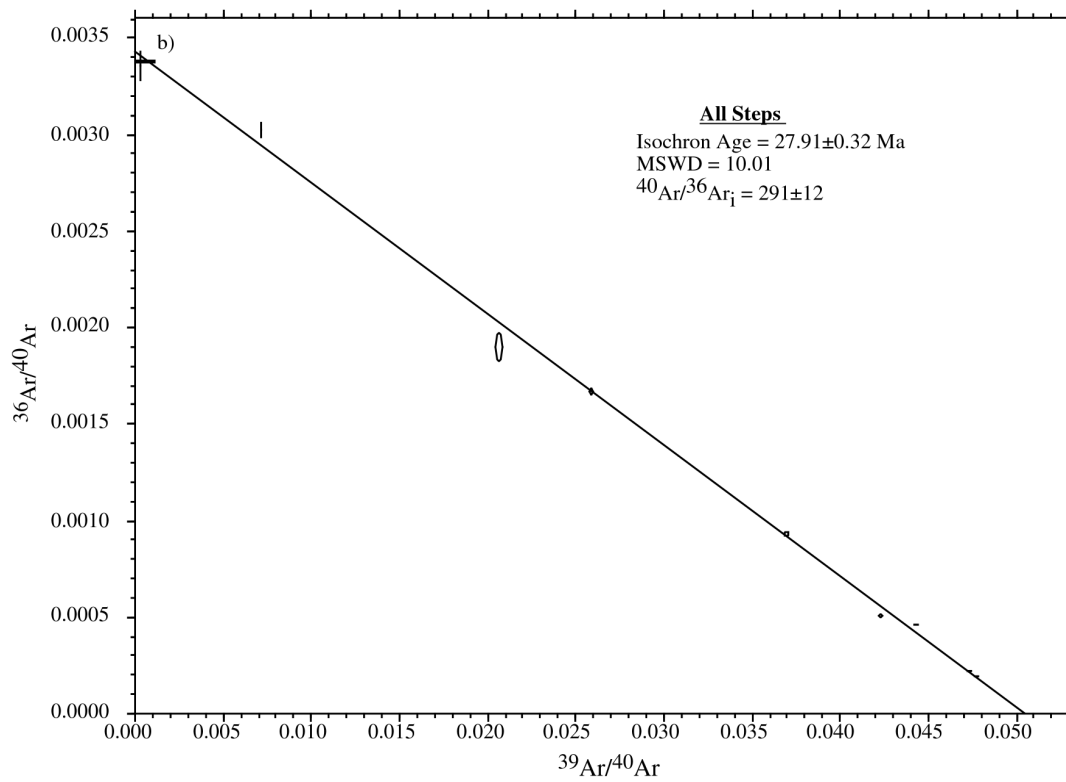
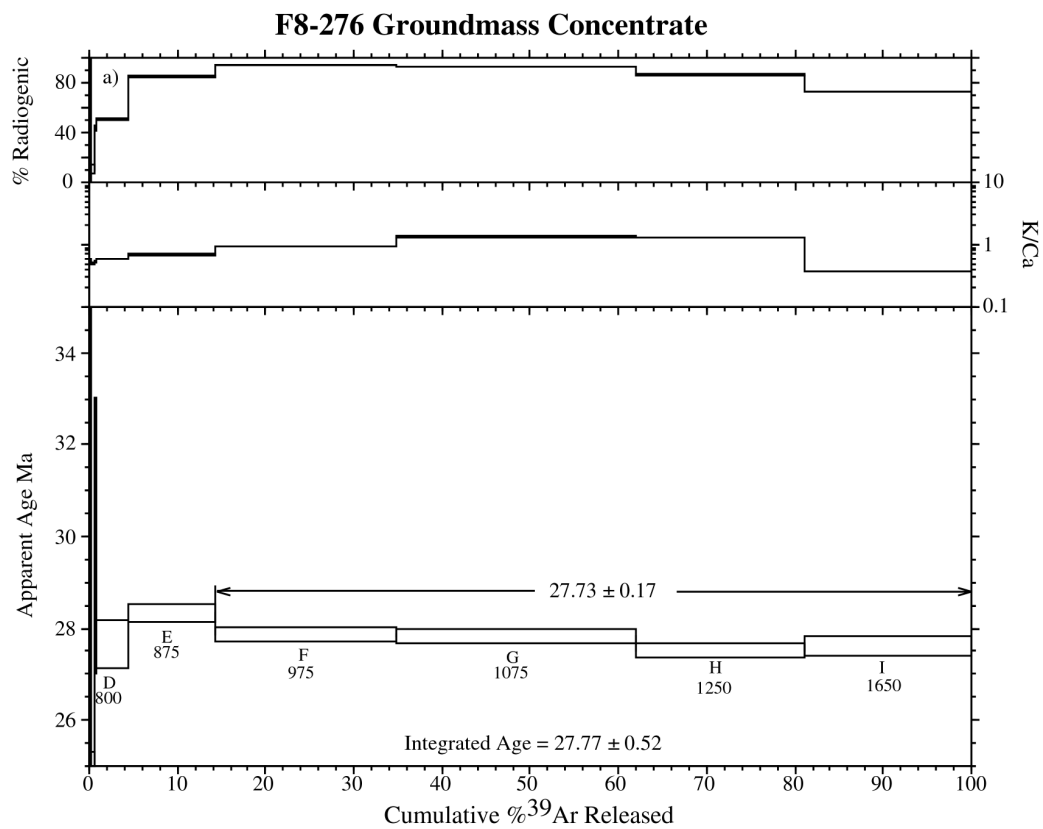


**Figure A5.** Age spectrum (a) and isochron (b) for resistance-furnace  $^{40}\text{Ar}/^{39}\text{Ar}$  of F8-276.

### F8-286 Groundmass Concentrate

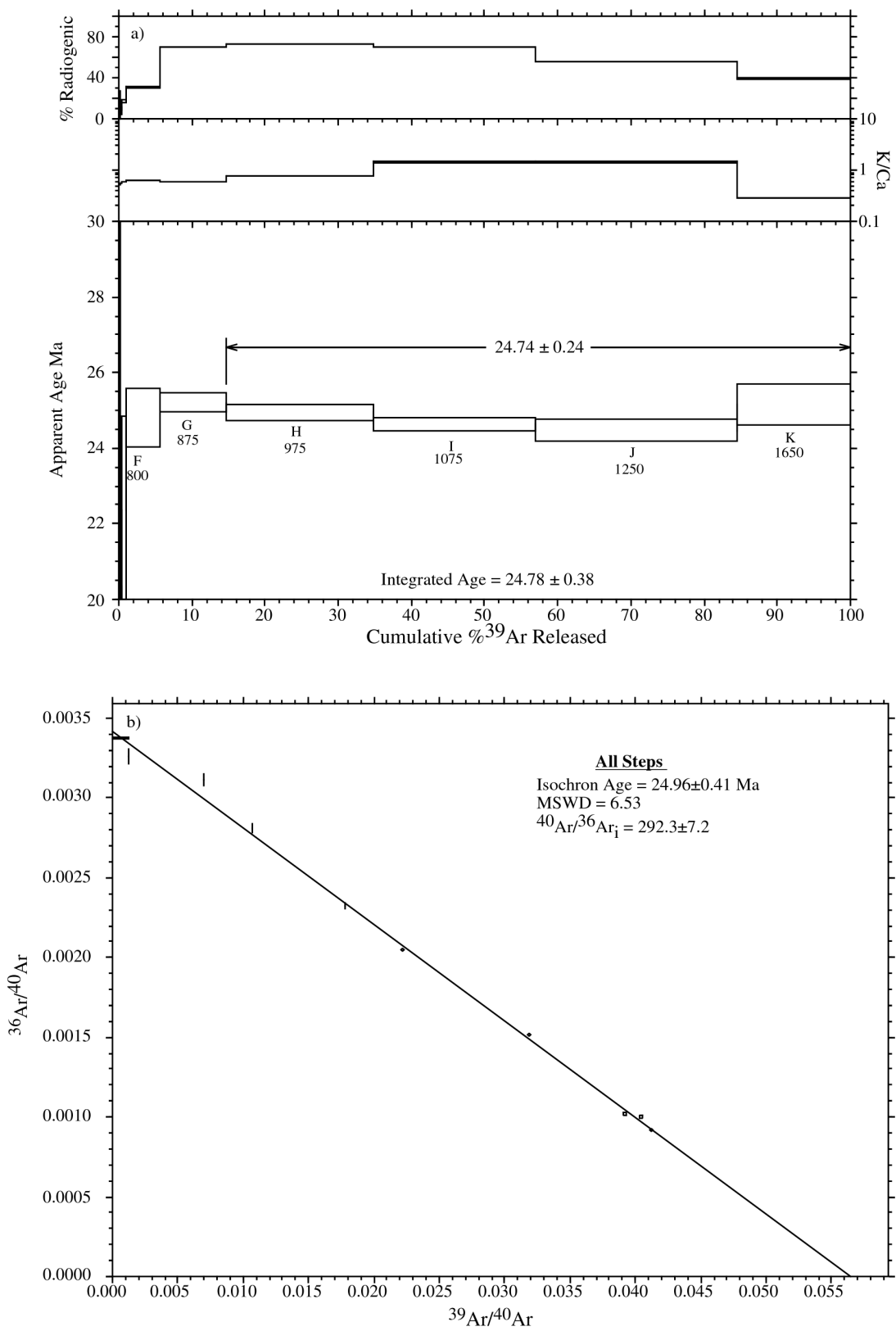


**Figure A6.** Age spectrum (a) and isochron (b) for resistance-furnace <sup>40</sup>Ar/<sup>39</sup>Ar of F8-286.

### F8-301 Groundmass Concentrate

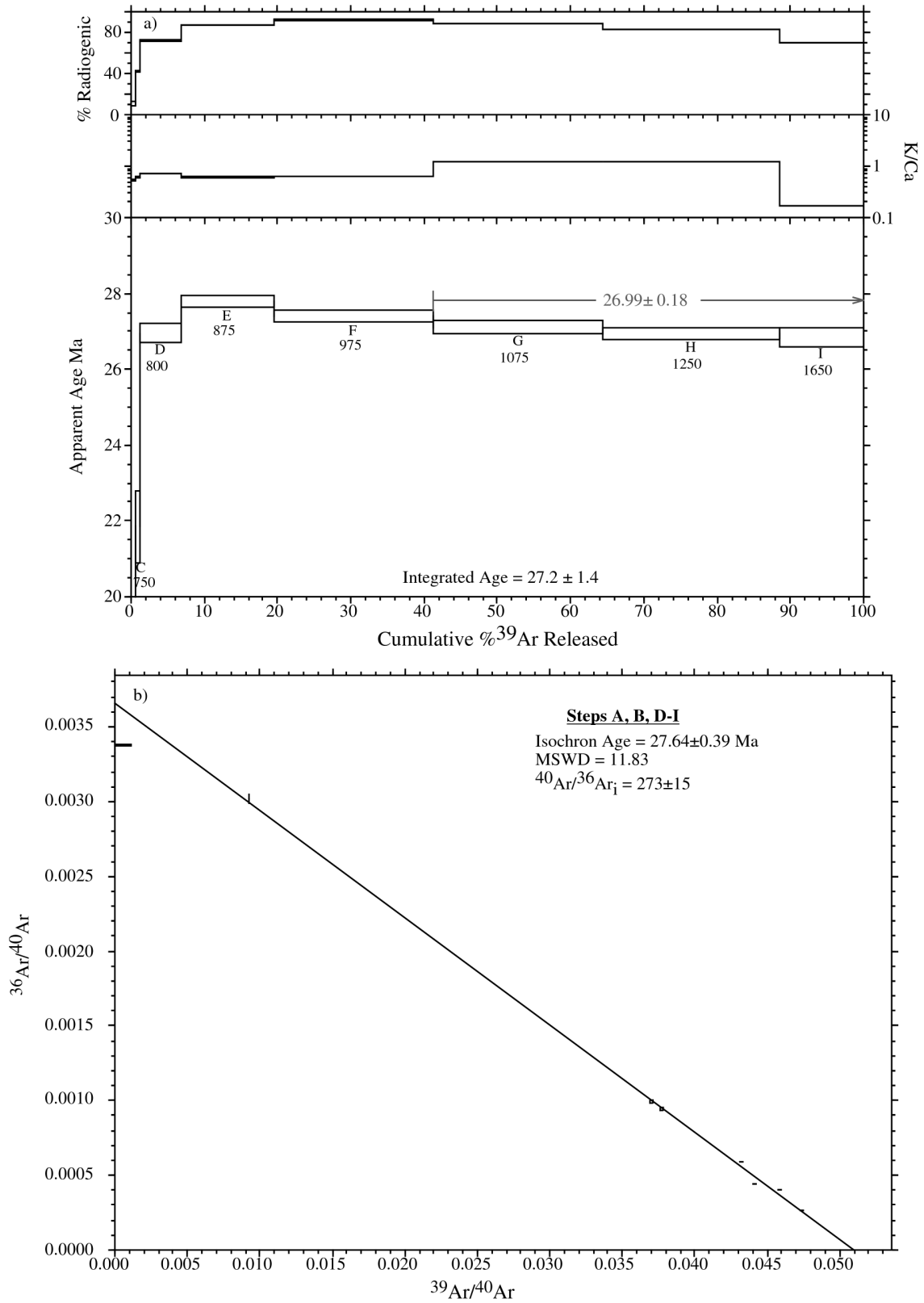


**Figure A7.** Age spectrum (a) and isochron (b) for resistance-furnace  $^{40}\text{Ar}/^{39}\text{Ar}$  of F8-301.

### F8-316 Groundmass Concentrate

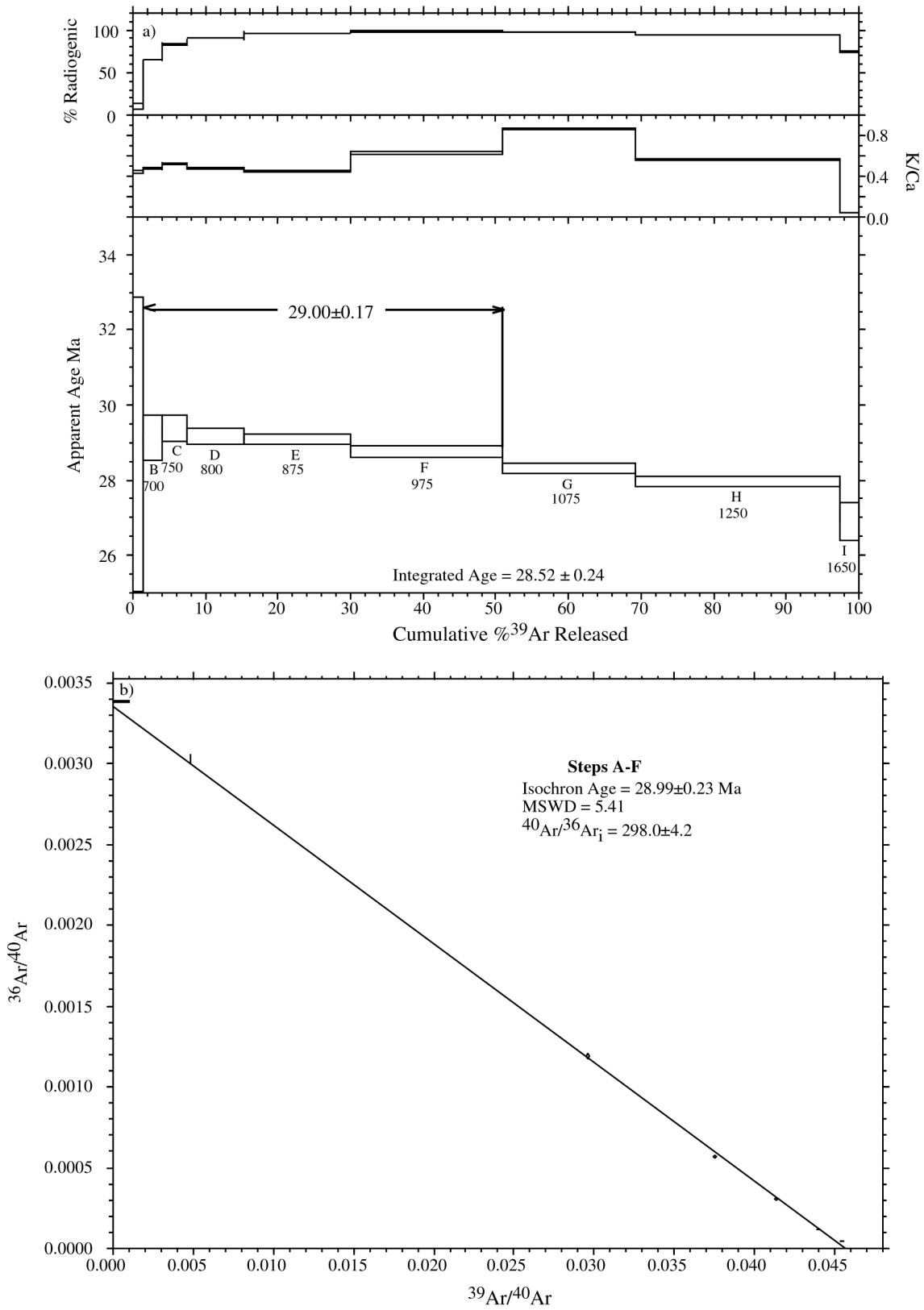


**Figure A8.** Age spectrum (a) and isochron (b) for resistance-furnace  $^{40}\text{Ar}/^{39}\text{Ar}$  of F8-316.

Sample F8-269 and to a lesser extent samples F8-301 and F8-316 yielded disturbed age spectra. In multi-phase samples such as groundmass concentrates,  $^{39}\text{Ar}$  can be displaced during irradiation from high-K phases into lower-K phases, although minor  $^{39}\text{Ar}$  may also be recoiled entirely out of the sample (Lo and Onstott, 1996, McDougall and Harrison, 1988). These recoil effects are illustrated in Figure A9. Recoil of  $^{39}\text{Ar}$  into high-temperature degassing phases, such as pyroxene (which would also have a low K/Ca), will result in high-temperature steps that are younger than early low-temperature steps. This is a possible explanation for the disturbed nature of F8-269 and F8-301. In cases where recoil is suspected, the integrated age is the best estimate for the age of the samples. The integrated ages of F8-269 ( $26.68 \pm 0.70$  Ma), F8-301 ( $27.2 \pm 1.4$  Ma) and F8-316 ( $28.52 \pm 0.24$  Ma) are, therefore, assigned as the preferred ages of these samples. We do caution that our confidence in these dates are not high as our confidence in the ages of the other samples.

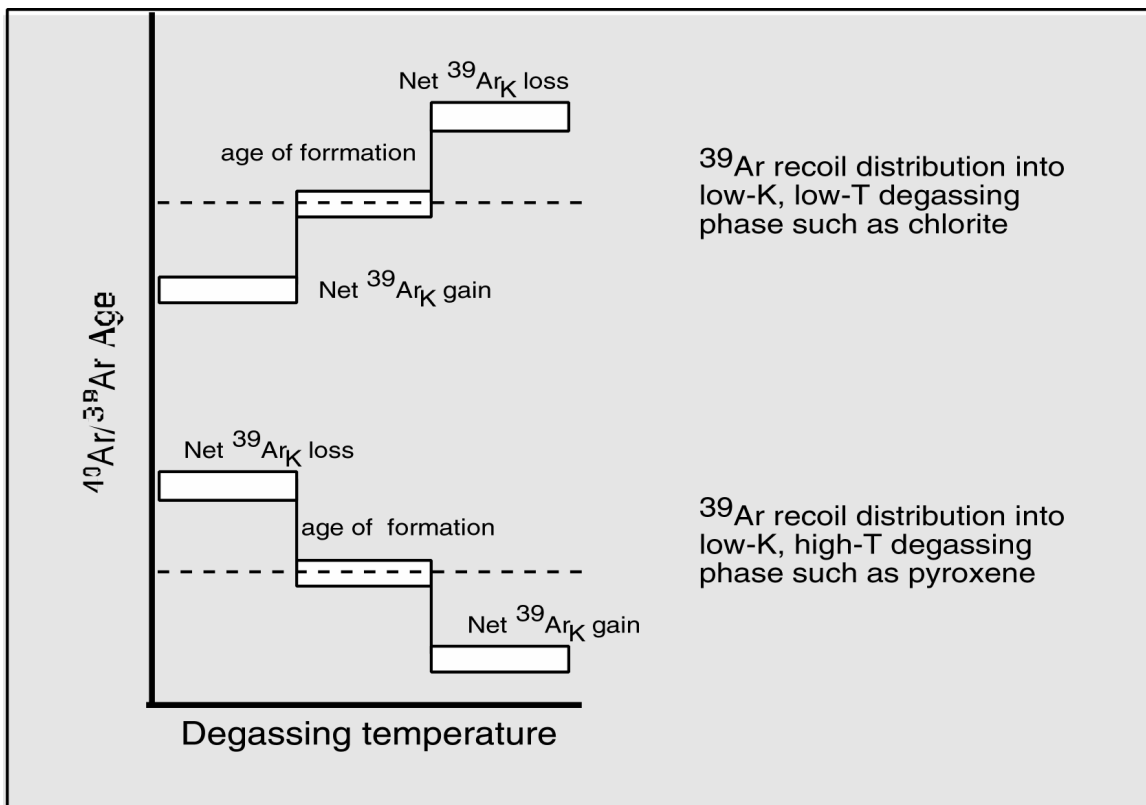


**Figure A9.** Cartoon showing potential effects of  $^{39}\text{Ar}$  recoil on an otherwise flat age spectrum.

## APPENDIX B

### Felsic lava and tuff samples

#### <sup>40</sup>Ar/<sup>39</sup>Ar analytical methods and results

The separated sanidine was analyzed by the laser total fusion method. These age data are displayed on probability distribution diagrams (Deino and Potts, 1992) as Figures B1-B8. Abbreviated analytical methods for the dated samples are given in Table B1, and details of the overall operation of the New Mexico Geochronology Research Laboratory are provided in Appendix D. The argon isotopic results are listed in Table B2 and summarized in Table B3.

Samples F8-277, F8-282, F8-288, F8-289, F8-295, F8-299, F8-302, and F9-165 yield simple gaussian distributions (Figures B1-B8) and all but F8-277 (Figure B1) and F8-299 (Figure B2) have acceptable MSWD values (Mahon, 1996). The errors on the weighted mean ages of those samples with unacceptable MSWD values have been adjusted to account for the high MSWD. The larger errors,  $\pm 2-3\%$ , for samples F8-282 and F8-289 versus  $\pm < 1\%$  for the other samples in this project are due to smaller crystal size and therefore smaller signal size. The preferred age for the eruption of F8-288 is the weighted mean of the pumice sanidine rather than the weighted mean of the matrix sanidine. This age was chosen as it had an acceptable MSWD and smaller error than the matrix sanidine which had an MSWD above the acceptable level.

#### *Discussion*

The interpretation of the data from these sanidine samples is very straightforward. The preferred age of eruption is the weighted mean of all sanidine crystals analyzed from the following samples: F8-277, F8-282, F8-289, F8-288, F8-295, F8-299, F8-302, F9-165 and F9-121. The eruption age of sample F9-167 is the weighted mean age of twelve of the fifteen analyzed crystals.

All ten weighted mean ages are shown on a probability distribution diagram (Figure 5, main text). This age compilation reveals a minimum of 5 eruptive intervals between  $\sim 18$  Ma and 28 Ma. Samples F9-165 ( $28.14 \pm 0.04$  Ma) and F8-277 ( $27.94 \pm 0.09$  Ma) have weighted mean ages similar to the mean age of the Bloodgood Canyon Tuff ( $28.05 \pm 0.04$  Ma, McIntosh et al., 1992).

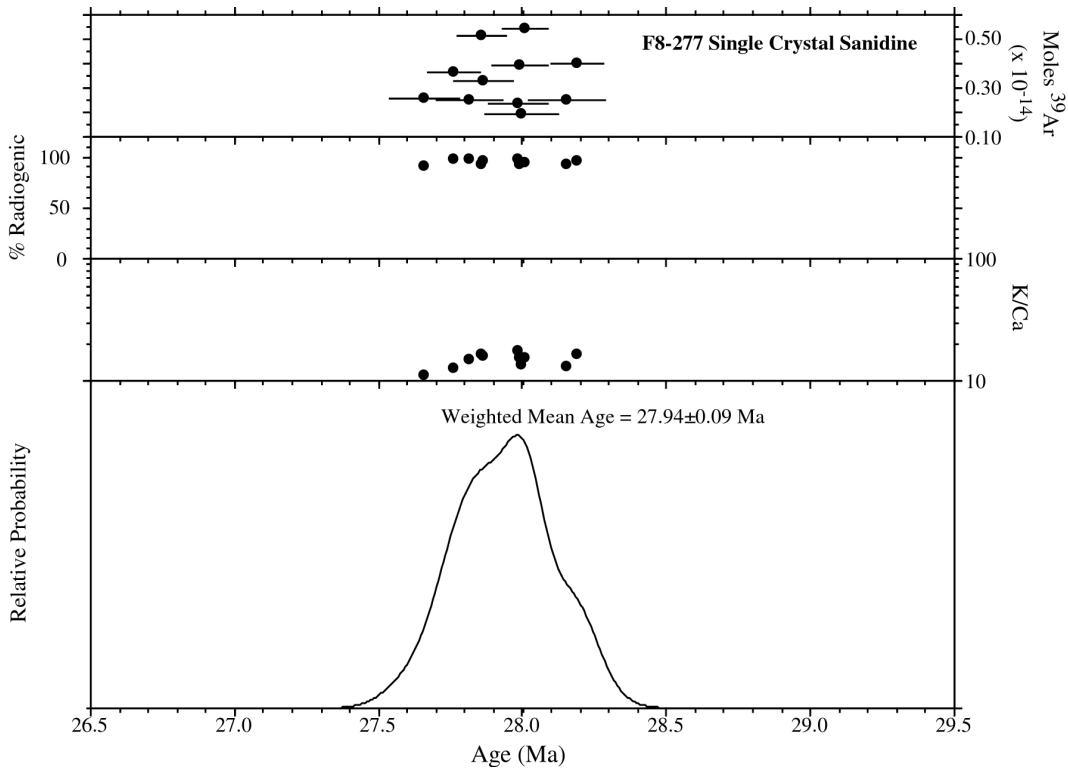


**Figure B1.** Age probability distribution diagram of sample F8-277.

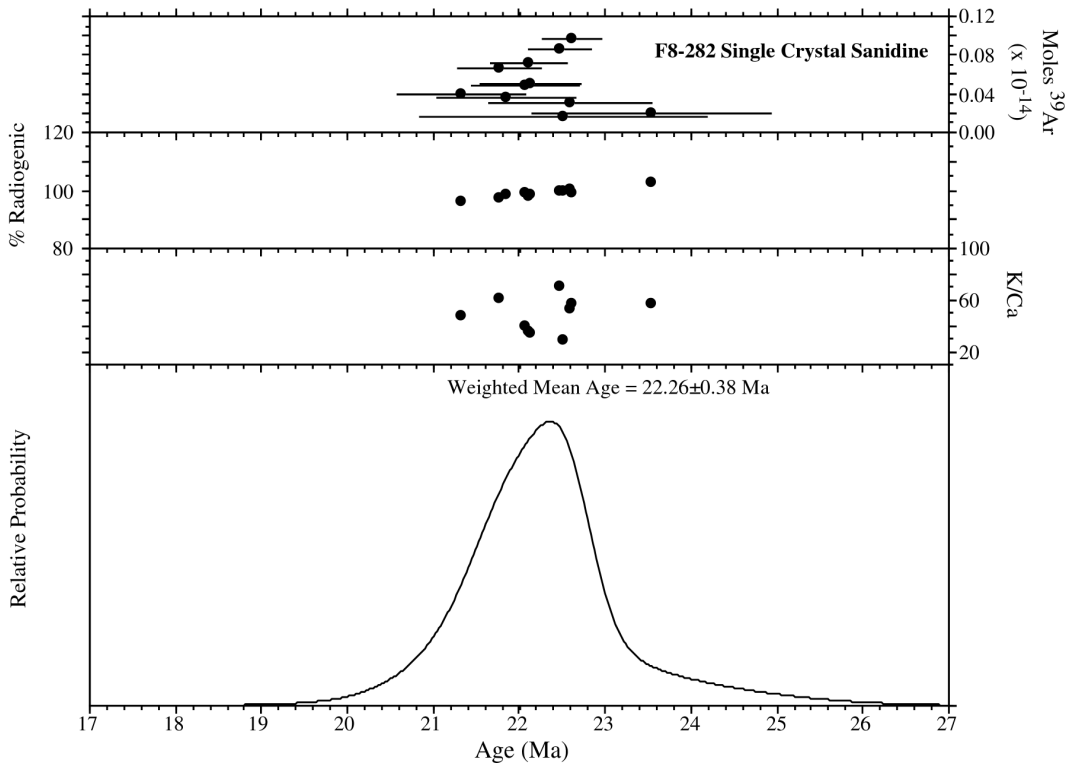


**Figure B2.** Age probability distribution diagram of sample F8-282.

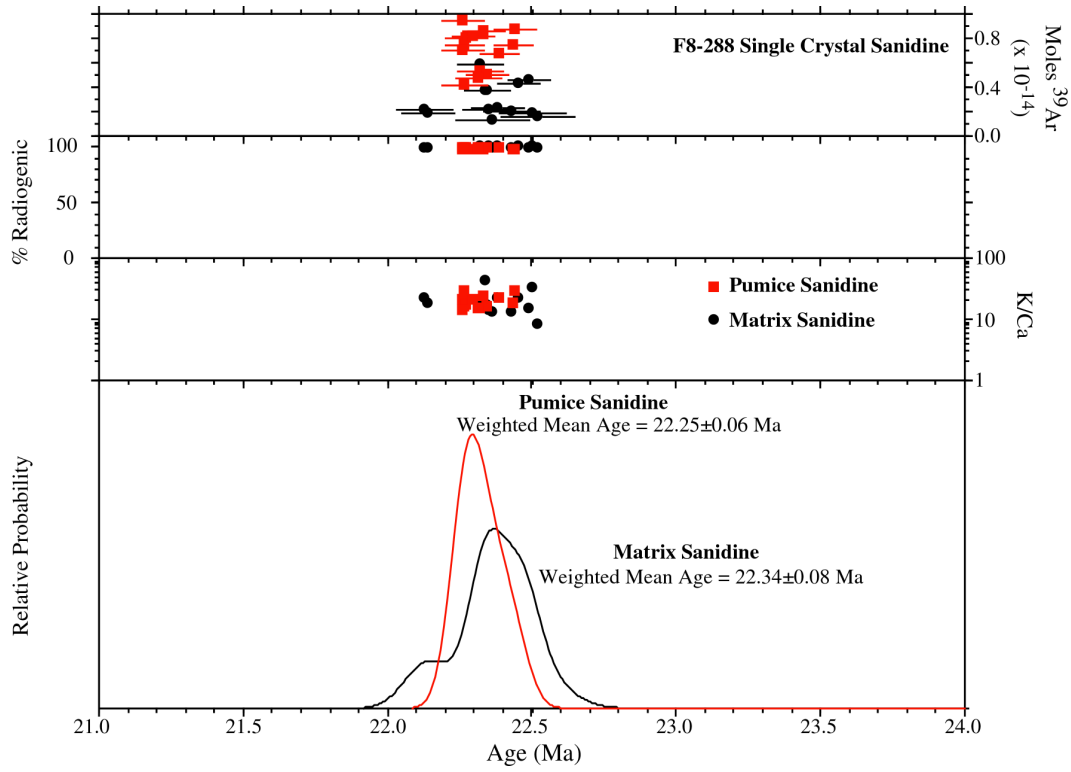


**Figure B3.** Age probability distribution diagram of sample F8-288.

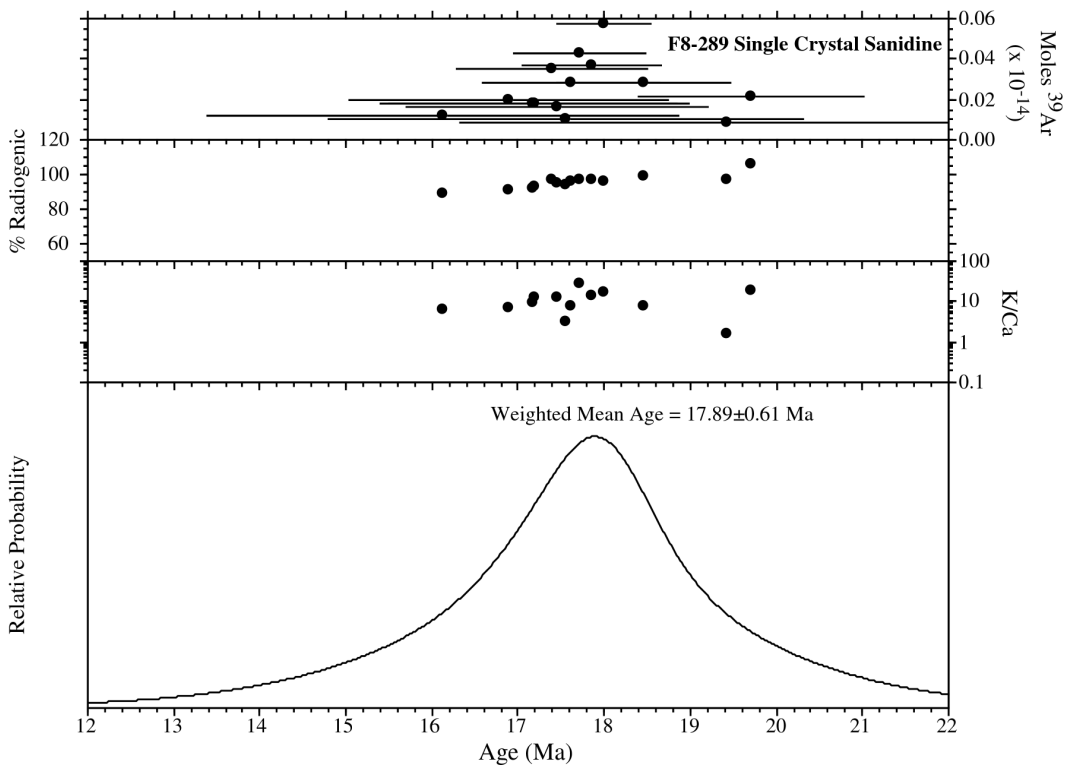


**Figure B4.** Age probability distribution diagram of sample F8-289.

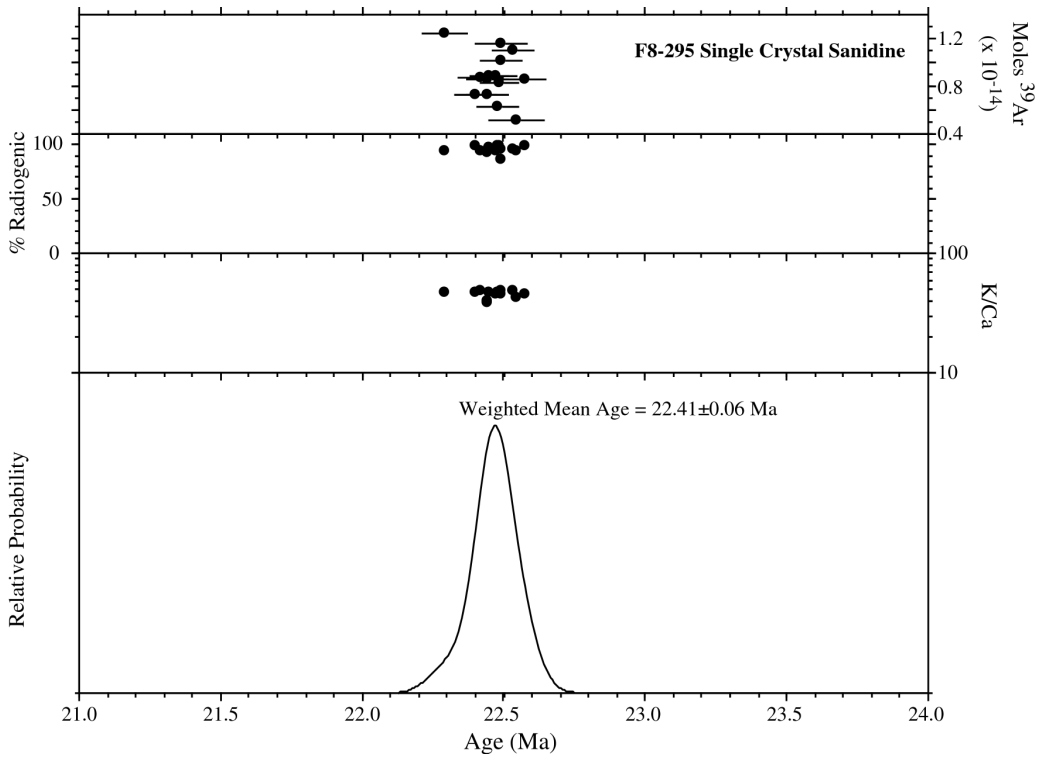


**Figure B5.** Age probability distribution diagram of sample F8-295.

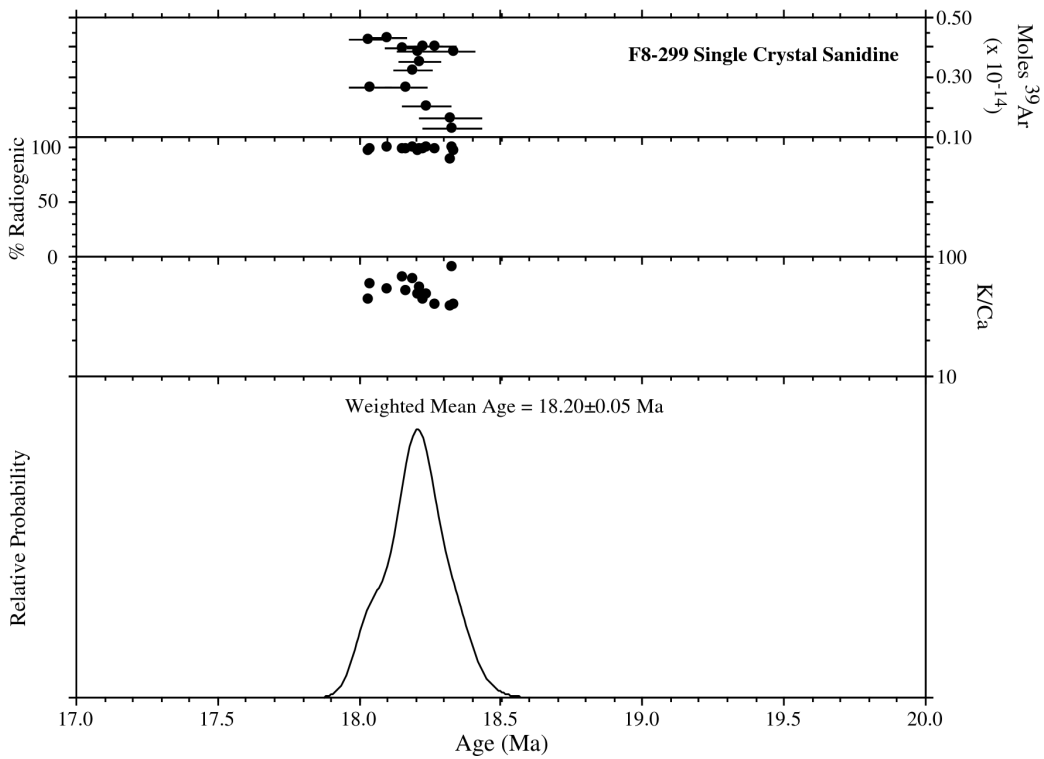


**Figure B6.** Age probability distribution diagram of sample F8-299.

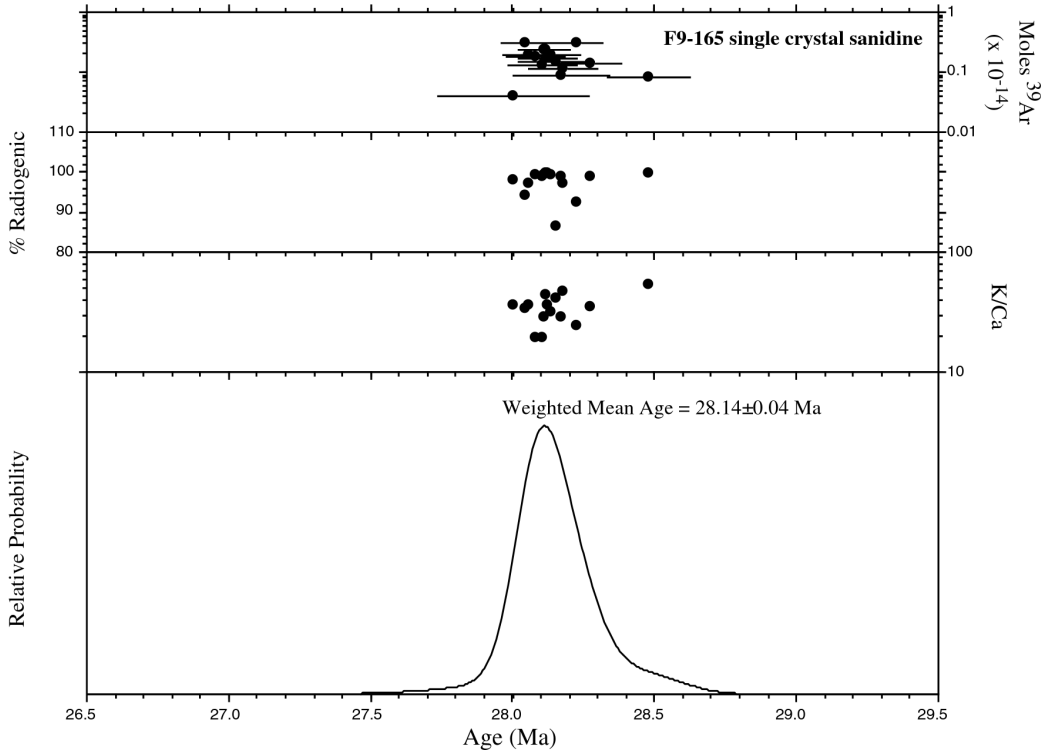


**Figure B7.** Age probability distribution diagram of sample F8-302.

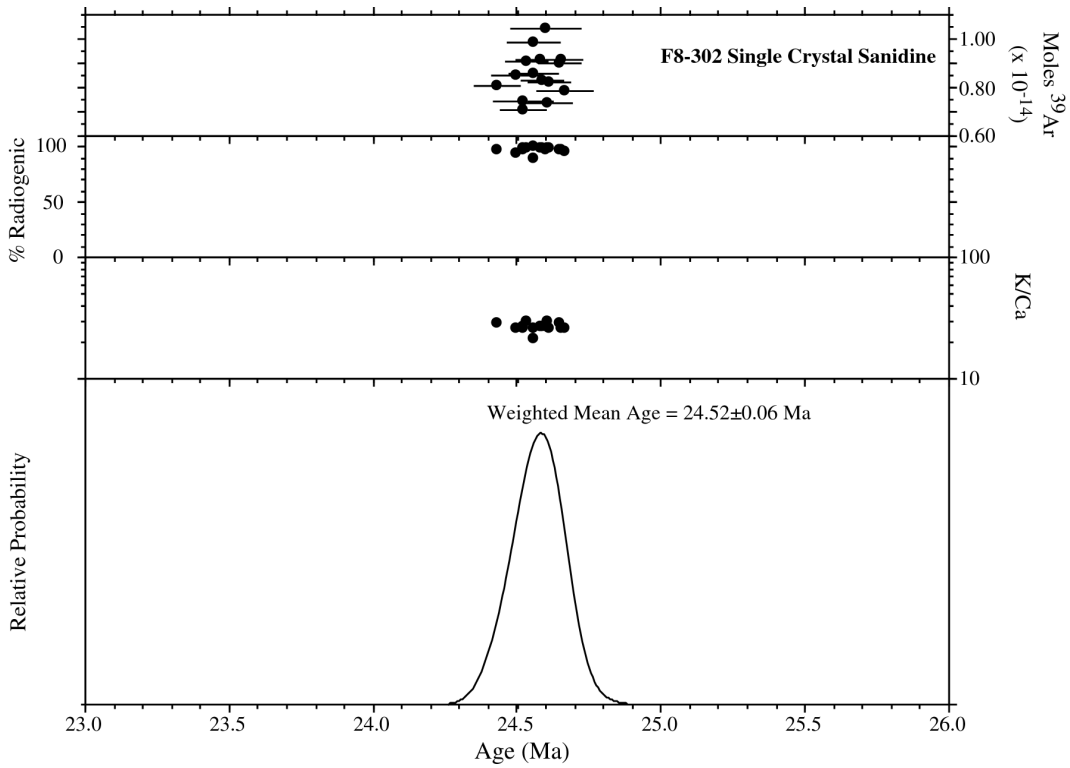


**Figure B8.** Age probability distribution diagram of sample F9-165.

**Table B1.** Abbreviated  $^{40}\text{Ar}/^{39}\text{Ar}$  analytical methods for dated samples.

<b>Sample preparation and irradiation:</b>
<ul style="list-style-type: none"> <li>Mineral phases concentrated by dissolving glass and matrix from the crushed rock in 15% HF. K-feldspar separated with standard heavy liquid, Franz Magnetic and hand-picking techniques.</li> <li>K-feldspars were loaded into a machined Al disc and irradiated for 7 hours in D-3 position, Nuclear Science Center, College Station, TX.</li> <li>Neutron flux monitor Fish Canyon Tuff sanidine (FC-1). Assigned age = 27.84 Ma (Deino and Potts, 1990) relative to Mmhb-1 at 520.4 Ma (Samson and Alexander, 1987).</li> </ul>
<b>Instrumentation:</b>
<ul style="list-style-type: none"> <li>Mass Analyzer Products 215-50 mass spectrometer on line with automated all-metal extraction system.</li> <li>Single crystals were fused by a 10 watt Synrad CO<sub>2</sub> laser.</li> <li>Reactive gases removed during a 2 minute reaction with 2 SAES GP-50 getters, 1 operated at ~450°C and 1 at 20°C. Gas also exposed to a W filament operated at ~2000°C and a cold finger operated at -140°C.</li> </ul>
<b>Analytical parameters:</b>
<ul style="list-style-type: none"> <li>Electron multiplier sensitivity averaged <math>1.68 \times 10^{-16}</math> moles/pA.</li> <li>Total system blank and background averaged 333, 10.0, 0.9, 1.8, <math>1.7 \times 10^{-18}</math> moles.</li> <li>J-factors determined to a precision of <math>\pm 0.1\%</math> by CO<sub>2</sub> laser-fusion of 4 single crystals from each of 4 radial positions around the irradiation tray.</li> <li>Correction factors for interfering nuclear reactions were determined using K-glass and CaF<sub>2</sub> and are as follows: <math>(^{40}\text{Ar}/^{39}\text{Ar})_{\text{K}} = 0.00020 \pm 0.0003</math>; <math>(^{36}\text{Ar}/^{37}\text{Ar})_{\text{Ca}} = 0.00028 \pm 0.000011</math>; and <math>(^{39}\text{Ar}/^{37}\text{Ar})_{\text{Ca}} = 0.00089 \pm 0.00003</math>.</li> </ul>
<b>Age calculations:</b>
<ul style="list-style-type: none"> <li>Weighted mean age calculated by weighting each age analysis by the inverse of the variance.</li> <li>Weighted mean error calculated using the method of (Taylor, 1982).</li> <li>MSWD values calculated for n-1 degrees of freedom.</li> <li>If the MSWD is outside the 95% confidence window (cf. Mahon, 1996; Table 1), the error is multiplied by the square root of the MSWD.</li> <li>Decay constants and isotopic abundances following Steiger and Jäger (1977).</li> <li>All final errors reported at <math>\pm 2\sigma</math>, unless otherwise noted.</li> </ul>

**Table B2.** Results of argon isotopic analysis. Isotopic ratios corrected for blank, radioactive decay, and mass discrimination, not corrected for interfering reactions. Individual analyses show analytical error only; weighted mean age error includes error in J and irradiation parameters. Analyses in *italics* are excluded from mean age calculations.

<b>F8-277, single crystal sanidine, J=0.0007771, NM-105, Lab#=50257</b>								
ID	<sup>40</sup> Ar/ <sup>39</sup> Ar	<sup>37</sup> Ar/ <sup>39</sup> Ar	<sup>36</sup> Ar/ <sup>39</sup> Ar (x 10 <sup>-3</sup> )	<sup>39</sup> Ar <sub>K</sub> (x 10 <sup>-15</sup> mol)	K/Ca	<sup>40</sup> Ar* (%)	Age (Ma)	±1σ (Ma)
06	21.94	0.0459	6.975	2.56	11.1	90.6	27.66	0.10
08	20.43	0.0400	1.640	3.63	12.8	97.6	27.76	0.07
01	20.54	0.0349	1.864	2.47	14.6	97.3	27.81	0.10
11	21.72	0.0311	5.749	5.16	16.4	92.2	27.86	0.07
03	20.71	0.0319	2.316	3.28	16.0	96.7	27.86	0.09
05	20.50	0.0296	1.293	2.35	17.2	98.1	27.99	0.08
02	21.74	0.0329	5.488	3.96	15.5	92.6	27.99	0.08
09	21.33	0.0384	4.101	1.94	13.3	94.3	28.00	0.11
07	21.24	0.0329	3.764	5.44	15.5	94.8	28.01	0.06
10	22.02	0.0386	6.061	2.49	13.2	91.9	28.15	0.12
04	20.99	0.0312	2.468	3.99	16.3	96.5	28.19	0.08
<b>weighted mean</b>								
MSWD = 3.4**			n=11		14.7 ± 1.9		27.94	0.09*
<b>F8-282, single crystal sanidine, J=0.0007771, NM-105, Lab#=50258</b>								
ID	<sup>40</sup> Ar/ <sup>39</sup> Ar	<sup>37</sup> Ar/ <sup>39</sup> Ar	<sup>36</sup> Ar/ <sup>39</sup> Ar (x 10 <sup>-3</sup> )	<sup>39</sup> Ar <sub>K</sub> (x 10 <sup>-15</sup> mol)	K/Ca	<sup>40</sup> Ar* (%)	Age (Ma)	±1σ (Ma)
05	15.91	0.0108	2.050	0.387	47.2	96.2	21.33	0.68
01	16.06	0.0083	1.476	0.665	61.5	97.3	21.77	0.43
02	15.88	0.0000	0.6537	0.363	-	98.8	21.85	0.75
09	16.01	0.0128	0.6043	0.478	39.8	98.9	22.07	0.56
14	16.24	0.0144	1.289	0.719	35.5	97.7	22.11	0.38
03	16.17	0.0152	0.9787	0.509	33.5	98.2	22.12	0.53
04	16.21	0.0073	0.2771	0.858	70.1	99.5	22.47	0.31
11	16.21	0.0175	0.1953	0.167	29.1	99.7	22.51	1.61
10	16.20	0.0095	-0.0474	0.304	53.6	100.1	22.59	0.88
13	16.38	0.0090	0.4914	0.975	56.9	99.1	22.61	0.29
12	16.47	0.0089	-1.4593	0.202	57.1	102.6	23.55	1.33
<b>weighted mean</b>								
MSWD = 0.69			n=11		48.4 ± 12.9		22.26	0.38*

**Table B2 (cont.).** Argon isotopic laser data.

<b>F8-288 matrix, single crystal sanidine, J=0.0007431, NM-103, Lab#=50117</b>								
ID	<sup>40</sup> Ar/ <sup>39</sup> Ar	<sup>37</sup> Ar/ <sup>39</sup> Ar	<sup>36</sup> Ar/ <sup>39</sup> Ar (x 10 <sup>-3</sup> )	<sup>39</sup> Ar <sub>K</sub> (x 10 <sup>-15</sup> mol)	K/Ca	<sup>40</sup> Ar* (%)	Age (Ma)	±1σ (Ma)
11	16.69	0.0225	0.3636	1.90	22.7	99.4	22.10	0.08
12	16.80	0.0286	0.7106	1.60	17.8	98.8	22.11	0.07
08	16.74	0.0263	0.0561	5.18	19.4	99.9	22.29	0.06
13	16.80	0.0124	0.2080	3.29	41.2	99.6	22.31	0.05
04	16.81	0.0303	0.2307	3.30	16.8	99.6	22.32	0.06
14	16.76	0.0363	0.0471	1.97	14.1	99.9	22.32	0.07
15	16.92	0.0388	0.5669	1.16	13.2	99.0	22.33	0.11
05	16.75	0.0236	-0.0571	1.99	21.6	100.1	22.35	0.07
01	16.95	0.0402	0.5026	1.77	12.7	99.1	22.40	0.08
02	16.81	0.0236	-0.0304	3.83	21.6	100.1	22.42	0.05
07	16.92	0.0336	0.2529	4.08	15.2	99.6	22.45	0.05
06	16.78	0.0160	-0.2697	1.67	31.8	100.5	22.47	0.09
09	17.02	0.0621	0.4954	1.41	8.2	99.2	22.49	0.11
10	14.18	0.0408	-13.1439	0.013	12.5	127.4	24.07	4.04
03	1190.2	6.326	2678.2	0.001	0.081	33.5	471	2072
<b>weighted mean</b> MSWD = 2.7**      n=14					19.2 ± 8.6		22.34	0.08*
<b>F8-288 pumice, single crystal sanidine, J=0.0007416, NM-103, Lab#=50119</b>								
ID	<sup>40</sup> Ar/ <sup>39</sup> Ar	<sup>37</sup> Ar/ <sup>39</sup> Ar	<sup>36</sup> Ar/ <sup>39</sup> Ar (x 10 <sup>-3</sup> )	<sup>39</sup> Ar <sub>K</sub> (x 10 <sup>-15</sup> mol)	K/Ca	<sup>40</sup> Ar* (%)	Age (Ma)	±1σ (Ma)
05	16.89	0.0231	0.7176	0.758	22.1	98.8	22.18	0.13
01	16.80	0.0242	0.3922	8.42	21.1	99.3	22.18	0.05
11	17.00	0.0357	1.067	6.25	14.3	98.2	22.19	0.05
02	16.81	0.0328	0.4091	6.58	15.5	99.3	22.19	0.05
14	16.92	0.0174	0.7804	3.66	29.3	98.6	22.19	0.06
06	16.99	0.0293	1.030	7.18	17.4	98.2	22.20	0.05
10	17.12	0.0249	1.376	7.27	20.5	97.6	22.22	0.05
13	16.80	0.0336	0.2811	4.16	15.2	99.5	22.24	0.06
09	16.93	0.0339	0.6777	4.75	15.1	98.8	22.25	0.06
04	17.15	0.0220	1.412	7.60	23.1	97.6	22.26	0.06
12	16.94	0.0312	0.6563	4.44	16.3	98.9	22.27	0.05
08	16.97	0.0238	0.6665	6.02	21.4	98.9	22.31	0.05
15	17.17	0.0282	1.234	6.57	18.1	97.9	22.36	0.05
03	17.25	0.0182	1.458	7.70	28.0	97.5	22.36	0.05
07	17.06	0.0319	0.6091	0.533	16.0	99.0	22.45	0.18
<b>weighted mean</b> MSWD = 1.5      n=15					19.6 ± 4.7		22.25	0.06*

**Table B2 (cont.).** Argon isotopic laser data.

**F8-289, single crystal sanidine, J=0.0007792, NM-105, Lab#=50262**

ID	<sup>40</sup> Ar/ <sup>39</sup> Ar	<sup>37</sup> Ar/ <sup>39</sup> Ar	<sup>36</sup> Ar/ <sup>39</sup> Ar (x 10 <sup>-3</sup> )	<sup>39</sup> Ar <sub>K</sub> (x 10 <sup>-15</sup> mol)	K/Ca	<sup>40</sup> Ar* (%)	Age (Ma)	±1σ (Ma)
12	12.89	0.0810	4.654	0.124	6.3	89.4	16.13	2.68
13	13.27	0.0713	4.098	0.196	7.2	90.9	16.88	1.79
09	13.38	0.0533	3.779	0.180	9.6	91.7	17.17	1.60
11	13.16	0.0386	2.976	0.179	13.2	93.3	17.19	1.74
14	12.86	0.0000	1.444	0.355	-	96.7	17.39	1.05
08	13.18	0.0421	2.400	0.167	12.1	94.6	17.46	1.69
04	13.31	0.1613	2.667	0.100	3.2	94.2	17.54	2.70
06	13.12	0.0665	1.821	0.280	7.7	95.9	17.62	0.97
10	13.04	0.0189	1.277	0.431	27.1	97.1	17.72	0.70
07	13.11	0.0368	1.163	0.370	13.9	97.4	17.86	0.75
05	13.34	0.0307	1.630	0.575	16.6	96.4	17.99	0.47
03	13.30	0.0659	0.3853	0.287	7.7	99.2	18.46	0.94
01	14.35	0.3201	1.624	0.089	1.6	96.8	19.43	3.03
02	13.25	0.0266	-2.8459	0.218	19.2	106.4	19.70	1.24
<b>weighted mean</b>								
MSWD = 0.34		n=14			11.2 ± 6.7		17.89	0.61*

**F8-295, single crystal sanidine, J=0.0007423, NM-103, Lab#=50118**

ID	<sup>40</sup> Ar/ <sup>39</sup> Ar	<sup>37</sup> Ar/ <sup>39</sup> Ar	<sup>36</sup> Ar/ <sup>39</sup> Ar (x 10 <sup>-3</sup> )	<sup>39</sup> Ar <sub>K</sub> (x 10 <sup>-15</sup> mol)	K/Ca	<sup>40</sup> Ar* (%)	Age (Ma)	±1σ (Ma)
03	17.63	0.0110	3.125	12.5	46.6	94.8	22.24	0.06
12	17.08	0.0109	0.9968	7.22	46.9	98.3	22.34	0.05
09	17.75	0.0104	3.214	8.75	48.9	94.7	22.36	0.06
05	17.71	0.0132	3.041	8.59	38.6	94.9	22.38	0.05
06	18.05	0.0130	4.154	7.32	39.4	93.2	22.38	0.05
13	17.30	0.0110	1.600	8.91	46.4	97.3	22.39	0.05
10	17.74	0.0111	3.057	8.85	45.9	94.9	22.41	0.05
15	17.04	0.0110	0.6710	6.32	46.5	98.8	22.42	0.05
08	17.02	0.0107	0.5934	8.29	47.6	99.0	22.42	0.05
11	17.48	0.0106	2.110	10.1	48.0	96.4	22.43	0.05
02	19.40	0.0112	8.615	11.6	45.5	86.9	22.43	0.07
01	17.69	0.0105	2.722	11.1	48.6	95.5	22.47	0.05
14	17.94	0.0118	3.538	5.15	43.1	94.2	22.49	0.07
04	16.98	0.0113	0.2086	8.51	45.2	99.6	22.52	0.05
<b>weighted mean</b>								
MSWD = 1.4		n=14			45.5 ± 3.1		22.41	0.06*

**Table B2 (cont.).** Argon isotopic laser data.

<b>F8-299, single crystal sanidine, J=0.0007412, NM-103, Lab#=50120</b>								
ID	<sup>40</sup> Ar/ <sup>39</sup> Ar	<sup>37</sup> Ar/ <sup>39</sup> Ar	<sup>36</sup> Ar/ <sup>39</sup> Ar (x 10 <sup>-3</sup> )	<sup>39</sup> Ar <sub>K</sub> (x 10 <sup>-15</sup> mol)	K/Ca	<sup>40</sup> Ar* (%)	Age (Ma)	±1σ (Ma)
04	13.93	0.0118	1.221	4.23	43.3	97.4	18.06	0.05
01	13.66	0.0085	0.2922	2.65	59.8	99.4	18.06	0.05
05	13.64	0.0095	0.0605	4.29	53.5	99.9	18.12	0.05
06	13.71	0.0077	0.1706	4.00	66.4	99.6	18.17	0.04
03	13.74	0.0099	0.2592	2.68	51.3	99.4	18.19	0.05
10	13.71	0.0077	0.0778	3.21	66.2	99.8	18.21	0.05
14	14.13	0.0106	1.468	3.85	48.3	96.9	18.22	0.05
15	13.74	0.0091	0.1299	3.52	55.8	99.7	18.23	0.05
11	13.77	0.0117	0.2098	4.00	43.7	99.6	18.24	0.04
12	13.68	0.0104	-0.1139	2.04	48.9	100.3	18.25	0.06
09	13.95	0.0126	0.7164	4.02	40.4	98.5	18.28	0.05
13	15.29	0.0130	5.111	1.61	39.1	90.1	18.34	0.09
07	13.73	0.0062	-0.2028	1.31	82.0	100.4	18.34	0.08
08	14.15	0.0127	1.230	3.83	40.2	97.4	18.35	0.05
02	16.81	0.0502	1.262	1.40	10.2	97.8	21.86	0.11
<b>weighted mean</b> MSWD = 2.9**      n=14					52.8 ± 12.3		18.20	0.05*
<b>F8-302, single crystal sanidine, J=0.0007441, NM-103, Lab#=50116</b>								
ID	<sup>40</sup> Ar/ <sup>39</sup> Ar	<sup>37</sup> Ar/ <sup>39</sup> Ar	<sup>36</sup> Ar/ <sup>39</sup> Ar (x 10 <sup>-3</sup> )	<sup>39</sup> Ar <sub>K</sub> (x 10 <sup>-15</sup> mol)	K/Ca	<sup>40</sup> Ar* (%)	Age (Ma)	±1σ (Ma)
07	18.81	0.0180	1.791	8.11	28.4	97.2	24.38	0.06
14	19.59	0.0195	4.265	8.51	26.1	93.6	24.45	0.07
09	18.86	0.0195	1.723	7.44	26.1	97.3	24.47	0.08
05	18.39	0.0187	0.1396	7.07	27.2	99.8	24.47	0.06
11	18.67	0.0172	1.042	9.09	29.6	98.4	24.49	0.05
15	18.39	0.0195	0.0489	8.58	26.1	99.9	24.51	0.06
10	20.53	0.0241	7.273	9.84	21.2	89.5	24.51	0.07
03	18.69	0.0189	0.9970	9.15	27.0	98.4	24.53	0.06
01	18.49	0.0192	0.2954	8.30	26.6	99.5	24.54	0.05
13	18.90	0.0191	1.651	10.4	26.7	97.4	24.55	0.10
04	18.49	0.0174	0.2501	7.39	29.3	99.6	24.55	0.07
08	18.48	0.0195	0.2181	8.18	26.1	99.7	24.56	0.05
12	18.79	0.0178	1.193	9.00	28.6	98.1	24.59	0.05
02	18.88	0.0199	1.465	9.14	25.7	97.7	24.60	0.06
06	19.17	0.0198	2.410	7.87	25.8	96.3	24.62	0.08
<b>weighted mean</b> MSWD = 1.0      n=15					26.7 ± 2.0		24.52	0.06*

**Table B2 (cont.).** Argon isotopic laser data.

<b>F9-121, single crystal sanidine, J=0.0007644, NM-123, Lab#=51225</b>								
ID	<sup>40</sup> Ar/ <sup>39</sup> Ar	<sup>37</sup> Ar/ <sup>39</sup> Ar	<sup>36</sup> Ar/ <sup>39</sup> Ar (x 10 <sup>-3</sup> )	<sup>39</sup> Ar <sub>K</sub> (x 10 <sup>-15</sup> mol)	K/Ca	<sup>40</sup> Ar* (%)	Age (Ma)	±1σ (Ma)
12	16.54	0.0133	0.4579	3.14	38.5	99.2	22.49	0.04
10	17.07	0.0112	2.212	4.49	45.5	96.2	22.50	0.04
06	16.57	0.0125	0.4543	2.30	40.7	99.2	22.53	0.07
11	16.59	0.0148	0.5113	2.79	34.4	99.1	22.54	0.06
07	16.83	0.0109	1.055	3.62	47.0	98.2	22.64	0.05
09	16.87	0.0146	1.130	4.51	35.0	98.0	22.66	0.04
01	16.56	0.0114	0.0548	2.88	44.8	99.9	22.68	0.05
08	16.71	0.0156	0.5553	2.26	32.8	99.0	22.68	0.06
02	16.80	0.0164	0.8371	2.31	31.2	98.5	22.69	0.06
03	16.99	0.0147	1.466	4.24	34.7	97.5	22.70	0.05
13	17.41	0.0127	2.877	4.18	40.3	95.1	22.70	0.05
05	16.91	0.0115	1.145	5.34	44.3	98.0	22.71	0.05
04	16.85	0.0140	0.7945	3.76	36.3	98.6	22.77	0.05
14	19.02	0.0119	8.025	4.88	42.8	87.5	22.81	0.06
<b>weighted mean</b>								
MSWD =3.8**		n=14			39.2 ± 5.2		22.64	0.05*

<b>F9-165, single crystal sanidine, J=0.0007648, NM-123, Lab#=51224</b>								
ID	<sup>40</sup> Ar/ <sup>39</sup> Ar	<sup>37</sup> Ar/ <sup>39</sup> Ar	<sup>36</sup> Ar/ <sup>39</sup> Ar (x 10 <sup>-3</sup> )	<sup>39</sup> Ar <sub>K</sub> (x 10 <sup>-15</sup> mol)	K/Ca	<sup>40</sup> Ar* (%)	Age (Ma)	±1σ (Ma)
08	20.87	0.0142	1.425	0.403	36.0	98.0	28.00	0.25
14	21.78	0.0149	4.375	3.15	34.3	94.1	28.05	0.07
06	21.13	0.0144	2.176	1.87	35.5	97.0	28.06	0.07
02	20.63	0.0262	0.4132	1.83	19.5	99.4	28.08	0.08
04	20.79	0.0261	0.9136	1.26	19.6	98.7	28.10	0.10
10	20.67	0.0176	0.4750	2.40	29.0	99.3	28.11	0.07
11	20.63	0.0115	0.3202	2.30	44.6	99.5	28.12	0.07
12	20.61	0.0140	0.2405	1.74	36.4	99.7	28.12	0.08
03	20.74	0.0159	0.6402	1.94	32.0	99.1	28.14	0.09
15	23.77	0.0126	10.85	1.47	40.5	86.5	28.16	0.11
01	20.82	0.0176	0.8396	0.891	29.1	98.8	28.17	0.15
07	21.18	0.0107	2.044	1.16	47.7	97.2	28.18	0.10
09	22.32	0.0209	5.795	3.14	24.4	92.3	28.22	0.07
05	20.87	0.0146	0.7415	1.35	35.0	99.0	28.27	0.09
13	20.84	0.0096	0.1409	0.833	53.1	99.8	28.48	0.12
<b>weighted mean</b>								
MSWD =1.1		n=15			34.4 ± 9.6		28.14	0.04*

**Table B2 (cont.).** Argon isotopic laser data.

<b>F9-167, single crystal sanidine, J=0.0007640, NM-123, Lab#=51226</b>								
ID	<sup>40</sup> Ar/ <sup>39</sup> Ar	<sup>37</sup> Ar/ <sup>39</sup> Ar	<sup>36</sup> Ar/ <sup>39</sup> Ar (x 10 <sup>-3</sup> )	<sup>39</sup> Ar <sub>K</sub> (x 10 <sup>-15</sup> mol)	K/Ca	<sup>40</sup> Ar* (%)	Age (Ma)	±1σ (Ma)
08	18.75	0.0121	0.4054	2.31	42.0	99.4	25.50	0.06
03	18.83	0.0162	0.5420	1.83	31.4	99.2	25.56	0.07
07	18.89	0.0132	0.5345	4.54	38.6	99.2	25.64	0.05
15	18.95	0.0084	0.6952	1.68	60.6	98.9	25.66	0.08
06	18.89	0.0115	0.4192	1.65	44.5	99.3	25.68	0.07
04	18.86	0.0116	0.3336	1.89	44.0	99.5	25.68	0.08
14	18.93	0.0134	0.5488	3.77	38.0	99.1	25.69	0.05
05	19.73	0.0153	3.047	3.76	33.3	95.4	25.77	0.06
01	19.08	0.0139	0.8230	2.23	36.6	98.7	25.78	0.06
10	18.90	0.0124	0.2152	1.43	41.2	99.7	25.78	0.08
11	18.88	0.0127	-0.1718	1.88	40.3	100.3	25.91	0.06
02	18.17	4.748	-1.4397	0.073	0.11	104.5	26.09	1.13
12	18.81	0.0142	-1.4365	0.646	36.0	102.3	26.33	0.13
13	18.99	0.0102	-1.7489	0.659	50.1	102.7	26.70	0.13
09	50.41	0.0151	1.610	1.09	33.8	99.1	67.55	0.16
<b>weighted mean</b>								
MSWD =2.9**			n=12		37.5 ± 13.9		25.69	0.05*

K/Ca = molar ratio calculated from reactor produced <sup>39</sup>Ar<sub>K</sub> and <sup>37</sup>Ar<sub>Ca</sub>.  
n= number of analyses used for weighted mean calculation.  
\* 2s error      \*\* MSWD outside of 95% confidence interval

**Table B3.** Table B3 Summary table of the eruption ages assigned to the Morenci Project samples dated with single crystal sanidine.

Sample	L#	Irrad	mineral	analysis	n	K/Ca	±2σ	Age	±2σ	MSWD
F8-277	50257	NM-105	single crystal sanidine	laser fusion	11	14.7	1.9	27.94	0.09*	3.4**
F8-282	50258	NM-105	single crystal sanidine	laser fusion	11	48.4	12.9	22.26	0.38*	0.69
F8-288	50117	NM-103	single crystal sanidine	laser fusion	14	19.2	8.6	22.34	0.08*	2.7**
F8-288	50119	NM-103	single crystal sanidine	laser fusion	15	19.6	4.7	22.25	0.06*	1.5
F8-289	50262	NM-105	single crystal sanidine	laser fusion	14	11.2	6.7	17.89	0.61*	0.34
F8-295	50118	NM-103	single crystal sanidine	laser fusion	14	45.5	3.1	22.41	0.06*	1.4
F8-299	50120	NM-103	single crystal sanidine	laser fusion	14	52.8	12.3	18.20	0.05*	2.9**
F8-302	50116	NM-103	single crystal sanidine	laser fusion	15	26.7	2.0	24.52	0.06*	1.0
F9-121	51225	NM-123	single crystal sanidine	laser fusion	14	39.2	5.2	22.64	0.05*	3.8**
F9-165	51224	NM-123	single crystal sanidine	laser fusion	15	34.4	9.6	28.14	0.04*	1.1
F9-167	51226	NM-123	single crystal sanidine	laser fusion	12	37.5	13.9	25.69	0.05*	2.9**

\* 2s error      \*\* MSWD outside 95% confidence level

## APPENDIX C: EVALUATING SAMPLES FOR SUITABILITY OF ANALYSIS

### Rhyolite

Thirteen samples of rhyolite lava and tuff from the Enebro Mountain Formation were submitted for single crystal total laser fusion analysis. Although very crystal-poor, all of the samples were judged in the field to have small feldspar phenocrysts. Subsequently all but one of these samples were found to be barren with respect to sanidine phenocrysts. The locations of these samples is given in Table C1.

**Table C1.** Location of barren (with respect to sanidine phenocrysts) rhyolite lava and tuff samples, Morenci area. UTM grid zone 12. F8-312 is a collection of pumice clasts gathered from three locations along a long outcrop.

Sample	UTM N	UTM E
19	3638775	649450
F8-260	3669340	654850
F8-262	3669665	651845
F8-263	3670710	652090
F8-264	3671400	650825
F8-267	3672825	650500
F8-283	3667035	660835
F8-304	3674450	661080
F8-305	3674335	660875
F8-307	3672990	662925
F8-311	3679500	658280
F8-312	3679590	658605
F8-312	3679625	658650
F8-312	3679675	658700

### Mafic lava

In order to select eight basaltic andesite groundmass concentrate samples for  $^{40}\text{Ar}/^{39}\text{Ar}$  analysis, microprobe analyses of 20 basaltic andesite lava samples were done by Nelia Dunbar at New Mexico Tech. Each sample was ranked for its suitability of  $^{40}\text{Ar}/^{39}\text{Ar}$  analysis based on three criteria: 1) presence of potassic feldspar suitable for Ar analysis as a groundmass phase or as rims on plagioclase, 2) presence of glassy groundmass that may contain excess Ar, 3) presence of secondary clay minerals that may adversely affect the Ar analysis. Samples were ranked as very good, good, moderate, or poor. Eight samples were chosen from this group based on their ranking (only good or very good samples were considered) and on their stratigraphic relevance. Table C2 summarizes the results of the evaluation process.

### Analytical methods

Microprobe analyses were performed using a Cameca SX-100 electron microprobe with 3 wavelength-dispersive spectrometers. Two types of analyses were performed. First, a potassium K-alpha x-ray map and backscatter image was collected of a selected area of the sample surface. The object of this analysis was to determine the location and distribution of K within the sample, and also to investigate the character (crystalline or glassy) of groundmass material. Secondly, quantitative analysis were performed in order to determine the composition of plagioclase, potassic feldspar rims and groundmass crystals or glass, and any alteration phases. Analyses were performed using a 15 kV accelerating voltage, and 20 nA beam current.

**Table C2** Suitability of Morenci basalt samples for  $^{40}\text{Ar}/^{39}\text{Ar}$  dating, based on microprobe analysis (Dunbar, 1999, personal communication). UTM grid zone 12 locations.

Sample #	Prospects	Comments	UTM N	UTM E
F8-257	Poor	Plagioclase has very K-rich rims (up to 7 wt% $\text{K}_2\text{O}$ ), but there is a large amount of alteration clay.	3664100	650130
F8-261	Poor	Some K-rich glass, but a large amount of alteration clay	3669370	651865
F8-266	Good	Plagioclase has very K-rich rims (8 wt% $\text{K}_2\text{O}$ ), only a small amount of alteration clay.	3671380	650935
F8-269	Good	Small amount of K-feldspar in the groundmass, but little alteration clay.	3674340	654240
F8-271	Good	Fine-grained K-feldspar in the interstitial groundmass, and only a small amount of alteration clay.	3674820	654810
F8-272	Good	Fine-grained K-feldspar in the interstitial groundmass, and only a small amount of alteration clay.	3674725	655125
F8-273	Very Good	Moderately-sized K-feldspar in the interstitial groundmass, and only a small amount of alteration clay.	3673885	655885
F8-275	Very Good	Small-sized K-feldspar in the interstitial groundmass, but no apparent alteration clay.	3663485	662610
F8-276	Good	K-rich rims on plagioclase, and only a small amount of alteration clay.	3663735	663610
F8-278	Poor	Small-sized K-feldspar, and a moderate to large amount of alteration clay.	3664465	664500
F8-280	Good?	Abundant K-feldspar in the interstitial groundmass, possibly low-K biotite or clay.	3665470	663405
F8-285	Very Good?	Plagioclase has thick, K-rich rims, possibly low-K biotite or clay.	3667456	660795
F8-286	Very Good	K in moderately-sized groundmass crystals, and only a small amount of alteration clay.	3641625	654650
F8-287	Moderate	Some interstitial K-feldspar and glass, but no apparent alteration clay.	3639000	651675
F8-301	Good	Some interstitial K-feldspar and a small amount of glass, but no apparent alteration clay.	3650435	649085
F8-310	Moderate	Some interstitial K-feldspar and also glass, but no apparent alteration clay.	3678440	658200
F8-314	Good	Some interstitial crystalline K-feldspar and a small amount of glass, but no apparent alteration clay.	3682440	656700
F8-315	Mod. to Poor	K-feldspar but no glass in the interstitial groundmass, but some alteration clays.	3682180	656550
F8-316	Good	K-rich as fine grained K-feldspar, only minor alteration phases present.	3663965	650145
F8-318	Poor	Former olivine phenocrysts are altered to smectite, possibly saponite.	3664060	650070

# APPENDIX D: PROCEDURES OF THE NEW MEXICO GEOCHRONOLOGY RESEARCH LABORATORY FOR THE PERIOD JUNE 1998 – PRESENT

by  
Matthew Heizler  
William C. McIntosh  
Richard Esser  
Lisa Peters

## <sup>40</sup>Ar/<sup>39</sup>Ar and K-Ar dating

Often, large bulk samples (either minerals or whole rocks) are required for K-Ar dating and even small amounts of xenocrystic, authigenic, or other non-ideal behavior can lead to inaccuracy. The K-Ar technique is susceptible to sample inhomogeneity as separate aliquots are required for the potassium and argon determinations. The need to determine absolute quantities (i.e. moles of <sup>40</sup>Ar\* and <sup>40</sup>K) limits the precision of the K-Ar method to approximately 1% and also, the technique provides limited potential to evaluate underlying assumptions. In the <sup>40</sup>Ar/<sup>39</sup>Ar variant of the K-Ar technique, a sample is irradiated with fast neutrons thereby converting <sup>39</sup>K to <sup>39</sup>Ar through a (n,p) reaction. Following irradiation, the sample is either fused or incrementally heated and the gas analyzed in the same manner as in the conventional K-Ar procedure, with one exception, no argon spike need be added.

Some of the advantages of the <sup>40</sup>Ar/<sup>39</sup>Ar method over the conventional K-Ar technique are:

1. A single analysis is conducted on one aliquot of sample thereby reducing the sample size and eliminating sample inhomogeneity.
2. Analytical error incurred in determining absolute abundances is reduced by measuring only isotopic ratios. This also eliminates the need to know the exact weight of the sample.
3. The addition of an argon spike is not necessary.
4. The sample does not need to be completely fused, but rather can be incrementally heated. The <sup>40</sup>Ar/<sup>39</sup>Ar ratio (age) can be measured for each fraction of argon released and this allows for the generation of an age spectrum.

The age of a sample as determined with the <sup>40</sup>Ar/<sup>39</sup>Ar method requires comparison of the measured <sup>40</sup>Ar/<sup>39</sup>Ar ratio with that of a standard of known age. Also, several isotopes of other elements (Ca, K, Cl, Ar) produce argon during the irradiation procedure and must be corrected for. Far more in-depth details of the determination of an apparent age via the <sup>40</sup>Ar/<sup>39</sup>Ar method are given in Dalrymple et al. (1981) and McDougall and Harrison (1988).

## **Analytical techniques**

### ***Sample preparation and irradiation details***

Mineral separates are obtained in various fashions depending upon the mineral of interest, rock type and grain size. In almost all cases the sample is crushed in a jaw crusher and ground in a disc grinder and then sized. The size fraction used generally corresponds to the largest size possible which will permit obtaining a pure mineral separate. Following sizing, the sample is washed and dried. For plutonic and metamorphic rocks and lavas, crystals are separated using standard heavy

liquid, Franz magnetic and hand-picking techniques. For volcanic sanidine and plagioclase, the sized sample is reacted with 15% HF acid to remove glass and/or matrix and then thoroughly washed prior to heavy liquid and magnetic separation. For groundmass concentrates, rock fragments are selected which do not contain any visible phenocrysts.

The NMGRL uses either the Ford reactor at the University of Michigan or the Nuclear Science Center reactor at Texas A&M University. At the Ford reactor, the L67 position is used (unless otherwise noted) and the D-3 position is always used at the Texas A&M reactor. All of the Michigan irradiations are carried out underwater without any shielding for thermal neutrons, whereas the Texas irradiations are in a dry location which is shielded with B and Cd. Depending upon the reactor used, the mineral separates are loaded into either holes drilled into Al discs or into 6 mm I.D. quartz tubes. Various Al discs are used. For Michigan, either six hole or twelve hole, 1 cm diameter discs are used and all holes are of equal size. Samples are placed in the 0, 120 and 240° locations and standards in the 60, 180 and 300° locations for the six hole disc. For the twelve hole disc, samples are located at 30, 60, 120, 150, 210, 240, 300, and 330° and standards at 0, 90, 180 and 270 degrees. If samples are loaded into the quartz tubes, they are wrapped in Cu foil with standards interleaved at ~0.5 cm intervals. For Texas, 2.4 cm diameter discs contain either sixteen or six sample holes with smaller holes used to hold the standards. For the six hole disc, sample locations are 30, 90, 150, 210, 270 and 330° and standards are at 0, 60, 120, 180, 240 and 300°. Samples are located at 18, 36, 54, 72, 108, 126, 144, 162, 198, 216, 234, 252, 288, 306, 324, 342 degrees and standards at 0, 90, 180 and 270 degrees in the sixteen hole disc. Following sample loading into the discs, the discs are stacked, screwed together and sealed in vacuo in either quartz (Michigan) or Pyrex (Texas) tubes.

#### ***Extraction line and mass spectrometer details***

The NMGRL argon extraction line has both a double vacuum Mo resistance furnace and a CO<sub>2</sub> laser to heat samples. The Mo furnace crucible is heated with a W heating element and the temperature is monitored with a W-Re thermocouple placed in a hole drilled into the bottom of the crucible. A one inch long Mo liner is placed in the bottom of the crucible to collect the melted samples. The furnace temperature is calibrated by either/or melting Cu foil or with an additional thermocouple inserted in the top of the furnace down to the liner. The CO<sub>2</sub> laser is a Synrad 10W laser equipped with a He-Ne pointing laser. The laser chamber is constructed from a 3 3/8" stainless steel conflat and the window material is ZnS. The extraction line is a two stage design. The first stage is equipped with a SAES GP-50 getter, whereas the second stage houses two SAES GP-50 getters and a tungsten filament. The first stage getter is operated at 450°C as is one of the second stage getters. The other second stage getter is operated at room temperature and the tungsten filament is operated at ~2000°C. Gases evolved from samples heated in the furnace are reacted with the first stage getter during heating. Following heating, the gas is expanded into the second stage for two minutes and then isolated from the first stage. During second stage cleaning, the first stage and furnace are pumped out. After gettering in the second stage, the gas is expanded into the mass spectrometer. Gases evolved from samples heated in the laser are expanded through a cold finger operated at -140°C and directly into the second stage. Following cleanup, the gas in the second stage and laser chamber is expanded into the mass spectrometer for analysis.

The NMGRL employs a MAP-215-50 mass spectrometer which is operated in static mode. The mass spectrometer is operated with a resolution ranging between 450 to 600 at mass 40 and isotopes are detected on a Johnston electron multiplier operated at ~2.1 kV with an overall gain of

about 10,000 over the Faraday collector. Final isotopic intensities are determined by linear regression to time zero of the peak height versus time following gas introduction for each mass. Each mass intensity is corrected for mass spectrometer baseline and background and the extraction system blank.

Blanks for the furnace are generally determined at the beginning of a run while the furnace is cold and then between heating steps while the furnace is cooling. Typically, a blank is run every three to six heating steps. Periodic furnace hot blank analysis reveals that the cold blank is equivalent to the hot blank for temperatures less than about 1300°C. Laser system blanks are generally determined between every four analyses. Mass discrimination is measured using atmospheric argon which has been dried using a Ti-sublimation pump. Typically, 10 to 15 replicate air analyses are measured to determine a mean mass discrimination value. Air pipette analyses are generally conducted 2-3 times per month, but more often when samples sensitive to the mass discrimination value are analyzed. Correction factors for interfering nuclear reactions on K and Ca are determined using K-glass and CaF<sub>2</sub>, respectively. Typically, 3-5 individual pieces of the salt or glass are fused with the CO<sub>2</sub> laser and the correction factors are calculated from the weighted mean of the individual determinations.

### ***Data acquisition, presentation and age calculation***

Samples are either step-heated or fused in a single increment (total fusion). Bulk samples are often step-heated and the data are generally displayed on an age spectrum or isochron diagram. Single crystals are often analyzed by the total fusion method and the results are typically displayed on probability distribution diagrams or isochron diagrams.

### ***The age spectrum diagram***

Age spectra plot apparent age of each incrementally heated gas fraction versus the cumulative % <sup>39</sup>Ar<sub>K</sub> released, with steps increasing in temperature from left to right. Each apparent age is calculated assuming that the trapped argon (argon not produced by *in situ* decay of <sup>40</sup>K) has the modern day atmospheric <sup>40</sup>Ar/<sup>36</sup>Ar value of 295.5. Additional parameters for each heating step are often plotted versus the cumulative %<sup>39</sup>Ar<sub>K</sub> released. These auxiliary parameters can aid age spectra interpretation and may include radiogenic yield (percent of <sup>40</sup>Ar which is not atmospheric), K/Ca (determined from measured Ca-derived <sup>37</sup>Ar and K-derived <sup>39</sup>Ar) and/or K/Cl (determined from measured Cl-derived <sup>38</sup>Ar and K-derived <sup>39</sup>Ar). Incremental heating analysis is often effective at revealing complex argon systematics related to excess argon, alteration, contamination, <sup>39</sup>Ar recoil, argon loss, etc. Often low-temperature heating steps have low radiogenic yields and apparent ages with relatively high errors due mainly to loosely held, non-radiogenic argon residing on grain surfaces or along grain boundaries. An entirely or partially flat spectrum, in which apparent ages are the same within analytical error, may indicate that the sample is homogeneous with respect to K and Ar and has had a simple thermal and geological history. A drawback to the age spectrum technique is encountered when hydrous minerals such as micas and amphiboles are analyzed. These minerals are not stable in the ultra-high vacuum extraction system and thus step-heating can homogenize important details of the true <sup>40</sup>Ar distribution. In other words, a flat age spectrum may result even if a hydrous sample has a complex argon distribution.

### ***The isochron diagram***

Argon data can be plotted on isotope correlation diagrams to help assess the isotopic composition of Ar trapped at the time of argon closure, thereby testing the assumption that trapped

argon isotopes have the composition of modern atmosphere which is implicit in age spectra. To construct an “inverse isochron” the  $^{36}\text{Ar}/^{40}\text{Ar}$  ratio is plotted versus the  $^{39}\text{Ar}/^{40}\text{Ar}$  ratio. A best fit line can be calculated for the data array which yields the value for the trapped argon (Y-axis intercept) and the  $^{40}\text{Ar}^*/^{39}\text{Ar}_K$  value (age) from the X-axis intercept. Isochron analysis is most useful for step-heated or total fusion data which have a significant spread in radiogenic yield. For young or low K samples, the calculated apparent age can be very sensitive to the composition of the trapped argon and therefore isochron analysis should be performed routinely on these samples (cf. Heizler and Harrison, 1988). For very old (>Mesozoic) samples or relatively old sanidines (>mid-Cenozoic) the data are often highly radiogenic and cluster near the X-axis thereby making isochron analysis of little value.

#### The probability distribution diagram

The probability distribution diagram, which is sometimes referred to as an ideogram, is a plot of apparent age versus the summation of the normal distribution of each individual analysis (Deino and Potts, 1992). This diagram is most effective at displaying single crystal laser fusion data to assess the distribution of the population. The K/Ca, radiogenic yield, and the moles of  $^{39}\text{Ar}$  for each analysis are also often displayed for each sample as this allows for visual ease in identifying apparent age correlations between, for instance, plagioclase contamination, signal size and/or radiogenic concentrations. The error ( $1\sigma$ ) for each age analysis is generally shown by the horizontal lines in the moles of  $^{39}\text{Ar}$  section. Solid symbols represent the analyses used for the weighted mean age calculation and the generation of the solid line on the ideogram, whereas open symbols represent data omitted from the age calculation. If shown, a dashed line represents the probability distribution of all of the displayed data. The diagram is most effective for displaying the form of the age distribution (i.e. gaussian, skewed, etc.) and for identifying xenocrystic or other grains which fall outside of the main population.

#### Error calculations

For step-heated samples, a plateau for the age spectrum is defined by the steps indicated. The plateau age is calculated by weighting each step on the plateau by the inverse of the variance and the error is calculated by either the method of Samson and Alexander (1987) or Taylor (1982). A mean sum weighted deviates (MSWD) value is determined by dividing the Chi-squared value by  $n-1$  degrees of freedom for the plateau ages. If the MSWD value is outside the 95% confidence window (cf. Mahon, 1996; Table 1), the plateau or preferred age error is multiplied by the square root of the MSWD.

For single crystal fusion data, a weighted mean is calculated using the inverse of the variance to weight each age determination (Taylor, 1982). Errors are calculated as described for the plateau ages above.

Isochron ages,  $^{40}\text{Ar}/^{36}\text{Ar}_i$  values and MSWD values are calculated from the regression results obtained by the York (1969) method.